Femtodynamics of Double Proton Transfer Reactions

A thesis presented to the University of London in partial fulfilment
of the requirements for the degree of Doctor of Philosophy

Carmen-María Redondo Marey

Department of Chemistry
University College London

August 2002

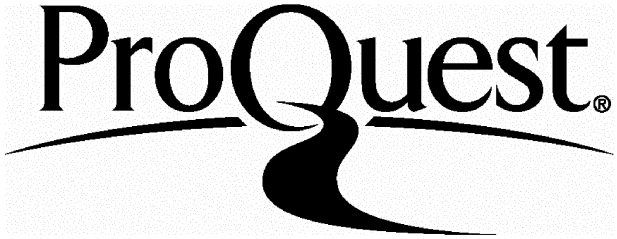

Acknowledgements

I would like to take this opportunity to thank those who have helped me during my PhD. Firstly I would like to thank my supervisor Prof. David Clary for his support and advice throughout my PhD. I would also like to thank Dr. Victor Guallar for providing some of *ab initio* data used in our calculations. I am also very grateful to Dr. Tanja van Mourik for her assistance with the *ab initio* calculations and for helping to proof read this thesis. I would like to thank the members of the Clary group past and present for providing an enjoyable working environment. Dr. Paul Krause and Dr. Luis S. Costa deserve a special mention for their useful comments and suggestions. This work was funded by a UCL Provost Studentship and by a Marie Curie TMR European Grant.

I would like to thank all my friends in Spain; their emails, visits and jokes have been a huge support during this time. I cannot forget all the friends I have made in London, they have made my life here easy and enjoyable. In particular, I am indebted to Maria Luz Endere and Pornpinmon Pianponsum for reminding me that there is life outside chemistry. I am especially grateful to Aurelio Rodriguez, his patience, support and affection have been essential.

Above all, I would like to thank my parents; I could not have made it without their love and encouragement.

To my parents Miguel and Carmina

"Nothing in life is to be feared. It is only to be understood."

Marie Curie

Abstract

The aim of this work is to develop a method to study excited-state double proton transfer reactions in biomolecules, looking mainly at their time scale. We focused our attention on the double proton transfer reaction in the 7-azaindole dimer. This reaction has been experimentally studied by Zewail and co-workers and Castleman and co-workers using femtospectroscopic techniques (resolution 10^{-15} s). In addition, the reaction is a model for that occurring in DNA base pairs.

The 7-azaindole dimer is a bifunctional molecule that contains two hydrogen-atom donor groups and two acceptor groups in close proximity. These groups form two hydrogen bonds between the two moieties of the molecule. During the reaction, the two hydrogen atoms move from one moiety of the molecule to the other. The goal is to predict the time scale of this reaction (the two proton transfer times).

A quantum tunnelling in a dissipative environment approach is used to study this process. This method considers the system composed of a tunnelling particle (the H atom) moving in a potential field, V, coupled to a bath that represents the rest of the molecule.

Our first approach was to use only two degrees of freedom to describe the process: the donor-atom hydrogen-atom distance and the donor-atom acceptor-atom distance (or intermolecular distance). The results were compared with the experimental ones.

To improve our results we introduced another degree of freedom in our calculations. It represents the other modes of the molecule, which had not been considered in the first approach. This improves agreement with the experiments.

Calculations considering different initial vibrationally excited states and different isotopic isomers (which show the importance of quantum tunnelling in this process) were also carried out and compared with the experiments.

Contents

List of Figures

List of Tables

Chapter 1

Introduction

1.1 Femtochemistry

At the turn of the 20th century the question for physical chemists was, how do reactions proceed and what are their kinetic rates ? [1]-[5] (and references therein). In an attempt to answer these questions Arrhenius, in 1889, formulated his well-known expression for the rate constant [6]. At this time it was already known that higher temperature implied two things: the molecules moved faster and the atoms oscillated more violently. Arrhenius' formula can then be interpreted assuming that when two molecules collide, they usually part again and nothing happens; but if the collision is sufficiently violent, the molecules disintegrate and their atoms recombine into new molecules. So, Arrhenius gave the first description on the change in rates of chemical reactions with temperature.

Five years later, Bodenstein published papers on understanding elementary reaction mechanisms. He modelled the reversible decomposition of HI into H_2 and I_2 as a simple molecular reaction between two HI molecules with a cyclic transition state. He assumed that the reaction evolved in a step-by-step sequence where one of the steps was slow and hence determined the overall course of the reaction while the other steps were immeasurably fast.

In the 1920s Lindemann and Hinshelwood developed an elementary mechanism with different steps for unimolecular gas phase reactions [7, 8]. Lindemann proposed

that, according to Arrhenius' law, a molecular reaction is due to intermolecular collisions. However, the reaction does not follow instantaneously the shock of activation, because the energy acquired by the molecule needs a certain time to be distributed. Depending on the order of magnitude of this lapse of time with respect to the frequency of the collisions and the pressures at which one operates, several cases can arise. By studying the decomposition of different molecules Hinshelwood showed that under strong pressure this type of reaction adopts an order one, under low pressure the order becomes two and with intermediate pressures, the reaction has an order ranging between one and two. He also showed that if an inert gas is introduced into the reaction medium it reduces the variation of the reaction order with respect to the pressure. Lindemann and Hinshelwood's work highlights then, three distinct reactional stages: activation, reaction and deactivation. It also constitutes the prelude to the theory of the "activated complex" [9]-[11].

In 1928, Rice, Ramsperger and Kassel formulated the RRK theory [12]. In this theory the rate at which the energized reactant molecule breaks down is treated as a function of the energy E that it contains. The theory assumes that the reaction rate is proportional to the number of ways of distributing E among the internal degrees of freedom of the reactant molecule. Marcus subsequently blended it with transition state theories to formulate the RRKM theory [13, 14]. This new theory looks into the way in which the various normal-mode vibrations and rotations contribute to the reaction. It also takes into account the zero-point energies.

All these theories and experimental works belong to the kinetics field. They provide an answer to the question of how reactions evolve and what factors determine their rates. But, the rate constant k(T) does not provide a detailed molecular picture of the reaction. k(T) is an average of the microscopic, reagent-state to product-state rate coefficients over all possible encounters. In order to quantitatively describe the details of chemical reactions answers are needed to the question of how reagent molecules approach, collide, exchange energy, sometimes break bonds and make new ones and finally separate into products. Providing an answer to this question is the goal of molecular reaction dynamics.

In this field two areas can be distinguished: theory and experiments. Both of them have experienced a big development in the last hundred years. So, from a theoretical point of view the first step was given in 1926 when Schrödinger formulated his famous equation. A year later Heitler and London published the quantum mechanical treatment of the H_2 molecule [15] and later on, London presented an approximate expression for the potential energy of triatomic systems such as H_3 [16].

At the same time Eyring and Polanyi started to work together. They used contour maps to represent the potential energy surface of a reaction, a ball rolling on this surface would describe the position of the atoms. They used semi-empirical methods, based in quantum mechanics but using experimental data for vibrational frequencies and energies of association. So, in 1931, Eyring and Polanyi provided a semi-empirical calculation of a potential energy surface (PES) of the H + H_2 reaction [17]; it was the first time one could think of the PES and the dynamics on it. In 1935 Eyring, Evans and Polanyi formulated the transition state theory [9]-[11]. The transition state of a chemical reaction is the brief period, often only millionths of a second long, when the starting materials have combined together but have not yet completely transformed themselves into the products of the reaction. This theory provided an explicit expression for Arrhenius' preexponential factor. In this way they completed the theory of reaction rates which gave an analytical formula for the rate constant which included the "frequency" for the passage through the transition state (typical value 10^{-13} s, the time scale of molecular vibrations). From a classical mechanics point of view, this estimate of time scale is consistent; the velocity of the nuclei is around 1 km.s^{-1} and the distances involved in a chemical reaction are around 1 Å, so the time scale is about 100 fs. Later on, Kramers' classical work modified the preexponential factor to include friction [18], but the description of the transition state is still similar to that formulated by Eyring, Evans and Polanyi.

In 1936 the first classical trajectory calculations were published. These calculations, carried out by Hirschfelder, Eyring and Topley on the H + H_2 reaction, showed the need of the femtosecond scale [19]. They used an analytical interatomic force expression for their calculations. In the 1960s, Karplus, Bunker and others [20] (and

references therein) showed a range for the time scales, from picoseconds to femtoseconds, depending on the reaction.

On the experimental side, in 1850 Wilhelmy reported the first quantitative rate measurements. He determined the homogeneous chemical kinetic rate law for acid catalyzed inversion of sucrose. In 1923 Hartridge and Roughton carried out experiments for solution reactions in flow tubes. They let two solutions arriving through separate tubes meet and be mixed, and then caused the mixture to flow swiftly through an outlet tube, in which the reaction could be observed as it proceeded. This method permitted measurement of reaction times down to thousandths of a second. Still many fast reactions could not be studied by this method for the simple reason that the substances cannot be mixed fast enough. In 1940 Britton Chance in his stopped-flow experiments reached the millisecond scale. He developed the new technique to study biochemical and biophysical processes in living organisms.

Around 1950, Eigen (relaxation method) and Norrish and Porter (flash photolysis) reached the microsecond time scale [21]. Norrish and Porter used a very powerful flash lamp to irradiate a substance which will be either converted into an activated form or its molecules will be broken up so as to yield groups with a high reactivity. It then becomes possible to study these newly formed molecules spectroscopically. Eigen showed that if, say, a solution of acetic acid is subjected to a high-tension electric pulse, more molecules of this substance are dissociated than would be the case otherwise. This takes a certain length of time. When the electric pulse is turned off, the solution goes back to its former equilibrium, this also takes some time, and that relaxation can be recorded. The recording methods of the Norrish-Porter and Eigen methods are similar. Eigen also showed that the absorption of sound in a solution could be used to estimate the velocity of fast reactions which take place in solution.

In the 1960s Polanyi [22] developed the method of infrared chemiluminescence, in which the extremely weak infrared emission from a newly formed molecule is measured and analysed. He used this method to elucidate the detailed energy disposal during chemical reactions. At the time it was known that molecules had three kinds of

motion: spinning or rotational energy, buzzing or vibrational energy, and the energy of movement from one point to another or translational energy. What was entirely unknown was the apportionment of the energy during a reaction between these three types of energy. Excess energy from the reaction is deposited as internal energy in the product molecules, which after some delay emit the energy in the form of infrared light. Spectroscopic analysis of this light reveals directly the quantum mechanical states which the product molecules occupied. This gives indirect but extremely important information on the multidimensional surface describing the potential energy for the system. Polanyi described how the existence and location of an energy barrier on the potential energy surface modifies the dynamics of the reaction. He showed that the product molecules in some cases belong to two different, well separated, classes with respect to the internal energy distribution. The method which he developed can be considered as a first step towards the present more sophisticated, but also more complicated, laser-based methods for the study of chemical reaction dynamics.

Lasers become available in the 1960s. With them it was possible to reach shorter time scales: picosecond time scales using mode-locking lasers and subpicosecond with dye lasers. In 1987 a 6 fs pulse was achieved and in 1991 Titanium:sapphire lasers became a common laboratory tool [23, 24]. Nowadays smaller femtosecond laser pulses are available.

Polanyi's experiments took place concurrently with the formation of the crossed molecular beam field. On the experimental side there was an important problem that could not be solved. The directions and velocities of the molecular motions in a gas or a liquid are mainly random, consequently the collisions between the molecules are ill-defined. The details of the reaction thus become blurred and could not be observed precisely enough. This problem was overcome by the use of molecular beams in, for example, the work of Herschbach and Lee [22]. Herschbach developed the method of crossed molecular beams, directed and well-defined fluxes of molecules, to and beyond the point where detailed studies of chemical reactions have been possible. Lee developed the method of crossed molecular beams further towards its use for general reactions. Most notably, he used this method for the study of important

reactions for relatively large molecules.

In the 1980s, Kinsey and others studied the dynamics of the decomposition of single molecules that have been photoexcited to an unstable electronic state. These studies provided a spectroscopic mean of following the motion of the transient state leading to photochemical fragmentation. This is accomplished by recording the spectrum of light emitted by the excited molecule.

All of these developments both theoretical and experimental set the ground work for the development of femtochemistry. Zewail made a major contribution into this field mainly into the experimental side but also on the theoretical one. He performed a series of experiments that were to lead to the birth of this new research field called femtochemistry. In 1986 he carried out an experiment on ICN [25, 26] in which his group was able, for the first time, to observe the passage through the transition state and to measure its "lifetime" with femtosecond resolution (the total time for the experiment was 200 fs). Later on, Zewail and his group studied the dissociation of NaI into Na + I, [27]-[29]. In this experiment the pump pulse excited the ion pair NaI, which has an equilibrium distance of 2.8 Å, to an excited form [Na-I]* which at this bond distance assumes a covalent bonding character. However, its properties change when the molecule vibrates: when the Na and I atoms are at their outer turning points, 10-14 Å apart, the structure is ionic, $[Na^+ \cdots I^-]^*$, as one electron has moved from Na to I. When the atoms move back together the bonding becomes covalent again: [Na-I]*, and so forth. A critical point during the vibration is when the distance is 6.9 Å. At this point the excited state and ground state are very close to each other and there is a great probability that the excited [Na-I]* will either fall back to its initial state [Na-I] or decay into sodium and iodine atoms.

What Zewail and his coworkers found was that they could follow the activated complex as it moved back and forth between covalent and ionic structures and, moreover, that bursts of free sodium atoms were produced in pace with these oscillations. This experiment showed that the wave packet was highly localised in the space of approximately 0.1 Å (dynamics at atomic-scale resolution) and its spreading was minimal up to a few picoseconds (a single-molecule trajectory). Vibrational coherence

was also observed during the entire course of the reaction (coherent trajectories in reactions) from reactants to products. It could then be said that on the femtosecond time scale, the description of the dynamics follows an intuitive classical picture.

Zewail's group conducted other key experiments on the H + CO_2 [30] ground state reaction. They showed that the intermediate HOCO lives for about 1 ps and that the OH bond making and the CO bond breaking are made in a nonconcerted pathway. In this case, comparison with theory was possible as there were several *ab initio* PES and dynamical calculations available.

From these experiments they inferred the basic concepts of femtochemistry. Firstly, the time scales and the location concept; the former one related to the vibrational and rotational motions and the later one to the deBroglie wavelength reaching the atomic scale for motion. Secondly, the concept of coherence connected with the state, orientation and nuclear wavepacket dynamics and the concept of single-molecule trajectory motion (instead of averaging). Thirdly, the concept of probing transition states and intermediates directly in real time. And finally, the concept of controlling reactivity with ultrashort light pulses.

Thus, they determined that in order to meet these requirements a femtosecond experiment should consist of a femtosecond pump (initiating) laser pulse and a femtosecond probe laser pulse [31]. This is known as a pump-probe configuration. The femtosecond pump (initiating) laser pulse allows the motion to be clocked (it defines the zero of time) and synchronises the motion of the millions of molecules used in the recording of molecular motion. The femtosecond probe laser pulse monitors the dynamics of the system. Laser-induced fluorescence was the first probe used but more recently mass-spectrometry, nonlinear optical techniques and Coulomb explosion are some of the probes used in the femtosecond experiments. A layout of a femtosecond experiment is showed in Figure 1.1.

In 1999 Zewail was awarded the Nobel Prize for his contributions to the development of femtochemistry [32] showing that it is possible with rapid laser techniques to see how atoms in a molecule move during a chemical reaction.

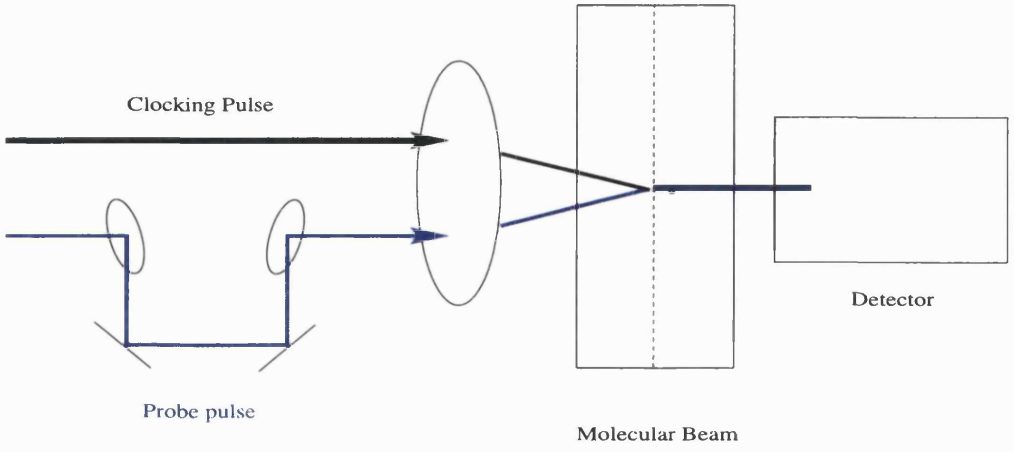

Figure 1.1: General layout of a femtosecond experiment.

In the last few years the applications of femtochemistry have spanned the different types of chemical bonds (covalent, ionic, dative, metallic, hydrogen and van der Waals bonds). The experiments are carried out using not only molecular beams but also studying processes on surfaces and on clusters (e.g. to understand and improve catalysts), in liquids and solvents (to understand the mechanism of the dissolving of, and reactions between, chemical substances in solution) and in polymers (e.g. to develop new materials for use in electronics). In addition, femtochemistry has been applied to the study of many important biological systems.

Knowledge of the mechanism of chemical reactions is important for our ability to control the reactions. A desired chemical reaction is often accompanied by a series of unwanted, competing reactions that lead to a mixture of products and hence the need for separation and cleansing. If the reaction can be controlled by initiating reactivity in a selected bond, this could be avoided.

As a summary, we can say that femtochemistry is the resolution in time of el-

ementary dynamics. It studies chemical processes that occur on the time scale of femtoseconds (10^{-15}s). Femtochemistry offers an opportunity to observe a molecular system in the continuous process of its evolution from reactants to transition states and then to products.

1.2 7-azaindole

Over the last thirty years a great deal of attention has been focused on 7-azaindole (7-AI), its dimer $(7\text{-AI})_2$ and its complexes with acids, alcohols, and water molecules. 7-azaindole is a biochemically important molecule as it is the basic chromophore of 7-azatryptophan [33], a noninvasive *in situ* optical probe of protein structure and dynamics. The dimer $(7\text{-AI})_2$ is a simple model for the hydrogen bonded base pair of DNA. $(7\text{-AI})_2$ is considered a prototype for fundamental studies of structure and electronic phenomena simulating those to be expected in DNA base pairs. The study of proton transfer reactions in this model could provide information on the possible role of tautomerism in mutation. This role was already emphasised by Watson and Crick [34] who pointed out that the genetic code might be disturbed by the unusual rare tautomeric forms of the base pairs, resulting from proton (or hydrogen atom) transfer reactions. Due to this interest the $(7\text{-AI})_2$ tautomerisation reaction has been widely studied in different environments: gas phase, solution and clusters [35]-[37]. Next I give a summary of all of this research going from the initial fluorescence spectra to the latest femtosecond technology in the experimental side and from semiempirical calculations to multidimensional *ab initio* potential energy surfaces in the theoretical one.

The first study of 7-azaindole was carried out in 1969 by El-Bayoumi and co-workers [38]. They obtained the ultraviolet absorption and the fluorescence spectra of 7-azaindole in solution. These spectra showed a long-wavelength absorption band (F1) due to the normal 7-AI monomer and a solvent-dependent band (F2) approximately 10000 cm^{-1} red shifted compared with the first band. They theorised that this F2 band could be a consequence of an excited state (ES) two-proton tautomerism in

the dimer. So, after excitation the ground state (GS) dimer could tautomerise to the excited tautomeric species which then emits fluorescence (F2 band). They assumed that a very low barrier or a high tunnelling rate allow a rapid thermal equilibration of the reaction in solution and that a much slower proton tunnelling rate prevents it from happening in rigid-glass solutions. The species involved in the tautomeric reaction are shown in Figure 1.2. Two years later El-Bayoumi's group [39] continued

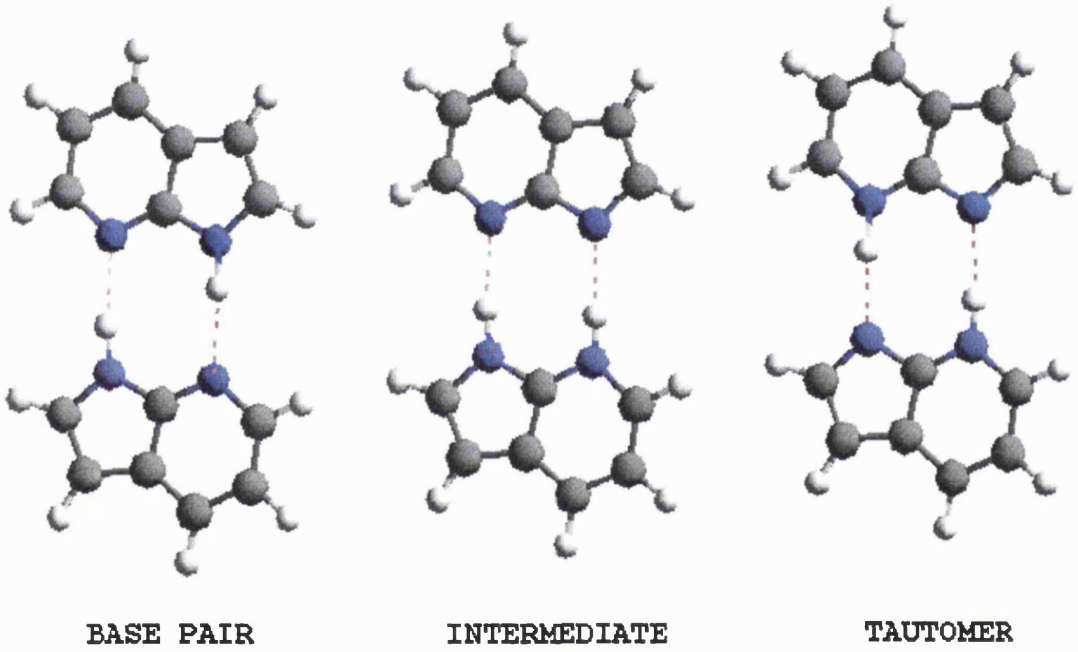

Figure 1.2: Molecular structures involved in the double proton transfer reaction of the 7-azaindole dimer.

studying this reaction. They confirmed that the fluorescence spectrum of 7-azaindole in 3-methylpentane consists of two bands: F1 with a maximum at 325 nm and F2 with a maximum at 480 nm. They assigned the F1 band to the monomer fluorescence and the F2 one to the $(7\text{-AI})_2$ tautomer fluorescence by comparing the spectrum with those of N-methyl-7-azaindole and 7-methyl-7H-pyrrolo[2,3-b]pyridine. The first of these compounds forms H-bonds and its spectrum only shows the F1 band. The sec-

ond compound has an analogous structure to the 7-AI tautomer and its spectrum only shows a band similar to F2. Studying the F2/F1 ratio they obtained an activation barrier for the tautomerisation reaction of approximately 1.4 kcal.mol^{-1}. It was also suggested that the proton tunnelling mechanism must be important in the reaction especially at very low temperatures. Some of these authors [40], in another study, investigated the effect of concentration, solvent, pH, excitation wavelength and isotopic change upon the F2/F1 ratio. They observed that the deuterium substitution enhances the F1 band at the expense of the F2 one as the tautomerisation reaction is less efficient in the deuterated sample. The ratio of proton tunnelling rates (obtained for the deuterated and nondeuterated compounds) was determined to be 2.9. They confirmed the existence of proton tunnelling as the F2/F1 ratio does not go to zero even at very low temperatures. This opinion is not shared by Bulska and Chodkowska [41] who maintained that no tunnelling mechanism is needed to explain the F2 fluorescence at low temperature. These authors explained that at these low temperatures the tautomeric fluorescence is overlapped by the isoenergetic monomeric phosphorescence. In order to probe this they measured the F2/F1 ratio variations with temperature, the curve approaches zero at temperatures when the phosphorescence was still not observable (120-130 K). So, they suggested that the proton transfer reaction occurs only via an activated process.

The first time-resolved fluorescence study of 7-AI (77 K, 10^{-2} M in 3-methylpenta ne) was carried out by El-Bayoumi *et al.* [42]. To slow down the reaction the indolic H was replaced by deuterium. They determined that while at high temperature the proton transfer can take place by both thermally activated and tunnelling mechanisms, at very low temperatures quantum tunnelling may be the only reaction mechanism. The efficiency of this mechanism in the $(7\text{-AI})_2$ tautomerisation reaction may be due to the coupling of the proton motion in the neighbouring hydrogen bonds. They suggested that the motion of the H in one of the hydrogen bonds (single proton transfer) creates an electronic field that reduces the potential barrier for the second proton transfer. The motion of the two hydrogen atoms is then correlated.

Four years later Hetherington *et al.* [43] carried out the first picosecond study of

the 7-azaindole tautomerisation reaction in solution. They showed that the double proton transfer reaction (DPTR) occurs in less than 5 ps in non-polar solvents at 298 K, and in approximately 1 ns at 77 K. They proposed two pathways for the reaction, a direct one for the nonequilibrated dimer and an indirect one for the thermally equilibrated dimers.

Catalán and Pérez [44] were the first to study theoretically the fluorescence of 7-AI . Using an all-valence electrons complete neglect of differential overlap (CNDO) method they found two $\pi \rightarrow \pi^*$ electronic transitions and one $n \rightarrow \pi^*$ transition localised between the other two. According to these semiempirical calculations the DPTR can take place in the first $\pi \rightarrow \pi^*$ excited singlet state. They underlined the dependence of the reaction mechanism on the intermonomeric separation. During the reaction this intermonomeric distance must change first to allow the proton transfer to take place and then to stabilise the tautomeric form.

In 1984 Kaya and co-workers [45] measured the electronic absorption and fluorescence spectra of free 7-AI , $(7\text{-AI})_2$ and 7-AI :water complexes in a supersonic beam. Their experimental results suggest that, in the ES, the dimer is displaced largely along the intermolecular coordinates and that the tautomeric form might be a stable structure. The GS dimer has $1A_g$ geometry and the excited states (upon dimer formation an ES of the monomer splits into two states) have $1B_u$ and $2A_g$ geometries which are one and two-photon allowed respectively from the GS. The $2A_g$ state is the one which undergoes the tautomerisation reaction. They found the reaction to be barrierless which contradicts the calculations by Catalán and Pérez [44] who found a barrier in the reaction (a barrier whose height varies with the intermonomeric distance). In a deeper study of the DPTR mechanism Fuke and Kaya [46] showed that one of the isomers (henceforth called the reactive isomer) undergoes a double proton transfer reaction even under collision-free conditions while the other isomer (the unreactive one) at high vibrational levels undergoes an intramolecular nonradiative relaxation. The dimeric spectrum exhibits a band at 120 cm^{-1} which can be assigned to an intermolecular N-H$\cdots$N symmetric stretch vibration. There is a dramatic enhancement of the DPTR rate by the excitation of this vibrational mode which is considered to

be the promoting mode of the tautomerisation reaction. This band corresponds to 107 cm^{-1} in the ES tautomer and to 129 cm^{-1} in the GS tautomer. The lifetime of the GS tautomer was estimated by these authors to be around 10 μs. Using transient absorption and fluorescence spectroscopic techniques Itoh and co-workers [47] studied the mechanism of the $(7\text{-AI})_2$ tautomerisation reaction in solution. They determined the reaction time to be 0.62 ns (0.79 ns for the deuterated form) at 77 K. At room temperature these values are 10.6 and 16.6 ns respectively. This large deuterium effect could be explained by the presence of an activation barrier of approximately 280 cm^{-1}. The decay time from the excited tautomer to the ground state tautomer is 19.0 μs. In the GS reverse reaction (from tautomer to dimer) they observed a large quantum tunnelling effect and the reaction time was now 41.3 μs (132 μs for the deuterated form).

Chou *et al.* [48] carried out some *ab initio* calculations (using 6-31G* as the basis set) and experimental work on 7-AI , 1:1 7-AI :acetic acid complex, $(7\text{-AI})_2$, 1:1 7-AI :methanol complex and 1:1 7-AI :water complex. They found that the GS $(7\text{-AI})_2$ tautomer has an energy 22.3 $kcal.mol^{-1}$ greater than that of the corresponding dimer while in the ES the tautomer energy is 1.8 $kcal.mol^{-1}$ lower than that of the dimer. To complete the energy profile of the reaction they used the experimental values obtained by Kaya and co-workers [45] for the $S_0 \rightarrow S_1$ transition. They estimated that the ES dimeric form is 23810 cm^{-1} higher than the GS dimeric form and the excited tautomer 32254 cm^{-1} higher than the ground state tautomeric form. The general schematic profile of the tautomerisation reaction is showed in Figure 1.3. In their calculations with 7-AI complexes (with alcohols, acids or water molecules) these authors found that the DPTR is energetically more favourable than in the dimer when the proton transfer reaction can be considered as a catalytic process (the molecular structure of the 7-azaindole partner remains the same along the reaction).

Zewail and co-workers [49] used femtosecond mass spectrometry to follow the phototautomerisation reaction of $(7\text{-AI})_2$ in the gas phase. The experimental set-up consists of an initial ultraviolet femtosecond pulse (305-310 nm) which excites the base pair (from a molecular beam) to the first electronically excited state.

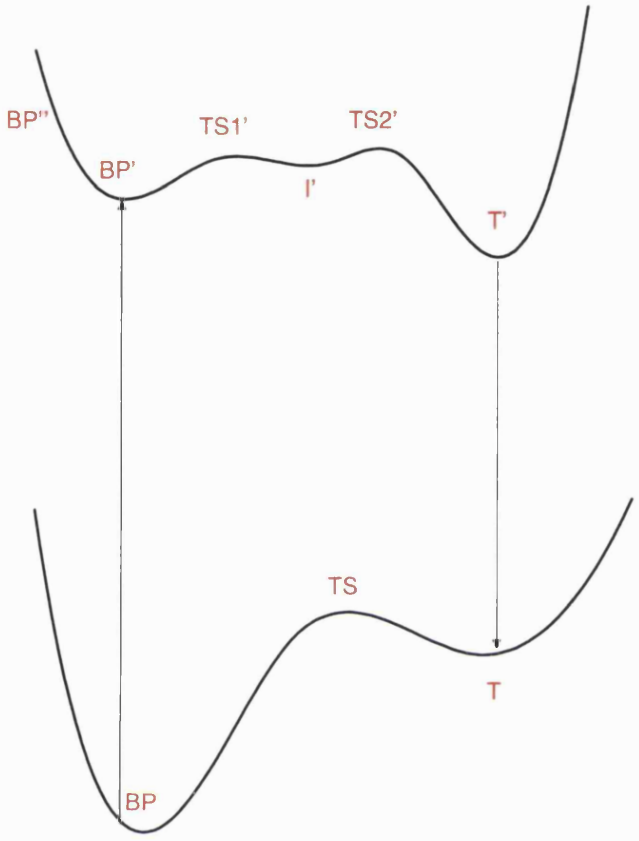

Figure 1.3: Schematic profile corresponding to the double proton transfer reaction. BP is the base pair, TS the transition state, I the intermediate and T the tautomer. Any symbol carrying ' or " denotes the excited state.

A second fs pulse (620 nm), delayed in time, probes the dynamics of the pair by exciting the bases above their ionisation threshold so that they can be monitored by time of flight (TOF) mass spectrometry. The zero of time is established *in situ* by identifying the ion signal that results when the two pulses coincide. They carried out a series of experiments at different N-H$\cdots$N symmetric stretch vibrational energies and with undeuterated and deuterated species. They obtained a series of experimental results which were not possible to fit to a single exponential but to a bi-exponential

function. This fact suggests that the DPTR occurs in two steps. Their results were the following: if the vibrational energy is 0.0 kcal.mol^{-1} the first transfer time is 650 fs and the second 3.3 ps; if the energy is 1.5 kcal.mol^{-1} the times are 200 fs and 1.6 ps respectively for the undeuterated species. This difference indicates the presence of a reaction barrier which was estimated to be 1.3 kcal.mol^{-1} for the first step and 2.6 kcal.mol^{-1} for the second one. The fact that the initial tautomerisation is on the femtosecond scale when the total vibrational energy is 0.0 kcal.mol^{-1} indicates that the proton transfer reaction is direct and does not involve the entire vibrational phase space of the pair; the motion is localised in the N-H$\cdots$N coordinate. If the vibrational energy is around 1 kcal. mol^{-1} the undeuterated transfer times are 360 fs and 1.7 ps, the double deuterated times are 3.0 ps and 25 ps and the monodeuterated times are 1.5 ps and 11 ps. These differences confirm the presence of a reaction barrier and that, at low energies, the reaction occurs through tunnelling.

Calculations on the ground and excited states of the dimer were reported in 1996 by Douhal *et al.* [50]. The GS was studied using the restricted Hartree Fock method while a Configuration Interaction (CI) all-single-excitations with spin-restricted Hartree Fock reference GS was used for the ES. The correlation energies for both the GS and the ES were evaluated with MP2. In all these calculations a 4-31G basis set was used. This is a very small basis set and so the results can only be considered as a qualitative guide. From these calculations they inferred that the GS base pair (BP) is completely symmetric (with two equivalent hydrogen bonds). As a vertical transition from the GS to the ES is symmetry forbidden, a small perturbation of the geometry and a vertical transition or a slightly non-vertical transition allows access to a base pair structure in the ES. This structure then relaxes to a non-symmetric base pair with less energy than the initial one and with the excitation fully localised in one moiety of the dimer. As the excitation is localised in one moiety and both the N$\cdots$N and the N-H motions are faster than the intramolecular vibrational energy redistribution, only one H atom shifts initially. This establishes the asymmetry of the reaction and the stepwise mechanism in accordance with the experimental results by Zewail's group [49]. This first jump occurs through tunnelling (energy

barrier of 1.2 kcal.mol^{-1}) originating from a zwitterionic intermediate species with both protons on the same side of the molecule. The second proton jump also occurs through tunnelling with an energy barrier of 0.11 kcal.mol^{-1}, which is very different from Zewail's experimental value of 2.6 kcal.mol^{-1}. Using the Configuration Interaction Singles and the Moller-Plesset second order perturbation (CIS-MP2) method these values change a lot; at this level of calculation there are no barriers, the reaction follows a downhill path with the energy of the intermediate being 5.9 kcal.mol^{-1} lower than that of the base pair and the tautomer's energy 15.9 kcal.mol^{-1} lower than that of the base pair. In the GS the reaction occurs in a concerted way. The tautomer's energy is 24.49 kcal.mol^{-1} higher than that of the BP (22.3 kcal.mol^{-1}) calculated by Chou and co-workers [48], the energy barrier in this case is 4.99 kcal.mol^{-1} higher than that of the tautomer and 28.48 kcal.mol^{-1} higher than that of the BP. Using CIS-MP2 these energies are 1.11 kcal.mol^{-1} and 18.80 kcal.mol^{-1} respectively.

In order to corroborate the spectra previously obtained by Fuke and Kaya [45] Lopez-Martens *et al.* [51] performed picosecond time resolved photoelectron spectroscopy of the $(7\text{-AI})_2$. They confirmed the presence of a nonreactive dimer which also has a double hydrogen-bonded structure. They suggested that the dimer could assume two different geometries (keeping the planar structure of the skeletal ring), a displaced by parallel geometry and an out-of-plane geometry, the former structure being the nonreactive one. Other authors [52] suggest that this unreactive dimer could have a T-shaped geometry or even that it could contain a water molecule. Lately Kasha and co-workers [53] have also found a new structure for the nonreactive dimer which only allows it to undergo a single proton transfer reaction. Lopez-Martens' group also reported that the reactant excited state lifetime is less than 5 ps. They suggest in accordance with Douhal's [50] calculations that the driving force for the tautomerisation reaction is the flow of charges through the excitation that makes the pyridinic nitrogen attract the hydrogen of the other moiety while the pyrrolic N-H bond is weakened.

Guallar *et al.* [54] using the restricted Hartree-Fock method and the complete active space SCF (CAS SCF) method, studied the GS dimerisation reaction and

using the CI all single excitations with a spin-restricted Hartree-Fock reference GS (CIS) method and the CAS SCF method studied the ES. For the GS they found that the base pair is formed of two identical monomers using both levels of calculation. For the first electronic excited state they found, with both methods, asymmetric structures. The CI coefficient reveals that in the ES only one moiety of the molecule is excited. It is seen that only one of the monomers has changed its geometry. This change comes along with a significant redistribution of the electronic charge that is the force leading to the stepwise mechanism of the double proton transfer and that reinforces both hydrogen bonds. So, when the intermolecular hydrogen bonds in the GS are rather weak, two moieties can be distinguished and the excitation of only one monomer to produce stronger intermolecular hydrogen bonds in the ES is possible. The resulting ES structure is clearly asymmetric and can be said to be formed by the interaction between a GS monomer and an ES monomer.

Castleman and co-workers [55] used the femtosecond-resolved Coulomb explosion technique to study the phototautomerisation of $(7\text{-AI})_2$. They used a pump photon beam of 312 nm, which initiates the reaction, then a high power 624 nm delayed pulse to accomplish the intense field ionisation and ensue the Coulomb explosion process and finally the ions produced are analysed with a time of flight mass spectrometer. The fragmentation of the initial dimer resulted in two identical moieties of mass 118 amu and after the first proton transfer the fragmentation of the intermediate species resulted in two different species one with mass 117 amu and the other with mass 119. After the second proton transfer the tautomer species is formed and its fragmentation produced again two identical species of 118 amu. These authors plotted the ratio of mass 119 to mass 118 with respect to the pump-probe delay obtaining a series of experimental data that fit to an equation describing the rate of an unimolecular consecutive reaction. From this fitting they obtained the two proton transfer times: 660 fs for the first proton transfer and 5 ps for the second one. These results are in very good agreement with those obtained by Zewail's [49] group using a completely different technique.

In 1999 Guallar *et al.* [56] obtained the *ab initio* excited state potential energy

surface of the tautomerisation reaction. They determined the PES in reduced dimensionality using the empirical valence bond approach (EVB) and *ab initio* calculations at CIS level of theory (with 6-31G as basis set). They found not just one but two intermediates in the reaction, one with zwitterionic electronic structure, the other with a covalent one and with lower energy. They reported that after excitation only one moiety of the molecule is excited (in agreement with previous reports [50, 54]) which creates an instantaneous charge imbalance that is responsible for the stepwise proton transfer (the concerted route is much higher in energy). They also studied the dynamics of the system using the semiclassical initial value representation method (SC-IVR) which was compared with full quantum calculations. They found that the proton transfer usually occurs about 100 fs after photoexcitation of the system. More details about the PES will be given in another chapter of this thesis.

Recently, Moreno *et al.* [57] carried out an *ab initio* study of this surface using a larger basis set, 6-31G(d), which includes d polarisation functions on the heavy atoms. The B3LYP hybrid density functional in conjunction with the 6-31G(d) basis was used to calculate the ground electronic state geometries and energies. A CIS level of calculation with spin-restricted Hartree-Fock reference ground state was used to optimise the geometries and to calculate the energies of the excited state. They showed that after the initial UV irradiation all the excitation is localised in one moiety of the molecule. This rupture of the molecular symmetry is then the driving force of the stepwise double proton transfer reaction. They also confirmed the presence of a neutral intermediate that has quite a different geometry from that of the zwitterionic one. This neutral intermediate belongs to an excited state whose potential energy surface is very high in energy in the BP and T region but that it is very stable in the intermediate one, for more details see Figures 3.3 and 3.9. So, at some point along the proton transfer coordinate, this potential energy surface crosses the surface corresponding to the first singlet excited state (which includes the base pair, zwitterionic and tautomer stationary points). They suggested that this crossing point is not far away from the zone where the intermediate is found. These calculations corroborate the previous work carried out by Guallar *et al.* [56].

In a series of papers Kasha and co-workers [53], [58], [59] show a completely different view of the $(7\text{-AI})_2$ tautomerisation reaction dynamics. They suggest that the reaction occurs in a concerted way (both protons are transferred at the same time). They considered the two ES states found by Fuke and Kaya [45] to be coupled and therefore the monomers are excited simultaneously in the dimer. The wavefunction must be then centro-symmetric and it should also be the driving force. This symmetric driving force will then provoke a concerted transfer. They think that this force is due to the electronic rearrangement that occurs on excitation of the GS to the ES. There is then a change in the dipole moment and the electronic density shifts from the pyrrolo ring to the pyridine one; this increases the acidity of the pyrrolo-N and the basicity of the pyridino-N. This group calculated the potential energy curve of the system using Hybrid Density Functional theory (HDF) for the ground state and CIS-6-31G**/B3LYP/6-31G** with S_0 geometry optimisation for the excited state. They found no intermediate minimum in the curve which has a barrier of 7.8-8.5 kcal.mol^{-1}. These authors also calculated the potential energy curve of the 119 amu cation (which was thought to be the intermediate of the reaction found by Castleman's and Zewail's groups). Their results suggest that if this were the intermediate it will trap the reaction preventing the second proton transfer. So, they considered that this cation does not appear naturally in the tautomerisation reaction but that its presence is due to the Coulomb explosion and photo-ionisation techniques used by Castleman's and Zewail's groups.

Their arguments were refuted by Castleman and co-workers [60] and Douhal *et al.* [61, 62] both from experimental and theoretical points of view. First of all, they pointed out that the intermediate detected by their groups is neutral and that it is only ionized for detection purposes. This is confirmed by the fact that the cation's abundance depends on the power of the probe pulse used in the Coulomb explosion technique. They underlined that every time the reaction is analysed a new set of molecules is used in the experiment. Also, if the 119 amu cation was produced after ionisation it should also be seen by Zewail's group as they also use a photoionisation technique in their experiments but it is only seen in Castleman's

experiments. Secondly, all the experiments done by Kasha's group with the cation are done under high solvation while Castleman's and Zewail's experiments are carried out in the gas phase. Thirdly and from a theoretical point of view, the reason Kasha's group do not find the reaction intermediate is that their calculations for the ES are done keeping the same symmetry for the dimer as that of the GS (they consider the reaction to follow the same path in the ES as in the GS). Following this reasoning, if the intermediate is not present in the GS it can not be found in the ES. Finally, Kasha's group still consider the wave function to be centrosymmetric while some calculations [56] have probed it to be localised in one part of the dimer in the ES.

In the last few years several more studies on the $(7\text{-AI})_2$ tautomerisation reaction in solution have been reported. Takeuchi and Tahara [63, 64] carried out a femtosecond fluorescence up-conversion study on the ESDPTR dynamics of the $(7\text{-AI})_2$ in a non-polar solvent (hexane). They observed a long lived fluorescence due to the tautomer with a finite rise time and a decay time of 3.2 ns. At short wavelengths they detected another band with two components: the fast one with a decay time of 1.1 ps and the ultrafast one with a decay time of 0.2 ps. They assigned the fast component to the fluorescence from the dimeric form in its ES (this value changes to 1.6 ps by isotopic substitution). So, 1.1 ps is the concerted proton transfer time at room temperature. The ultrafast component was assigned to a fluorescence from the dimeric form in an excited state that is initially populated but then decays to the normal ES state (this value is independent of isotopic substitution). They believe that the stepwise process is impossible because if the zwitterionic intermediate exists it should emit some fluorescence in the region studied (it is not seen in the experiments) and also if the ultrafast component were the first proton transfer time it should be altered by deuteration and it is not.

Zewail's group [65, 66] has also studied the $(7\text{-AI})_2$ tautomerisation reaction in solution (hexadecane or 3-methylpentane) using the fluorescence up-conversion technique. They concluded that the first proton transfer takes place in 130 fs for the undeuterated dimer (280 fs for the deuterated one) and that the second proton transfer occurs in 1 ps for the undeuterated species (5 ps for the deuterated one). These

results are very similar to those reported in the gas phase and were obtained without excess of vibrational energy (0,0 transition). They believed that their results are different to those described by Takeuchi and Tahara [63, 64] because those experiments have been performed with an excitation energy much higher than the one corresponding to the 0,0 transition. They suggested that the 200 fs assigned by Takeuchi and Tahara to relaxation between two different ES are in reality used in intramolecular vibrational-energy redistribution (IVR) and in vibrational relaxation (VR). They consider that Takeuchi and Tahara may not have enough isotopic substitution in their experiments with the deuterated species and to draw reliable conclusions from them (this could be due to the exchange of D atoms by H atoms present in the water of the environment).

Kasha's group [67] has also examined this reaction. They reported that for the undeuterated species at 227 K and in 10^{-4}M solution in 2-methylbutane they only observed the fluorescence due to the tautomeric form of the dimer while for the monodeuterated species under the same conditions they observed only the fluorescence due to the dimeric form.

Finally, Moreno *et al.* [57] using the isodensity surface-polarised continuum model (IPCM), studied the effect of solvent polarity on this tautomerisation reaction. They concluded that as this polarity increases both intermediates (zwitterionic and neutral) are stabilised, mostly the neutral one. In general, they suggested a similar energy profile for the reaction in solution to the one it has in the gas phase.

1.3 This Research

In this thesis a quantum tunnelling in a dissipative environment theory is applied to the study of excited-state double proton transfer reactions in biomolecules. Attention is focused on the double proton transfer reaction in the 7-azaindole dimer. The times of these proton transfer reactions are calculated and compared with the experimental values obtained by Zewail and co-workers [49] and Castleman and co-workers [55] using different femtospectroscopic techniques. Various initial vibrational energies and

different isotopic isomers are used to observe the influence of these two variables on the final proton transfer times. The calculations are also carried out using different potential energy surfaces. The results obtained in this work throw some light on the reaction mechanism which has been subject of discussion over the last few years.

The remaining part of this thesis is divided into four chapters. In the first one the theory behind our calculations is presented with details about the quantum tunnelling in a dissipative environment method. The second one shows the different potential energy surfaces used in the calculations. The third one shows the results of our calculations and the final one gathers a discussion of the results and our conclusions.

Chapter 2

Method

2.1 Hydrogen Bond and Proton Transfer Reactions

There is a wide literature about the hydrogen bond and proton transfer reactions since both play a central role in many different chemical and biological phenomena. In this Chapter we will focus our attention on the different methods developed to study proton transfer reactions when the potential describing the system is asymmetric.

The hydrogen bond and proton transfer reactions have attracted a lot of attention since Watson and Crick [34] formulated their stereo model for DNA. They suggested that DNA consists of a double helix, where the strands are sugar-phosphate chains joined by pairs of nucleotide bases held together by hydrogen bonds. They also indicated that proton transfer reactions along the hydrogen bonds joining these DNA chains could disturb the genetic code causing errors (mutagenesis) in DNA replication.

While studying these mutations Löwdin [68, 69] carried out some of the first detailed theoretical studies on the hydrogen bond. In these studies, he found that a hydrogen bond is essentially a proton shared between two electron pairs associated with different atoms. He considered that the total effect could be represented by a double well potential, the two wells being either symmetric or asymmetric. When the proton moves, in a classical approach, it can only jump from one well to the other if its energy is higher than the barrier height. But Löwdin, using quantum theory, found that the proton (considered as a wavepacket) may penetrate into classically

forbidden regions. This phenomenon is known as the tunnel effect and it is one of the characteristic features of the hydrogen bond. He also determined that if the double well is symmetric, the probability of finding the proton is the same in the two wells. However, for an asymmetric potential, a large part of the wavepacket may remain in the deeper well, whereas only a smaller part of the packet will actually oscillate between the two positions. The tunnelling time (the time that the proton takes to get from one well to another) will then depend on the height and the form of the barrier. The barrier's shape depends not only on the atoms involved in the hydrogen bond but also on the neighbouring ones.

Bell [70] in his book about the tunnel effect confirmed the differences between the tunnel effect in a symmetric double well potential and the same effect in an asymmetric one. He determined that these differences can be attributed to the fact that the introduction of asymmetry destroys the exact state of resonance between the two wells. The wave functions cannot be classed as symmetric or antisymmetric (as in the symmetrical case) and the probability of finding the proton is no longer the same in the two wells. In the asymmetric case slight departures from symmetry always produce a large decrease in the tunnelling frequency.

Nieto and co-workers [71] studied the propagation of a given wavepacket in a double well potential. They considered that in any symmetric double well potential the ground and first excited states are almost degenerate. The ground vibrational state has a symmetric wave function and the first vibrationally excited state has an antisymmetric one. The time taken for a wavepacket, initially located on one side, to get to the other side is, in this case, given by:

$$\tau = \frac{\pi\hbar}{(E_1 - E_0)} \tag{2.1}$$

where E_1 and E_0 are, respectively, the energies of the first and ground vibrationally excited states. The wavepacket tunnels back and forth in multiples of this oscillation time. Nieto and co-workers showed that these considerations cannot be applied if the potential describing the system is asymmetric. They concluded that the probability of quantum mechanical tunnelling from one well to another is a very sensitive function

of the shape of the potential. They showed that while in the symmetric case the particle tunnels through the barrier coherently (the wavepacket retains its shape), in the asymmetric one the probability of finding the particle in the second well is very small and the wavepacket will not retain its shape after it tunnels (the tunnelling is not coherent). In this case to ensure decay from a relative minimum there must be either dissipation or coupling to other modes.

Taking this idea further, Razavy [72] studied two different cases for an asymmetric double well potential. In both of them the tunnelling of the wavepacket from a minimum in the presence of dissipative forces was studied. The first case considered these forces acting everywhere. The second one considered them acting in part of the space. For the first case it was found that the wavepacket always decays into the deeper well and remains there. In the second case, the final position of the wavepacket was found to be dependent on the shape of the potential, the strength of damping and the initial location of the wavepacket.

For proton transfer reactions, along with the mechanism involving quantum tunnelling dynamics, there is another competing mechanism. This one moves the system along the heteroatomic distance until it reaches a region where the barrier vanishes. Both channels might together bring the system from the reactant to the product well. Douhal [73] and Limbach and Manz [74] confirmed that a way to discriminate between these two different dynamics is to study the H/D isotope effect on the rate of the transfer.

Syage [35] adopted a method developed by Bernstein and co-workers [75] for calculating tunnelling probabilities. He considered that two degrees of freedom are needed to describe any proton transfer reaction. One coordinate is the distance between the hydrogen atom and one of the heteroatoms involved in the hydrogen bond and the other is the distance between the two heteroatoms surrounding the hydrogen atom. However, Zewail and co-workers [76] suggested that a minimum of four different coordinates are needed. These include the two previously considered by Syage plus the solvent coordinate, which takes into account the fluctuations in the relative energy of reactant and product caused by solvent modes and, finally, a group of coordinates cor-

responding to product acceptor modes that reduce the energy gap between reactant and product.

Another aspect to consider is the fact that most of these proton transfer reactions occur in an electronically excited state. Weller [77] was the first to study these excited state proton transfer reactions. He laid the foundation of their mechanism, known as excited-state intramolecular proton transfer or ESIPT, which is still used to explain the behaviour of some compounds that undergo proton transfer reactions. Catalán *et al.* [78] concluded that the signature of an excited state proton transfer reaction is the emission of strongly Stokes shifted fluorescence following absorption of UV photons. This spectral feature is the result of both the exothermal behaviour of the excited singlet state potential curve that governs the process while the proton transfer develops, and the endothermal behaviour of the potential curve for the process in the ground state. These combined effects bring the two electronic states involved in the emission dramatically nearer. While the curve for the electronically excited state is that which dictates whether the proton transfer is to take place, the role played by the curve for the ground state is spectroscopically as relevant because it contributes to the Stokes shift and is responsible for the spectral envelope with no vibronic structure that is observed in the fluorescence of compounds undergoing an excited state proton transfer process. The nature of the state that governs the proton transfer is quite important since an n,π^* state is believed to facilitate hydrogen abstraction whereas a π,π^* state is thought to facilitate the proton transfer.

Limbach and Manz [74] considered that the difficulties to simulate a proton transfer reaction are increased when it takes place in an excited state. This is due to the presence of additional and competing processes such as internal conversion, intersystem crossing, and the difficulty to evaluate *ab initio* potential energy surfaces and wavepacket dynamics with adequate accuracy. However, from an experimental point of view the fact that the proton transfer reaction takes place in an excited state provides a simplification as the propagation of selected states can be easily followed in the gas phase or molecular beams.

A final point to take into account is that in many cases more than one proton

is transferred in the same system. These multiproton transfer reactions have been theoretically and experimentally studied by many different groups i.e. [79]-[82]. Each of these groups focused their attention on a different aspect of these reactions. For example, some of them studied if the multiproton transfer reaction takes place synchronously or asynchronously and if the reaction is an intramolecular one (both proton donor group and proton acceptor group are in the same molecule) or an intermolecular one (the proton exchange takes place between one molecule and the solvent). They determined that in the first case (intramolecular reaction) the proton transfer mechanism is determined purely by intramolecular factors, characteristic of a given chromophore, while for the intermolecular case the solvent role is key in determining the process of the proton transfer reaction.

Considering all this information some conclusions can be drawn. The tunnel effect in an asymmetric double well potential presents clear differences with the same process in a symmetric potential. We saw in Figure 1.3, that the potential corresponding to the 7-azaindole dimer phototautomerisation reaction is highly asymmetric. Therefore, we need to find a method suitable to simulate proton transfer reactions with an asymmetric potential. The proton transfer times obtained in this simulation will be compared with those from Zewail's and Castleman's experiments [49, 55]. So, following Zewail's work [76], and taking into account that the experiments were carried out in the gas phase, it can be said that three coordinates will be needed to describe the double proton transfer reaction of 7-azaindole dimer. One coordinate will be the distance between one of the N atoms and the H atom, another one the distance between the two N atoms involved in the hydrogen bond and the third one will actually be a group of coordinates corresponding to the product acceptor modes. To a first approximation, as the proton transfer reaction is a very fast process (femtosecond time-scale for the first proton transfer and picosecond one for the second proton transfer), the proton transfer can be described as being localised on the N—H$\cdots$N bond and hence only the first two coordinates will be needed to simulate the process.

2.2 Simulating a Proton Transfer Reaction

In the last few years many theoretical methods have been developed to simulate proton transfer reactions and to obtain the proton transfer times. For example, in 1969 Brickmann and Zimmermann [83] examined these reactions. They considered a double well potential for the reaction. These authors found that the probability of finding the proton has a relative maximum in each well. The question was then how long the proton lingers in one well before it tunnels into the other. This time was called the lingering time and it can be determined as a function of several characteristic potential parameters: the height of the potential barrier, the separation between the wells and the difference between the minima of the potential wells. It was defined as a function of the probability of finding the proton in the second well at time t and the mean probability of finding the proton in the second well at any time. This method can be applied to any double well potential but, it only seems to work well with symmetric or weakly antisymmetric potential functions.

Brickmann [84] carried out another study in proton transfer in a double well potential. He made a detailed study of this phenomenon considering only a one dimensional case in which the influence of the other degrees of freedom is neglected. As he considered the multidimensional case (taking into account the coupling between the proton motion and the thermal vibrations along the other coordinates) he used an additional fluctuating potential for the vibrations which were not considered explicitly. This method is also only easy to apply when the potential is symmetric or weakly antisymmetric so is not suitable for our system.

In 1980 Babamov and Marcus [85] devised a method for treating the transfer of a light particle such as a hydrogen atom or a proton between two heavy particles. They studied collinear reactions such as AH + B $\rightarrow$ A + HB. They mainly worked on the case of A=B. In this situation the reaction has a symmetric double well potential. They neglected the nonadiabatic effects and used polar coordinates to treat the dynamics of the system.

In the same year Miller *et al.* [86] developed the reaction path Hamiltonian method

to study the dynamics of polyatomic molecules. In this method the kinetic part of the Hamiltonian is exact and the potential energy is approximated as a harmonic valley about the reaction path. The reaction path is the steepest descent path (in mass-weighted Cartesian coordinates) connecting saddle points and minima. In a later work Carrington and Miller [87] pointed out that the reaction path method was not suitable to study proton transfer reactions. They showed that in these transfer processes the reaction path has, in some regions, a large curvature. This curvature is due to the coupling between the reaction coordinate motion and other degrees of freedom; large curvature thus means large coupling. So, they developed a new method, known as the reaction surface Hamiltonian, for treating these more complex processes. The key idea is to introduce two degrees of freedom that can undergo arbitrarily large amplitude motion. For atom transfer reactions these coordinates would be the bond lengths of the bond being broken and the bond being formed. The basic physical assumption is that once we have described the two important degrees of freedom correctly for arbitrarily large displacements it should be a much better approximation to characterise the remaining degrees of freedom as small amplitude (i.e. harmonic) motions. They used this method to study the intramolecular hydrogen atom transfer in malonaldehyde [88].

In 1988 Sato and Iwata [89] proposed a model Hamiltonian to analyse the observed promotion of the proton transfer reaction by the intermolecular stretching. They used the two dimensional finite element method to solve the Schrödinger equation. They showed that when the intermolecular stretching mode is excited the proton transfers from one site to the other over the ridge, taking a detour path. However, when the intermolecular mode is in the lowest state, the proton transfers under the barrier with the tunnelling mechanism. They used a symmetric double well potential for their calculations.

There is a group of methods, known as system-bath methods, based on the fact that in proton transfer reactions some degrees of freedom are strongly coupled to the proton (the system) and only weakly coupled to the rest of the degrees of freedom of the molecule (the bath). In these reactions there are several degrees of freedom

which are strongly anharmonic (the system) while the rest of the degrees of freedom (the bath) are generally harmonic.

Following this approach, Miller and Schwartz [90] carried out a system-bath decomposition of the reaction path Hamiltonian method [86]. They considered that the reaction coordinate and the few strongly coupled modes are the system whose dynamics should be treated accurately, and the remaining (many) weakly coupled modes constitute the bath that will be incorporated as a perturbation. So, these authors treated the system-bath coupling by straightforward quantum mechanical perturbation theory which will only be sufficient if the coupling between the system and the bath is weak.

Using the same idea, Caldeira and Leggett [91] studied the effect of dissipation on quantum tunnelling. They considered a system, characterised by some coordinate Q, which is subject to a potential $V_{sys}(Q)$ which has a single metastable minimum. To study the effect of dissipation, they started with an isolated system and then they introduced terms which couple the system to its environment, producing the effect of dissipation. So, they considered dissipation as the transfer of energy from the single degree of freedom of the system to the set of degrees of freedom that characterise the environment. It is assumed that the energy, once transferred, effectively disappears into the environment and is not recovered within any time of physical interest.

Hron and Razavy [92] also studied this phenomenon of quantum tunnelling in a dissipative environment. They formulated the wave equation of the problem by considering a many-body system in which the central particle is subject to an arbitrary force law, and at the same time is coupled to a bath of noninteracting harmonic oscillators. In this method they wrote a many-body Schrödinger equation for the whole system, and then eliminated the wave functions of all the oscillators. This results in a many-channel Schrödinger equation for the motion of the central particle.

Also following this system-bath approach, Horsewill and co-workers [93] studied, in 1998, the proton transfer reaction in the hydrogen bonds of carboxylic acid dimers in the solid state. They found that the proton displacement is always accompanied by changes in the equilibrium positions of the other atoms in the molecule so the

potential energy surface of the reaction is multidimensional. To a first approximation the potential energy along the trajectory of the particle through the multidimensional potential energy surface may be described as a double minimum potential and consequently the dynamics of the proton may be modelled as that of a particle in a double well potential which is coupled to a bath of phonons.

In the same year, Manz and co-workers [94] modelled the hydrogen transfer in malonaldehyde using this system-bath idea. Some coordinates were chosen as the system, the remaining degrees of freedom were then treated as harmonic oscillators coupled linearly to the H atom coordinate by means of a coupling function. In this study they neglected some of the intramolecular bath modes as well as possible solvent modes.

Also in 1998 Anderson *et al.* [95] proposed a simple method known as locally propagating gaussians to treat the bath modes in a system-bath approach. In this method they described the bath by a set of Gaussians and let the Gaussian position, momentum and width parameters be dependent on its site in the system. Each site couples to others by the overlap of their Gaussians. In this approach very little computational resources are necessary for the bath part, so that very large systems can be handled. Inter-bath correlations are also handled (within the Gaussian approximation) by letting the Gaussian tensor width parameters be site and time dependent.

There are also a group of methods known as mixed quantum-classical methods. These methods describe the system with full quantum mechanics while the many degrees of freedom of the bath are handled more approximately using classical mechanics. The most common of these methods follow the Ehrenfest model [96] where one simultaneously integrates the time-dependent Schrödinger equation for the system and the classical equations of motion for the bath. Another approach is the time-dependent self-consistent field method or TDSCF [97] were the bath wavefunction is taken to be an infinitely narrow Gaussian wavepacket above its classical trajectory; this method only works well if the system is coupled weakly to many bath modes. Other mixed quantum-classical methods are surface-hopping models [98, 99] in which the quantum motion of the system is assumed to be adiabatic except for localised

transitions from one adiabatic quantum state to another; this method works very well when the system consists of the electronic degrees of freedom of a molecular system. The most accurate treatment of the system-bath dynamics is possible when the bath is a set of harmonic modes that are linearly coupled to the system, so the bath can be integrated out analytically using the Feynman path integral method [100].

In 1997 Sun and Miller [101] developed a semiclassical-classical method to study the dynamics of complex molecular systems. In this method they use a semiclassical approach to study the dynamics of the system (they used the initial value representation method [102]) and a classical approach to study the bath. The advantage of this semiclassical-classical approach is that the dynamics of both the system and bath are treated by classical mechanics giving a more consistent treatment than that given by the quantum-classical methods. Miller and co-workers [56] used this method to study the dynamics of the double proton transfer reaction in the $(7\text{-AI})_2$.

After considering all of these methods the method developed by Hron and Razavy [92] was thought to be the most suitable one for the study of the 7-azaindole dimer phototautomerisation reaction. It allowed us to use any kind of potential for the central particle (in this case the hydrogen atom) and to introduce as many coordinates as needed to simulate the double proton transfer reaction. This method, known as the quantum tunnelling in a dissipative environment method, will be described in detail in the next Section.

2.3 Quantum Tunnelling in a Dissipative Environment

The 7-azaindole dimer phototautomerisation reaction can be described as a problem of quantum tunnelling in a dissipative environment [92] by considering a many-body system in which the central particle is subject to a force and at the same time is coupled to a bath of noninteracting harmonic oscillators. In the 7-azaindole dimer case the central particle will be the H atom which jumps from one N atom to another.

In this way the Hamiltonian of the problem can be written as:

$$H(Q,q) = H_{sys}(Q) + H_{bath}(q) + V_{coup}(Q,q) \tag{2.2}$$

where $H_{sys}(Q)$ is the Hamiltonian corresponding to the central particle or to the anharmonic degrees of freedom of the molecule which will be henceforth called "the system". $H_{bath}(q)$ is the bath's Hamiltonian associated to the harmonic degrees of freedom of the molecule (or weakly coupled degrees of freedom). $V_{coup}(Q,q)$ is the coupling potential between the system and the bath and Q and q are respectively the coordinates that describe the system and the bath, each of them being one or more variables.

The Schrödinger equations for the system and bath will be given by:

$$H_{sys}(Q)\phi_\alpha(Q) = E_\alpha\phi_\alpha(Q) \tag{2.3}$$

$$H_{bath}(q)\psi_m(q) = E_m\psi_m(q) \tag{2.4}$$

where the Hamiltonians, in atomic units ($\hbar = 1$), can be expressed as:

$$H_{sys}(Q) = \frac{-1}{2\mu_Q}\frac{\partial^2}{\partial Q^2} + V_{sys}(Q) \tag{2.5}$$

$$H_{bath}(q) = \frac{-1}{2\mu_q}\frac{\partial^2}{\partial q^2} + V_{bath}(q) \tag{2.6}$$

where μ_Q and μ_q, are the reduced masses associated with the system or with the bath, respectively. $V_{sys}(Q)$ and $V_{bath}(q)$ are the corresponding potential energy surfaces which will be considered, in detail, in the next Chapter.

$\phi_\alpha(Q)$ and $\psi_m(q)$ can be expanded as:

$$\phi_\alpha(Q) = \sum_i A_{\alpha,i} v_i(Q) \tag{2.7}$$

$$\psi_m(q) = \sum_j A_{m,j} v_j(q) \tag{2.8}$$

where v_i and v_j are DVR functions. The discrete variable representation (DVR) method [103]-[108] will be used to solve the Equations 2.3 and 2.4. It will allow us to obtain $A_{\alpha,i}$, $A_{m,j}$, E_α and E_m and therefore, $\phi_\alpha(Q)$ and $\psi_m(q)$ will also be determined. A detailed description of this method will be given in the next Subsection.

On the other hand, the time-independent Schrödinger equation for the whole problem can be written as:

$$H(Q,q)\Psi_E(Q,q) = E_E\Psi_E(Q,q) \tag{2.9}$$

where H(Q,q) is the Hamiltonian described in Equation 2.2 and $\Psi_E(Q,q)$ will be given by:

$$\Psi_E(Q,q) = \sum_{m,\alpha} A_{E,m\alpha}\phi_\alpha(Q)\psi_m(q). \tag{2.10}$$

The coefficients $A_{E,m\alpha}$ and the energy values E_E, in Equation 2.9, can be obtained by substituting H(Q,q) and $\Psi_E(Q,q)$ by their values in Equations 2.2 and 2.10 and then by diagonalising the following matrix

$$E = \langle\Psi_{E'}|H|\Psi_E\rangle = (E_\alpha + E_m)\delta_{\alpha'\alpha}\delta_{m'm} + \langle\psi_{m'}(q)\,\phi_{\alpha'}(Q)\,|\,V_{coup}(Q,q)\,|\,\psi_m(q)\,\phi_\alpha(Q)\rangle. \tag{2.11}$$

In order to solve this equation we need to know the form of the coupling potential $V_{coup}(Q,q)$. There are different types of coupling but, to a first approximation, the coupling between a central particle and a bath of harmonic oscillators can be expressed by:

$$V_{coup}(Q, q) = \varepsilon Qq \tag{2.12}$$

being

$$\varepsilon = \frac{\alpha\omega\Omega}{(\alpha^2 + \omega^2)} \tag{2.13}$$

where ω is the frequency of the oscillator, Ω is the strength of the coupling to the heat bath and α is a parameter. The expression in Equation 2.12 will be used in most of our calculations to obtain the coupling potential $V_{coup}(Q,q)$, see Section 3.1 and Subsection 3.2.1.

Once E_E and $A_{E,m\alpha}$ have been obtained we have the stationary states corresponding to Equation 2.9. In order to study the evolution in time of the system and the bath as a whole we use the time-dependent Schrödinger equation which can be written as:

$$i\left(\frac{\partial\Psi(Q, q, t)}{\partial t}\right) = H(Q, q, t)\Psi(Q, q, t) \tag{2.14}$$

and the solution to this equation will be given by:

$$\Psi(Q, q, t) = \sum_E B(E) \exp^{-iE_E t} \Psi_E(Q, q) \tag{2.15}$$

being E_E and Ψ_E, respectively, the eigenvalues and eigenfunctions previously obtained and B(E) some coefficients that we need to determine. To obtain these coefficients we can consider Equation 2.15 at time t equal to zero:

$$\Psi(Q, q, 0) = \Psi_0(Q, q) = \sum_E B(E)\Psi_E(Q, q) \tag{2.16}$$

where Ψ_0(Q,q) is the initial wavepacket.

So, if we know the characteristics and the form of the initial wavepacket we will be able to determine the B(E) coefficients. This information can be drawn from the experimental work carried out by Zewail's and Castleman's groups [49, 55]. They excited the 7-azaindole dimer from its ground electronic state to the first electronically excited state. Considering a vertical transition the molecule retains its shape. So, by solving the time-independent Schrödinger equation for the 7-azaindole dimer phototautomerisation reaction in its ground electronic state and obtaining its first eigenfunction the initial wavepacket Ψ_0(Q,q) can be determined.

The Hamiltonian for the system in its ground electronic state can be expressed as:

$$H^0_{sys}(Q^0)\,\phi^0_\alpha(Q^0) = E^0_\alpha\,\phi^0_\alpha(Q^0) \tag{2.17}$$

where ^{0} denotes the ground electronic state. The expression for the bath's Hamiltonian can be written as:

$$H^0_{bath}(q^0)\,\psi^0_m(q^0) = E^0_m\,\psi^0_m(q^0). \tag{2.18}$$

Solving these equations using the DVR method and following a similar process to that described previously for the excited state we can write that the first eigenfunction in the electronic ground state is:

$$\Psi^0_E(Q^0, q^0) = \sum_{m,\alpha} A^0_{E,m\alpha}\,\phi^0_\alpha(Q^0)\,\psi^0_m(q^0). \tag{2.19}$$

Ψ^0_E can be expressed as a function of ϕ_α(Q) and ψ_m(q) as:

$$\Psi^0_E(Q, q) = \sum_{m,\alpha} D_{m,\alpha}\,\phi_\alpha(Q)\,\psi_m(q) \tag{2.20}$$

by combining expressions 2.19 and 2.20 the $D_{m,\alpha}$ coefficients can be obtained. So, we have two different expressions for the initial wavepacket:

$$\Psi(Q,q,0) = \Psi_0(Q,q) = \sum_E B(E)\,\Psi_E(Q,q) \tag{2.21}$$

$$\Psi^0_E(Q,q) = \sum_{m,\alpha} D_{m,\alpha}\phi_\alpha(Q)\psi_m(q). \tag{2.22}$$

By associating these two expressions the B(E) coefficients are determined

$$B(E) = \sum_{m,\alpha} D_{m,\alpha}\, A^*_{m,\alpha}. \tag{2.23}$$

Now, we can study the time evolution of the initial wavepacket using Equation 2.15.

We can also define the probability of finding the particle in any region as:

$$P(t) = \int\int |\Psi(Q,q,t)|^2 dQdq \tag{2.24}$$

and substituting Equation 2.15 into Equation 2.24

$$P(t) = \sum_{E'}\sum_{E} B(E')\,B(E)^*\,\exp^{-i(E'-E)t}\,P(E',E) \tag{2.25}$$

where

$$P(E',E) = \int_{q_{mi}}^{q_M}\int_{Q_{mi}}^{Q_M} \Psi_{E'}(Q,q)\,\Psi_E(Q,q)\,dQ\,dq \tag{2.26}$$

Integrating Q and q between their minimum and maximum values P(t) must be equal to 1 for any given time t as the Ψ_E functions are normalised. The minimum values (q_{mi} and Q_{mi}) refer to the Q and q coordinates that describe the 7-azaindole dimer base pair geometry. The maximum ones (q_M and Q_M) to the Q and q coordinates that describe the 7-azaindole dimer tautomer geometry. If Q_M describes the 7-azaindole dimer at the first transition state geometry then when the first proton jumps from one N atom to another (going from the base pair structure to the intermediate one)

the probability becomes 0. The time at which this probability is 0 is the first transfer time τ_1. If Q_M describes the 7-azaindole dimer at the second transition state geometry then the time at which the probability becomes 0 is the second proton transfer time τ_2. So, in order to obtain these proton transfer times we need to solve the time-independent Schrödinger equation for the ground and first electronically excited states. Then the initial wavepacket expression has to be determined and finally the time evolution of the system-bath group needs to be studied.

2.3.1 DVR Method

In order to apply the quantum tunnelling in a dissipative environment method [92] different equations of the form:

$$H(x)\,\psi_c(x) = E_c\,\psi_c(x) \tag{2.27}$$

need to be solved. This can be done using the DVR method [103]-[108]. In these equations H(x) and $\psi_c(x)$ are given by:

$$H(x) = \frac{-1}{2\mu}\frac{\partial^2}{\partial x^2} + V(x) \tag{2.28}$$

$$\psi_c(x) = \sum_k A_{c,k}\,v_k(x). \tag{2.29}$$

A reference potential that comprises V(x) needs to be chosen. In our calculations this reference potential was taken to be a box. The eigenfunctions and the eigenvalues for this kind of potential are well known:

$$\phi_n(x) = \left(\frac{2}{(b-a)}\right)^{\frac{1}{2}} \sin\frac{\pi n(x-a)}{b-a} \tag{2.30}$$

$$E_n = \frac{n^2\pi^2}{2\mu(b-a)^2} \tag{2.31}$$

where a and b are the edges of the box, x is the coordinate and n is the quantum number. These functions $\phi_n(x)$ are used as basis functions to obtain DVR-functions following this expression:

$$v_k(x) = \sum_{n=1}^{N} B_{kn}\phi_n(x) \tag{2.32}$$

where N is the total number of functions used in the expansion. The coefficients B_{kn} are obtained by diagonalising the matrix

$$\langle \phi_m | x | \phi_n \rangle \tag{2.33}$$

where x is the coordinate operator. These DVR-functions $v_k(x)$ are orthogonal and they are localised around their corresponding eigenvalues which are given by:

$$x_k = a + \frac{k(b-a)}{N+1}. \tag{2.34}$$

These are called DVR-points and they form a grid of equally spaced points.

As the $v_k(x)$ functions are localised a new parameter V_{max} can be introduced. This parameter truncates the basis set according to $V(x_k) \leq V_{max}$. In this way the N value is determined. Also, due to the localised nature of the DVR-functions the potential energy matrix of the system is diagonal:

$$\langle v_k | V(x) | v_{k'} \rangle = V(x_k)\delta_{kk'}. \tag{2.35}$$

Once $v_k(x)$ and x_k are obtained the Hamiltonian matrix of the system can be calculated using:

$$H_{k'k} = \langle v_{k'} | H | v_k \rangle = \langle v_{k'} | T + V | v_k \rangle = \langle v_{k'} | T | v_k \rangle + \langle v_{k'} | V | v_k \rangle \tag{2.36}$$

where the first factor $\langle v_{k'} | T | v_k \rangle$ can be obtained by calculating

$$\int_a^b v_{k'}(x) \left(\frac{-1}{2\mu} \frac{\partial^2}{\partial x^2} \right) v_k(x)\, dx \tag{2.37}$$

and the second factor can be easily evaluated by using Equation 2.35. Thus, the Hamiltonian matrix can be calculated. By diagonalising it gives E_c and ψ_c

$$\psi_c(x) = \sum_k A_{c,k} v_k(x) = \sum_k \sum_n A_{c,k} B_{kn} \phi_n(x). \tag{2.38}$$

This DVR method will be used several times in the implementation of the quantum tunnelling in a dissipative environment method.

Chapter 3

Potential Energy Surfaces

As we saw in the introduction, Catalán and Pérez [44] were the first to theoretically study the 7-azaindole dimer phototautomerisation reaction. Using a semiempirical method they found that the double proton transfer reaction takes place in the first ($\pi \rightarrow \pi^*$) excited singlet state. They underlined the importance of the intermonomeric separation in this reaction.

Years later Douhal *et al.* [50] carried out some *ab initio* calculations on the ground and first excited singlet electronic states of the dimer. Their results will be used in Section 3.1 to obtain a two dimensional potential energy surface for the $(7\text{-AI})_2$ double proton transfer reaction in its ground and first excited state.

The first multidimensional potential energy surface for this reaction was developed in 1999 by Guallar *et al.* [56] using the empirical valence bond method [110]-[111]. This surface will be discussed in detail in Section 3.2.

In the previous Chapter we saw that in the quantum tunnelling in a dissipative environment approach the reaction's total potential energy surface, V(Q,q), can be expanded as a function of several contributions according to the following expression:

$$V(Q,q) = V_{sys}(Q) + V_{bath}(q) + V_{coup}(Q,q) \tag{3.1}$$

where $V_{sys}(Q)$ and $V_{bath}(q)$ are the potential energy surfaces associated respectively with the system and the bath, and $V_{coup}(Q,q)$ is the coupling potential between the system (Q) and the bath (q) coordinates. So, in this Chapter the potential energy

surfaces for the ground and first excited singlet electronic state of the 7-azaindole dimer will be obtained and then expressed as a function of $V_{sys}(Q)$, $V_{bath}(q)$ and $V_{coup}(Q,q)$.

3.1 Two Dimensional Potential Energy Surface

In order to obtain the potential energy surfaces for the ground and first excited states of the $(7\text{-AI})_2$ phototautomerisation reaction we made use of the *ab initio* points reported by Douhal *et al.* [50]. This group studied the ground electronic state using the restricted Hartree Fock method whereas the calculations for the excited state were made at the CI all-single-excitations with a spin restricted Hartree Fock reference ground state level of calculation. In all these calculations a 4-31G basis set was used. Douhal *et al.* localised the stationary points corresponding to the base pair, the transition states, the intermediate (if any) and the tautomer molecular configurations of the $(7\text{-AI})_2$ in its ground and first electronic excited states.

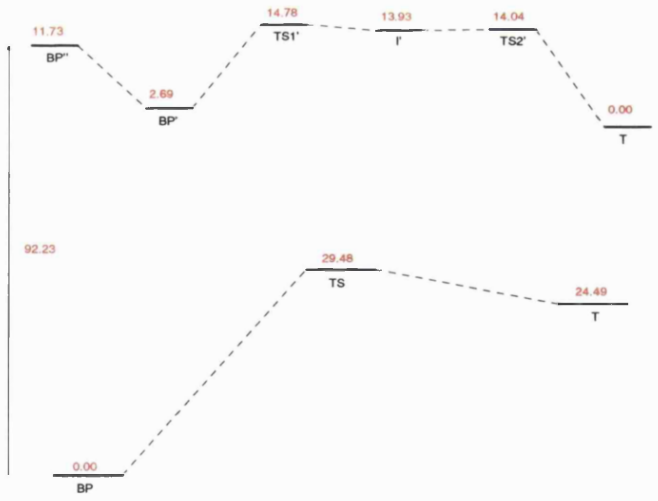

Figure 3.1: Relative potential energies (in kcal.mol^{-1}) for the double proton transfer process in the ground and first electronically singlet excited states of the $(7\text{-AI})_2$. The values correspond to Douhal's calculations [50].

Figure 3.1 shows the schematic energy profile of the $(7\text{-AI})_2$ double proton transfer reaction. The optimised geometries associated with these molecular configurations are shown in Figure 3.2.

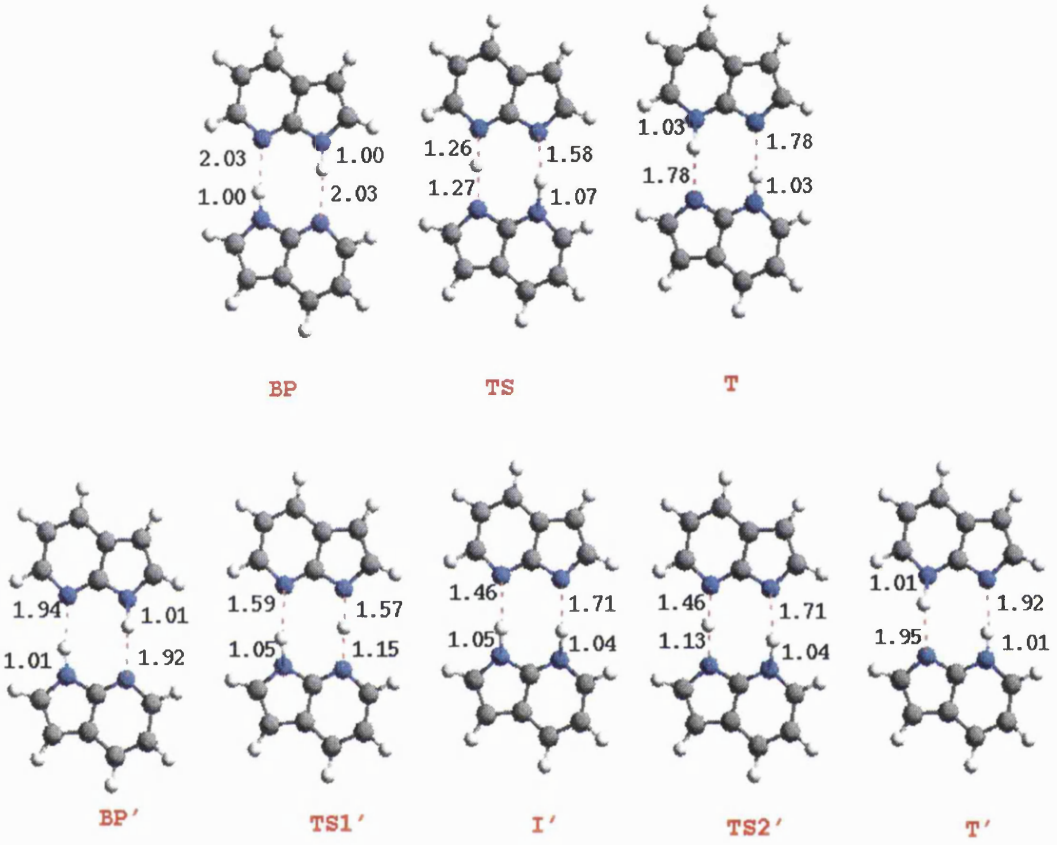

Figure 3.2: Geometries and internal hydrogen bond distances (Å) for the structures involved in the 7-azaindole dimer phototautomerisation reaction. BP is the base pair, TS the transition state, I the intermediate and T the tautomer. Any symbol carrying ' denotes the excited state.

These geometries are very similar to those obtained by other groups [48, 54, 57] using different levels of theory and different basis sets in the calculations. The *ab initio* points are slightly different from those calculated by Chou *et al.* [48] (only for the ground state) and by Moreno *et al.* [57] (for both the ground and the first excited state). For the ground state both Chou's and Moreno's groups reported smaller energy values but in all of these calculations a large endothermicity for the double proton transfer reaction in the ground state was found. For the excited state, Moreno's group

obtained higher energy values than those reported by Douhal's group but the general profile of the reaction is similar. The differences between these calculations can be seen in Figure 3.3.

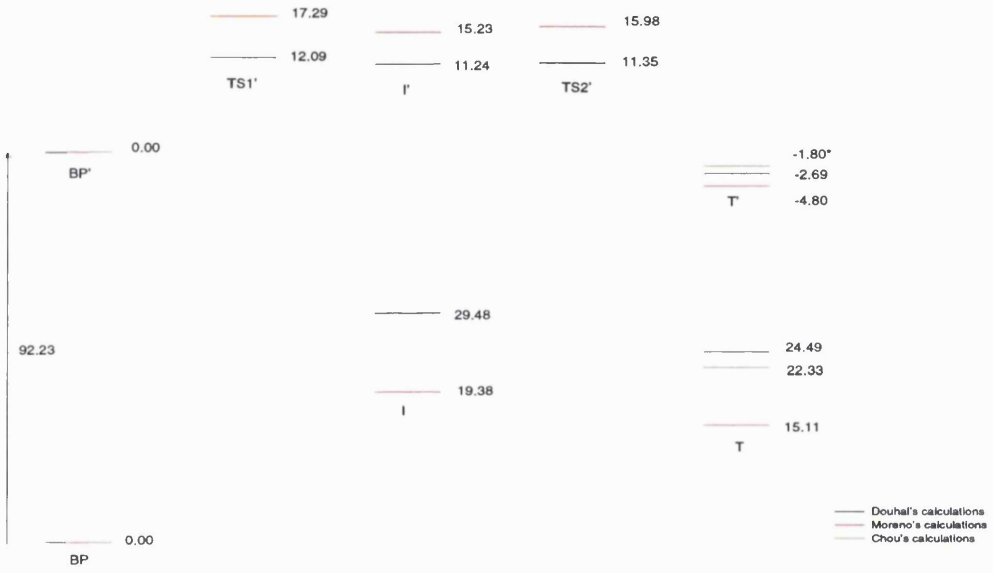

Figure 3.3: Comparison of the relative potential energies (in kcal.mol^{-1}) obtained by different groups for the double proton transfer process in the ground and first electronically singlet excited states of the (7-AI)$_2$. The * value was obtained by adding the 0-1 transition energy value obtained experimentally by Fuke and co-workers to the ground state T energy obtained by Chou and co-workers.

In Douhal's calculations the geometries were optimised keeping frozen all the interatomic distances but the hydrogen displacement r_1 and the intermonomeric separation r_2. This approach is considered to be a good one as both experimental and theoretical studies have underlined the importance of the role played by the N$\cdots$N symmetric stretch motion on the dynamics of the (7-AI)$_2$ phototautomerisation reaction [35, 44, 49, 50]. Also, as the proton transfer takes place very quickly (femtosecond to picosecond time scale) it can be said that the proton motion is direct so it does not involve the entire vibrational space of the pair. The proton motion is then described

as being localised in the N-H$\cdots$N coordinate and therefore, in this first approach, the N-H bond is considered to be the system and the N$\cdots$N bond the bath (the influence of the rest of the molecule is ignored). So, in the quantum tunnelling in a dissipative environment approach, we can say that r_1 describes the system movements, so $r_1 \equiv Q$, and r_2 constitutes the bath, so $r_2 \equiv q$. These coordinates are pictured in Figure 3.4.

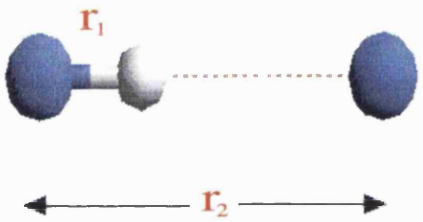

Figure 3.4: Coordinates for the $(7\text{-AI})_2$ double proton transfer where r_1 is the hydrogen displacement distance and r_2 the intermonomeric separation distance.

In order to apply the quantum tunnelling in a dissipative environment method we need to know the value of $V_{sys}(Q) \equiv V(r_1)$, $V_{bath}(q) \equiv V(r_2)$ and $V_{coup}(Q,q)$. As in these calculations the coupling potential was obtained using the following expression:

$$V_{coup}(Q, q) = \varepsilon Q q, \tag{3.2}$$

we need to determine the value of ε.

The *ab initio* data reported by Douhal and co-workers define the $V(Q,q) \equiv V(r_1,r_2)$ potential energy surface. The $V_{bath}(q) \equiv V(r_2)$ potential is given by:

$$V_{bath}(q) \equiv V(r_2) = \frac{1}{2}\,\mu_{NN}\,(\omega_{NN})^2(r_2 - r_2^0)^2 \tag{3.3}$$

where μ_{NN} is the reduced mass of the NN molecule (12763.0175 m_e), ω_{NN} is the vibrational frequency which was experimentally determinated by Fuke and Kaya [46]

to be 120 cm^{-1} and r_2^0 is the equilibrium distance. The r_2^0 and ε values will be determined in the next two Subsections and finally, the value of $V_{sys}(Q)$ will be obtained using Equation 3.1.

3.1.1 Ground State Potential Energy Surface

In order to obtain the value for the coupling term, ε, for this ground state potential energy surface we carried out some DFT calculations using the B3LYP functional and the 6-31G* basis set using Gaussian-98 [109]. The DFT points obtained in these calculations are shown in Appendix A. By comparing the value of these DFT points (V(Q,q)) at different $r_2 \equiv q$ distances (keeping the same $r_1 \equiv Q$ distance) and taking into account that the $V_{bath}(q)$ value is known at each of these points, we were able to estimate the ε value to be -0.000309 $E_h.a_0^{-2}$. The r_2^0 for calculating V(q) was considered to be -1.66 a_0 (the distance at which both monomers are closest to each other).

Once the value of $V_{bath}(q)$ and ε are known we can obtain $V_{sys}(Q)$ according to:

$$V_{sys}(Q) = V(Q,q) - V_{bath}(q) - \varepsilon Qq. \tag{3.4}$$

The final values for V(Q,q), $V_{sys}(Q)$, $V_{bath}(q)$ and εQq are given in Table 3.1.

	r_1^*	r_2^*	$V(r_1,r_2)^*$	$V(r_2)$	$\varepsilon r_1 r_2$	$V(r_1)$
BP	0.00	0.00	0.000000	0.005257	0.000000	-0.005257
TS	1.60	-1.66	0.047000	0.000000	0.000821	0.046179
T	2.95	-0.83	0.039000	0.001314	0.000756	0.036929

Table 3.1: Potential data and corresponding geometries, in atomic units, for the ground state potential energy surface. The data with * are obtained from Douhal's calculations but given in atomic units and taking the base pair (BP) geometry and the $V(r_1, r_2)^{BP}$ potential as reference.

These $V_{sys}(Q) \equiv V(r_1)$ data describe a double well potential and, as it was suggested by Löwdin [69], in this case the potential energy surface can be expressed as a sum of two Morse functions:

$$V_{sys}(Q) \equiv V(r_1) = D_{e_1}(\exp^{-2\alpha_1(r_1-r_{e_1})} - 2\exp^{(-\alpha_1(r_1-r_{e_1}))}) + D_{e_2}(\exp^{-2\alpha_2(r_{e_2}-r_1)} - 2\exp^{(-\alpha_2(r_{e_2}-r_1))}) + X \quad (3.5)$$

where D_{e_1}, D_{e_2}, α_1 (5.985 a_0^{-1}), α_2 (5.8 a_0^{-1}) are the Morse parameters. The α_1 and a_2 values, in parentheses, were obtained by fitting Equation 3.5 to the $V(r_1)$ data shown in Table 3.1 using a least squares method. D_{e_1} is the energy difference between the BP configuration and the TS configuration, D_{e_1}=0.051436 E_h. D_{e_2} is the energy difference between the TS configuration and the T configuration, D_{e_2}=0.009250 E_h. r_1 is the distance between the H and the N atoms, r_{e_1} is the same r_1 distance in the BP geometry (0.00 a_0) and r_{e_2} is the same value in the T geometry (2.95 a_0), X is the energy value at the TS configuration X=0.046179 E_h. The final ground state potential profile is shown in Figure 3.5.

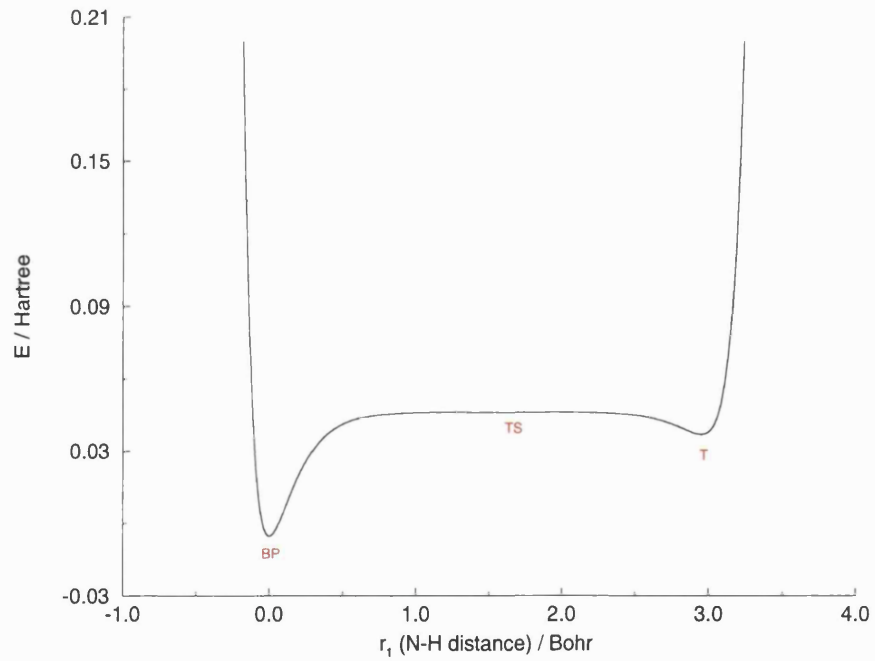

Figure 3.5: Potential energy curve, $V(r_1)$, for the $(7\text{-AI})_2$ double proton transfer reaction in its ground state.

3.1.2 First Excited State Potential Energy Surface

In this case the $V(r_2)$ potential can also be obtained using Equation 3.3, where r_2^0 is now equal to -1.51 a_0 (r_2^0 being the distance at which, in this excited state, the monomers are closer to each other). In this case, we cannot carry out *ab initio* calculations to determine the value of ε as these calculations would be too expensive, so we considered different possible values for the coupling term ranging from -0.0007 to 0.0000 $E_h.a_0^{-2}$ (in steps of 0.0002 $E_h.a_0^{-2}$, ε=0 means no coupling). $V_{sys}(Q)$ can then be determined using the expression in Equation 3.4, the data provided in Table 3.2 and the different values for the coupling term ε.

	r_1*	r_2*	$V(r_1,r_2)$ *	$V(r_2)$
BP'	0.04	-0.34	0.0043	0.00261100
TS_1'	1.17	-1.32	0.0235	0.00000689
I'	1.43	-1.51	0.0222	0.00000000
TS_2'	1.59	-1.36	0.0224	0.00004290
T'	3.53	-0.32	0.0000	0.00270150

Table 3.2: Potential data and corresponding geometries for the $(7\text{-AI})_2$ double proton transfer reaction in its first electronic excited state. The data carrying * are from Douhal's calculations but given in atomic units and taking BP's geometry and $V(r_1, r_2)^{T'}$ as reference.

The $V_{sys}(Q)$ potential obtained using these data is a three-well potential that can be fitted to a polynomial expression using a least squares method. So, the final expression for the $V_{sys}(Q)$ potential is given by:

$$V_{sys}(Q) = \sum_{n=0}^{19} a_n Q^n. \tag{3.6}$$

Different sets of a_n are obtained for $Q \leq 1.17\ a_0$, $1.17\ a_0 < Q \leq 1.59\ a_0$ and Q

> 1.59 a_0. These coefficients took different values for the different ε values. The resulting potential energy curves are named in Table 3.3 and plotted in Figure 3.6.

PES	1	2	3	4	5
ε	-0.0007	-0.0005	-0.0003	-0.0001	0.0000

Table 3.3: Labels of the potential energy surfaces obtained using the data in Table 3.2 and the different ε values.

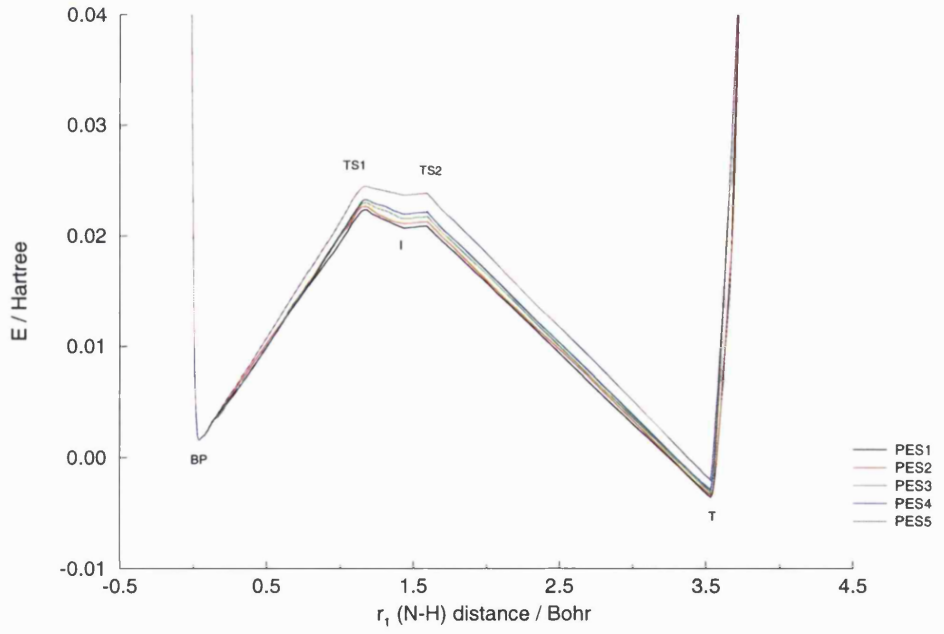

Figure 3.6: Potential energy curves, $V(r_1)$, for the $(7\text{-AI})_2$ double proton transfer reaction in its first excited state.

3.2 Multidimensional Potential Energy Surface

In 1999 Guallar *et al.* [56] obtained the first multidimensional excited state potential energy surface for the $(7\text{-AI})_2$ phototautomerisation reaction. Their calculations showed that the concerted proton transfer displacements involve higher energy configurations than the stepwise ones. They carried out some *ab initio* calculations at the CIS level of theory with a 6-31G basis set. These calculations showed that for most of the nuclear configurations the lowest excited state corresponds to an eigenstate (V_Z) in which a partial charge separation takes place during the first proton transfer. This V_Z eigenstate has associated a zwitterionic intermediate I_Z. For some other molecular configurations another eigenstate (V_C) becomes the lowest singlet excited state. In this case the intermediate structure I_C has a covalent character as the charge associated with the first proton transfer is neutralised by the intermonomer electron transfer excitation. The geometry of I_C is quite different from that of I_Z. The covalent intermediate has longer H-bond distances and the monomer units are more separated than in the zwitterionic intermediate. This is due to the fact that in the covalent intermediate there is no direct electric attraction between the two monomer units.

For most of the nuclear configurations V_C has a much higher energy than V_Z but in some areas the energy of V_C becomes smaller than that of V_Z. So V_Z and V_C must cross at some point along the proton transfer coordinate. As the energy of the V_C eigenstate rises quickly when we move away from the intermediate zone, the crossing zone is probably not far away from the zone where the intermediate is found. Taking these facts into account Guallar *et al.* developed the excited state potential energy surface of the system using the empirical valence bond method (EVB) [110]-[111] but contrary to this method the authors computed the two potential energy surfaces V_Z and V_C.

Following this approach the lowest potential energy surface, i.e. the Born-Oppenheimer PES $V_{B.O.}$, will be then given, in the intermediate region, by the root of this 2x2 secular determinant:

$$\begin{vmatrix} V_Z - V_{B.O.} & V_{ZC} \\ V_{ZC} & V_C - V_{B.O.} \end{vmatrix} \tag{3.7}$$

whereas in the rest of the space it will be given by:

$$V_{B.O.} = V_Z(r_1, r_2). \tag{3.8}$$

V_Z and V_C are the potential energy surfaces corresponding respectively to the zwitterionic and covalent eigenstates. V_{ZC} are the exchange or resonant matrix elements which match the energy gap at the crossings between the PESs. In Guallar *et al.* calculations these resonant elements were approximated as constants ($\sim$1.5 kcal.mol^{-1}).

The two potential energy surfaces V_Z and V_C were computed according to the reaction surface model [87, 88] as a function of two large amplitude motion [88] coordinates r_1, r_2 and one global coordinate R. r_1 describes the proton displacements, r_2 the intermonomer separation and R the average motion of the locally harmonic degrees of freedom of the molecule. The introduction of R allows the authors to reduce the dimensionality of the surface from N to 3 (N being the number of atoms of the molecule). So, V_Z and V_C are given by the following expression:

$$V^{\xi}(r_1, r_2, R) \sim V_0^{\xi}(r_1, r_2) + \frac{1}{2}\left(\omega_R^{\xi}(r_1, r_2)\right)^2 \left(R - R_0^{\xi}(r_1, r_2)\right)^2 \tag{3.9}$$

where $\xi \equiv$(Z,C), $V_0^{\xi}(r_1,r_2)$ are the CIS reaction surface potentials, and $\omega_R^{\xi}(r_1,r_2)$ are the average frequencies obtained in terms of a reference geometry (r_1^0,r_2^0). These coordinates refer to the r_1 and r_2 values that describe the dimer geometry at the base pair configuration. A scheme, with the complete process followed by Guallar *et al.* to obtain the potential energy surface is given in Figure 3.7.

The final expression for the Born-Oppenheimer potential energy surface of the system, in the intermediate area, will be given by:

$$V_{B.O.}(r_1, r_2, R) = \frac{1}{2}\left[V_0^Z + V_0^C + \frac{1}{2}(\omega_R^Z)^2(R - R_0^Z)^2 + \frac{1}{2}(\omega_R^C)^2(R - R_0^C)^2\right]$$
$$\pm \frac{1}{2}\left[\left(V_0^Z - V_0^C + \frac{1}{2}(\omega_R^Z)^2(R - R_0^Z)^2 - \frac{1}{2}(\omega_R^C)^2(R - R_0^C)^2\right)^2 + 4V_{ZC}^2\right]^{\frac{1}{2}}. \tag{3.10}$$

In this formula, and henceforth, $V_0^Z(r_1,r_2)$, $V_0^C(r_1,r_2)$, $\omega_0^Z(r_1,r_2)$, $\omega_0^C(r_1,r_2)$, $R_0^Z(r_1,r_2)$ and $R_0^C(r_1,r_2)$ have been referred to as V_0^Z, V_0^C, ω_0^Z, ω_0^C, R_0^Z and R_0^C respectively.

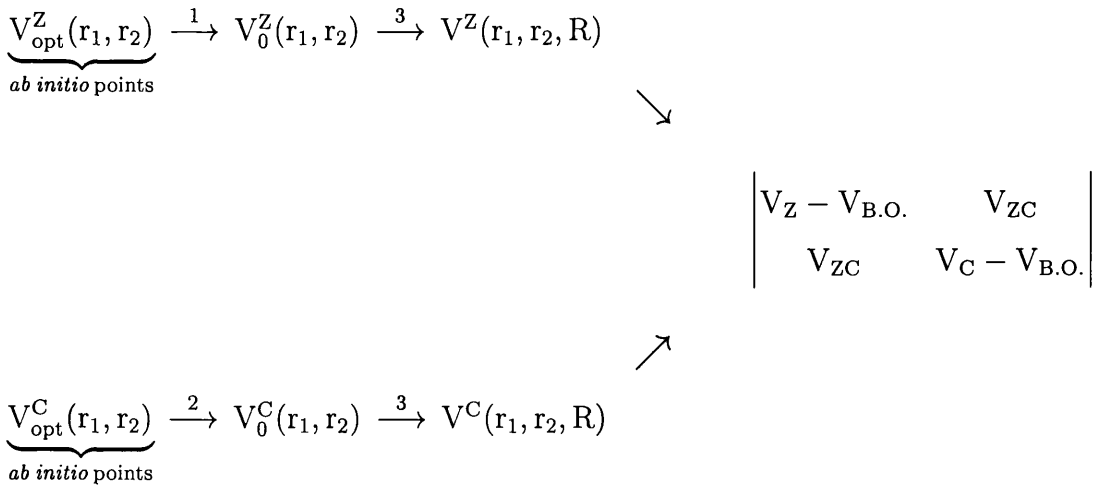

Figure 3.7: Scheme followed by Guallar *et al.* to obtain a multidimensional potential energy surface for the (7-AI)$_2$ phototautomerisation reaction. 1. V_0^Z is obtained from the *ab initio* data using the Lagrange form of the interpolation polynomial. 2. V_0^C is obtained from the *ab initio* data using a quadratic approximation. 3. V^Z and V^C are obtained respectively from V_0^Z and V_0^C using the reaction surface model.

A plot of the V_0^Z and V_0^C surfaces is shown in Figure 3.8. Their corresponding minimum energy paths (MEP) are shown in Figure 3.9. It must be noted that in these calculations the r_1 and r_2 distances that describe the BP configuration were taken as a reference so $r_1^{BP}=r_1^0=0$ a_0 and $r_2^{BP}=r_2^0=0$ a_0.

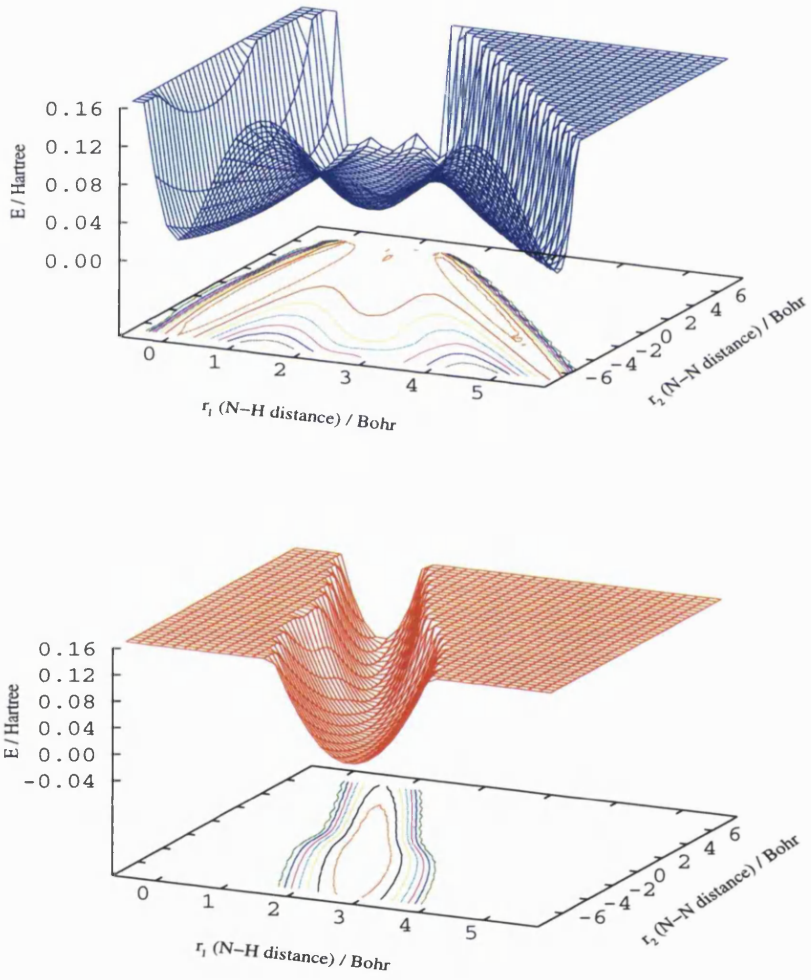

Figure 3.8: Potential energy curves, $V_0^Z(r_1,r_2)$ in blue and $V_0^C(r_1,r_2)$ in red, obtained with the data provided by Guallar *et al.*

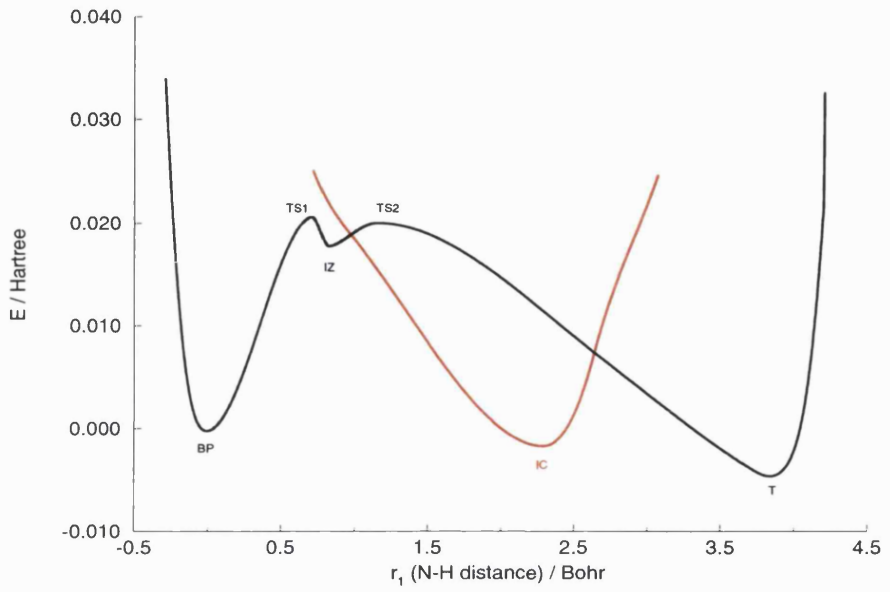

Figure 3.9: Minimum energy paths corresponding to the $V_0^Z(r_1,r_2)$ and $V_0^C(r_1,r_2)$ surfaces shown in Figure 3.8. The zwitterionic MEP is plotted in black and the covalent one in red.

3.2.1 Two Dimensional Approach

In order to carry out our calculations we considered, in a first approach, only a two dimensional surface so we could compare the results obtained with this new surface with those obtained using the previous one. In this case, the N-H bond ($Q \equiv r_1$) will constitute the system and the N$\cdots$N bond the bath ($q \equiv r_2$). In the expressions given by Equations 3.8 and 3.10 we will neglect the terms that include the R contribution. The final expression for V(Q,q) in the intermediate region will be given by:

$$V(Q,q) = V(r_1,r_2) = \frac{1}{2}\left(V_0^Z + V_0^C\right) \pm \frac{1}{2}\left[\left(V_0^Z - V_0^C\right)^2 + 4V_{ZC}^2\right]^{\frac{1}{2}} \tag{3.11}$$

and in the base pair and tautomeric area by:

$$V(Q,q) = V(r_1,r_2) = V_0^Z(r_1,r_2). \tag{3.12}$$

In order to obtain the $V_{sys}(Q)$ potential we will apply a similar approach as that used in the previous Section. The $V_{bath}(q)$ potential can be obtained using Equation 3.3, in this case $r_2^0 = 6.00\ a_0$, it is the distance at which the monomers are closest. The coupling term ε was estimated to range between -0.0007 and 0.0000 $E_h.a_0^{-2}$ as in the previous case. $V_{sys}(Q)$ can then be determined using the expression in Equation 3.4 and the data provided in Table 3.4.

	r_1	r_2	$V(r_1,r_2)$	$V(r_2)$
BP'	-0.0030	-0.7783	-0.000198	0.087650
TS_1'	0.7068	6.0000	0.020556	0.000000
IZ'	0.8291	6.0000	0.017778	0.000000
TS_2'	1.1523	5.4998	0.020028	0.000477
IC'	2.2891	-3.0290	-0.001705	0.155868
T'	3.8365	-0.7783	-0.004622	0.087650

Table 3.4: Potential data and corresponding geometries, in atomic units, for the first excited PES of $(7\text{-AI})_2$. The data in the first three columns were obtained by Guallar and co-workers.

The V(Q) potential obtained using these data and the different ε values is a four-well potential which can be fitted to a polynomial expression:

$$V(Q) = \sum_{n=0}^{19} a_n Q^n. \tag{3.13}$$

Different values for the a_n coefficients were obtained for $Q \leq 0.7068\ a_0$, for $0.7068\ a_0 < Q \leq 1.1523\ a_0$ and for $Q > 1.1523\ a_0$. The final potential energy curves are labelled in Table 3.5 and plotted in Figure 3.10.

PES	6	7	8	9	10
ε	-0.0007	-0.0005	-0.0003	-0.0001	0.0000

Table 3.5: Labels of the potential energy surfaces obtained using the data in Table 3.4 and the different ε values.

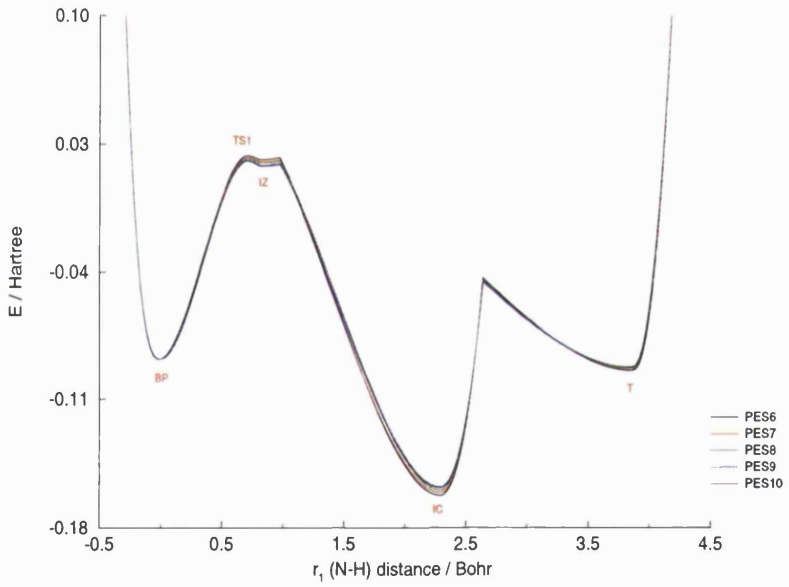

Figure 3.10: Potential energy curves, $V(r_1)$, obtained with the data provided by Guallar *et al.* and with different ε values.

3.2.2 Three Dimensional Approach

In this case the N-H and the N···N bonds form the system ($Q \equiv r_1$, r_2) and the rest of the molecule, described by the R coordinate, constitutes the bath ($q \equiv R$). These coordinates are plotted in Figure 3.11. The N-H and the N···N bond distances are the ones that change most along the reaction.

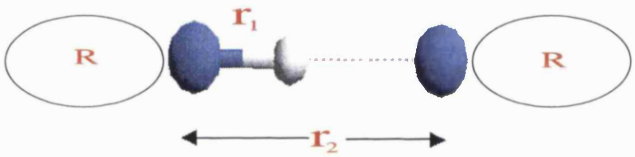

Figure 3.11: Coordinates used to obtained the three dimensional potential energy surface for the $(7\text{-AI})_2$ double proton transfer reaction. r_1 is the proton displacement distance, r_2 is the intermonomeric distance and R is a global coordinate that describes the distance's variations in the rest of the molecule.

The potential energy surface will be then given by Equations 3.8 and 3.10. As there are no data available for the R_0^C value we assumed it was equal to R_0^Z. In these expressions ω_R^Z is $\sim 900\,cm^{-1}$ in the base pair region, $\sim 600\,cm^{-1}$ in the tautomer region and $\omega_R^Z = \omega_R^C = \omega_R \sim 350\,cm^{-1}$ in the intermediate one. The values of ω_R are plotted in Figure 3.12.

So, the final expression we use to calculate the surface, in the base pair and tautomeric area, is:

$$V_{B.O.}(r_1, r_2, R) = V_0^Z(r_1, r_2) + \frac{1}{2}\left[\omega_R^2(R - R_0)^2\right] \tag{3.14}$$

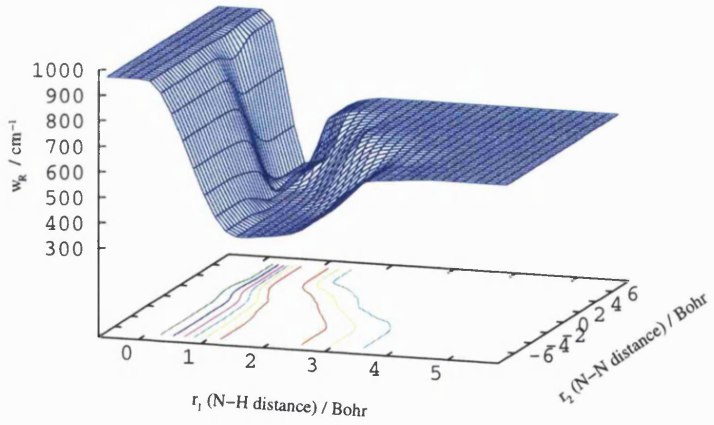

Figure 3.12: Values of the harmonic frequency ω_R as a function of the r_1 and r_2 distances.

whereas in the intermediate area it will be:

$$V_{B.O.}(r_1, r_2, R) = \frac{1}{2}\left[V_0^Z + V_0^C + \omega_R^2(R - R_0)^2\right] \pm \frac{1}{2}\left[(V_0^Z - V_0^C)^2 + 4V_{ZC}^2\right]^{\frac{1}{2}}. \tag{3.15}$$

In this three dimensional approach, $V_{sys}(Q)$ will be then given by:

$$V_{sys}(Q) = V(r_1, r_2) = V_0^Z(r_1, r_2) \tag{3.16}$$

in the base pair and tautomeric areas; in the intermediate area it will be given by:

$$V_{sys}(Q) = \frac{1}{2}\left[V_0^Z + V_0^C\right] \pm \frac{1}{2}\left[(V_0^Z - V_0^C)^2 + 4V_{ZC}^2\right]^{\frac{1}{2}}. \tag{3.17}$$

The negative value of the second term in this expression was chosen to minimise the total value for the potential energy surface $V_{B.O.}(r_1,r_2,R)$.

We now need to calculate the bath potential $V_{bath}(q)$ and the coupling potential $V_{coup}(Q,q)$. Equation 3.1 can be rearranged as:

$$V(Q,q) - V_{sys}(Q) = V_{bath}(q) + V_{coup}(Q,q). \tag{3.18}$$

So, by subtracting Equation 3.17 from Equation 3.15

$$V(Q,q) - V_{sys}(Q) = V(q) + V_{coup}(Q,q) = \frac{1}{2}\omega_R^2(R - R_0)^2, \tag{3.19}$$

in the intermediate area. The same expression is obtained for the base pair and tautomeric area by substracting Equation 3.16 from Equation 3.14. In this expression both ω_R and R_0 depend on r_1 and r_2. So, the expression in Equation 3.19 depends explicitly on R and implicitly on r_1 and r_2.

By definition we know that the bath potential, $V_{bath}(q)$, depends only on the q coordinate (in this case q≡R) and that it has the shape of a harmonic oscillator (the bath degrees of freedom do not change much during the reaction). So, we can say that:

$$V(q) = \frac{1}{2}\left(\omega_R(r_1^0, r_2^0)\right)^2 \left(R - R_0(r_1^0, r_2^0)\right)^2, \tag{3.20}$$

where r_1^0 and r_2^0 are the r_1 and r_2 values that describe the dimer geometry at the base pair configuration. We have $\omega_R(r_1^0,r_2^0)$= 900 cm^{-1} and $R_0(r_1^0,r_2^0)$= 0.00 a_0.

Once $V_{bath}(q)$ is known $V_{coup}(Q,q)$ can be obtained using the expression in Equation 3.19:

$$\begin{aligned} V_{coup}(Q,q) =& \frac{1}{2}\left(\omega_R(r_1, r_2)\right)^2 \left(R - R_0(r_1, r_2)\right)^2 \\ & - \frac{1}{2}\left(\omega_R(r_1^0, r_2^0)\right)^2 \left(R - R_0(r_1^0, r_2^0)\right)^2 \end{aligned} \tag{3.21}$$

This expression can be rewritten as:

$$V_{coup}(Q,q) = \frac{1}{2}\left[(\omega_R(r_1,r_2))^2 - \left(\omega_R(r_1^0,r_2^0)\right)^2\right] R^2 - \frac{1}{2}(\omega_R(r_1,r_2))^2\left[2RR_0(r_1,r_2) - (R_0(r_1,r_2))^2\right]. \quad (3.22)$$

The values for R_0^Z=R_0^C=R_0 are given in Figure 3.13. The coupling potential, V_{coup}(Q,q), is plotted in Figure 3.14 and the final potential energy surface is shown in Figure 3.15.

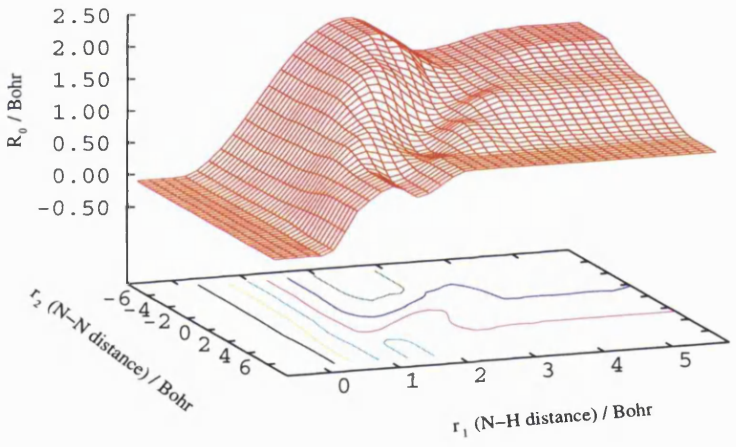

Figure 3.13: Equilibrium position R_0 as a function of the $r_1$and r_2 coordinates.

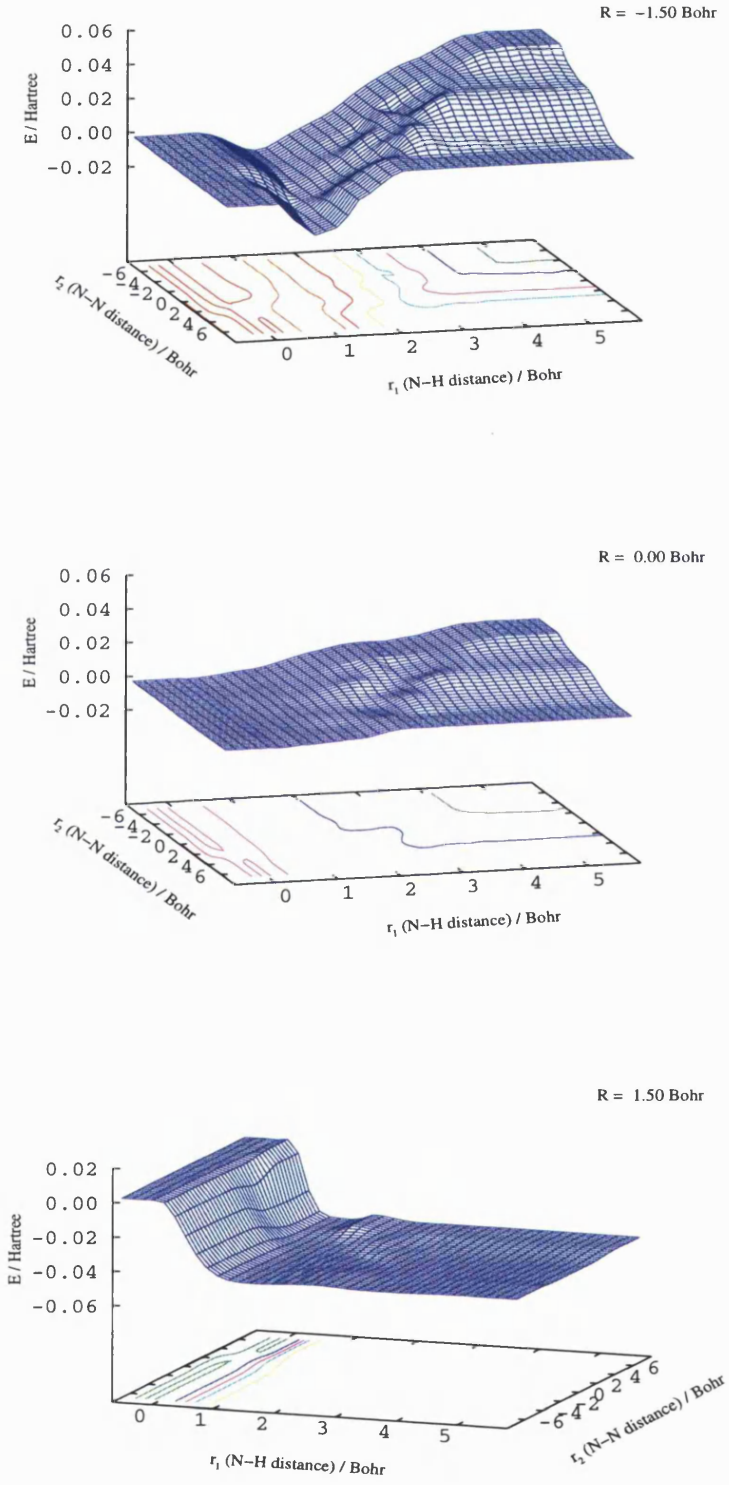

Figure 3.14: Three dimensional coupling potential energy surface as function of the r_1, r_2 and R coordinates. It is important to notice the change of the coupling potential energy surface with the global coordinate R.

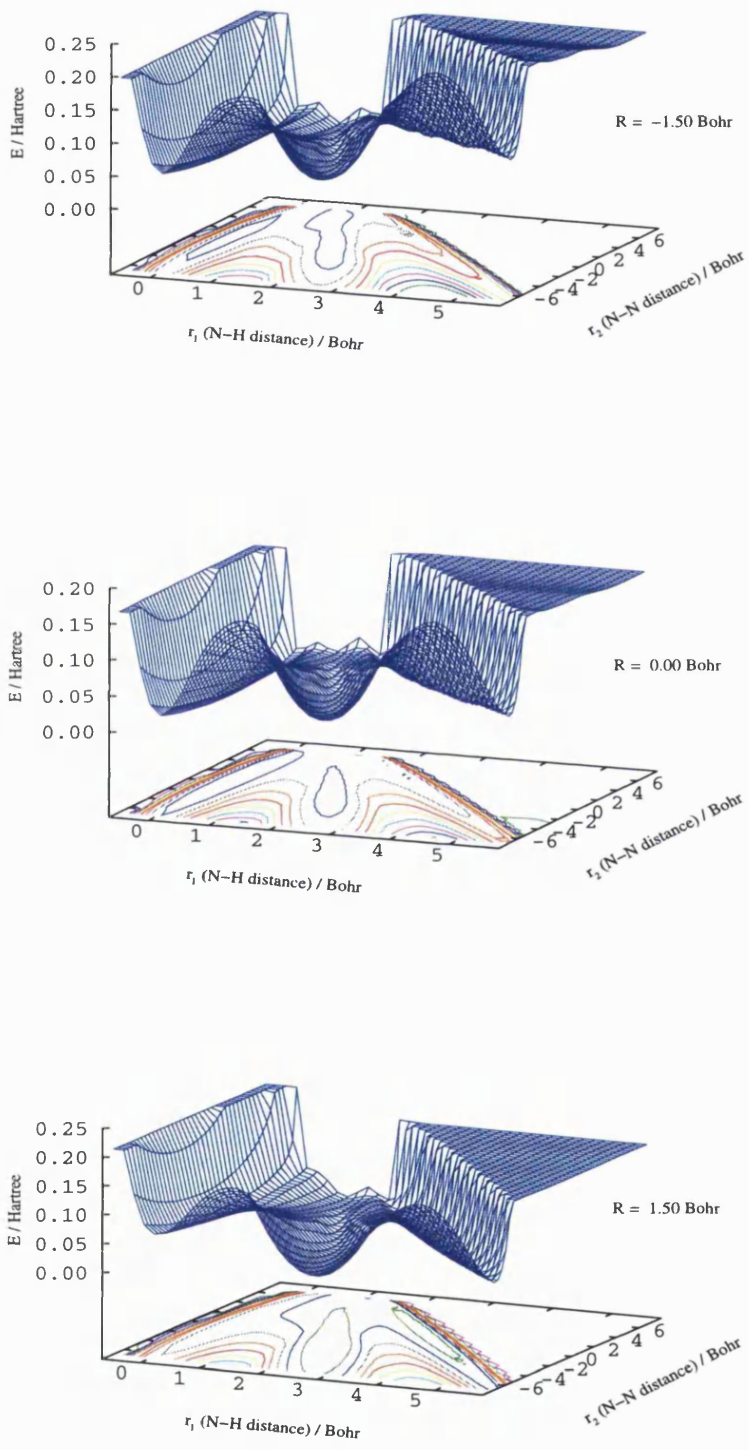

Figure 3.15: Three dimensional potential energy surface as function of the r_1, r_2 and R coordinates. The variation of the well depth with the R coordinate can be seen.

Chapter 4

Results

In this Chapter we will present the results obtained on applying the quantum tunnelling in a dissipative environment method, described in Chapter 2, to the 7-azaindole dimer double proton transfer reaction using the potential energy surfaces depicted in Chapter 3. The final aim of this work is to obtain the proton/deuterium transfer times of the $(7\text{-AI})_2$ phototautomerization reaction.

In the next Sections we will present the results of our work giving, in each case, some numerical details about the calculations and comparing our results with the experimental ones when possible.

4.1 General Numerical Details

All our calculations were carried out following the same procedure. The first step was always to solve the Hamiltonian equations corresponding to the system and to the bath:

$$\mathrm{H_{sys}(Q)}\phi_\alpha(\mathrm{Q}) = \mathrm{E}_\alpha\phi_\alpha(\mathrm{Q}) \tag{4.1}$$

$$\mathrm{H_{bath}(q)}\psi_\mathrm{m}(\mathrm{q}) = \mathrm{E_m}\psi_\mathrm{m}(\mathrm{q}) \tag{4.2}$$

The first of these equations is solved using the DVR method described in Subsection 2.3.1. The second equation, corresponding to the bath, is solved analytically as the potential involved in this equation is always a harmonic one. So, the $\psi_\mathrm{m}(\mathrm{q})$

functions are given by:

$$\psi_m(q) = N_m H_m(y) \exp^{-\frac{y^2}{2}} \tag{4.3}$$

where N_m are the normalisation constants

$$N_m = \left(\frac{1}{\alpha \pi^{0.5} 2^m m!}\right)^{0.5}, \tag{4.4}$$

$H_m(y)$ are the Hermite polynomials and $y = \frac{q-q^0}{\alpha}$. q^0 is the q value at which the $V_{bath}(q)$ potential reaches its minimum and $\alpha = \frac{1}{\sqrt{\mu\omega}}$, being μ the corresponding reduced mass and ω the frequency associated with the $V_{bath}(q)$ potential.

The E_m energies can be determined, in atomic units, by:

$$E_m = (m + 0.5)\omega \tag{4.5}$$

where m is the corresponding vibrational quantum number, m=0,1,...,$Z_m - 1$, and Z_m is the number of $\psi_m(q)$ used in the calculations.

The second step in our calculations, was to determine the initial wavepacket. This wavepacket will be a function of the Q and q coordinates:

$$\Psi_0(Q, q) = \Psi(Q)\Psi(q). \tag{4.6}$$

The final form of this wavepacket depends on the coordinates involved in the calculations. Its calculation will be seen in detail in the next Sections.

Once the initial wavepacket is determined it has to be described as a function of the $\phi_\alpha(Q)$ and $\psi_m(q)$ functions using the expression:

$$\Psi_0(Q, q) = \sum_{m,\alpha} D_{m\alpha}\, \phi_\alpha(Q)\, \psi_m(q). \tag{4.7}$$

By comparing this expression with the previous one, Equation 4.6, we are able to obtain the $D_{m\alpha}$ coefficients.

The third step is to solve the time independent Schrödinger equation of the system, Equation 2.9, using the $\psi_m(q)$ and $\phi_\alpha(Q)$ functions as the basis set to determine the $\Psi_E(Q, q)$ functions, their coefficients $A_{E,m\alpha}$ and their corresponding energies E_E.

Different Numerical Recipes algorithms [112] and Nag routines [113] were used to solve the linear equations and eigenvalue problems. This is the most time-consuming and computer memory demanding step in all the calculations.

In order to study the time evolution of the initial wavepacket the time dependent Schrödinger equation was considered. Its solution can be written as:

$$\Psi(Q,q,t) = \sum_{E} B(E) \exp^{-iE_E t} \Psi_E(Q,q) \tag{4.8}$$

where the B(E) coefficients can be obtained by comparing this expression at t=0

$$\Psi(Q,q,0) = \sum_{E} B(E)\Psi_E(Q,q) \tag{4.9}$$

to the expression in Equation 4.7.

Finally, the probability of finding the particle (in our case the H or D atoms) in a given region can be calculated using the following expression

$$P(t) = \int\int |\Psi(Q,q,t)|^2 dQdq. \tag{4.10}$$

In all our calculations this integral was calculated integrating q over its maximum and minimum values (all the q space) while Q was integrated between its minimum value and the value at the corresponding transition state (TS) geometry (if $Q \leq Q_{TS}$ the H/D has not jumped while if $Q > Q_{TS}$ the H/D has already moved). The time at which this integral reaches its minimum value is considered to be the transfer time (always some part of the initial wavepacket remained trapped in the first well).

4.2 Ground State Calculations

4.2.1 Numerical Details

In these calculations, the first we carried out, Q≡r_1 (N-H distance) and q≡r_2 (N-N distance). The calculations were done on the PES described in Section 3.1.1 and plotted in Figure 3.5.

For the system 200 $\phi_\alpha(r_1)$ functions were used in the calculations (obtained, using the DVR method, from 400 equally spaced DVR functions). The number of $\phi_\alpha(r_1)$ functions used was determined by introducing a maximum value for the $V_{sys}(Q)$ potential, $V_{sys}(Q)$= 0.10 E_h, and taking then all the $\phi_\alpha(r_1)$ functions whose corresponding energy E_α is $\leq$ 0.10 E_h. The $V_{sys}(Q)$ potential and the $\phi_\alpha(r_1)$ functions were plotted in a grid of 402 points.

For the bath only 10 $\psi_1(r_2)$ functions were used. It was found that increasing the number of these functions did not make significant changes in the final results.

In these calculations the initial wavepacket was chosen to be a gaussian wavepacket in the r_1 coordinate. This wavepacket was centred on the first well of the ground state potential energy surface (r_1 = 0.00 a_0). We considered that at this point only the first $\psi_m(r_2)$ state was occupied so the final form of the initial wavepacket is given by:

$$\Psi_0(r_1, r_2) = \sqrt{\frac{\alpha}{\pi^{0.5}}} \exp^{-0.5(\alpha(r_1 - r_1^0))^2} \psi_0(r_2) \tag{4.11}$$

where α is a coefficient that determines the width of the wavepacket. We set it to be $\alpha = 15$ in our calculations. Changes in this parameter determine the percentage of the wavepacket that tunnels through the barrier. Higher α values determine narrower wavepackets with more percentage of the wavepacket going through the barrier, but the P(t) function always reaches its minimum value at the same t value. The reduced masses used in the calculations were the following, μ_{NH} = 1713.80695 m_e, μ_{ND} = 3209.665345 m_e (both associated with the r_1 coordinate) and μ_{NN}=12763.0175 m_e (this one being related to the r_2 coordinate). r_2 was integrated over the whole r_2

space while the integration limits for r_1 were -0.2332 a_0 (minimum value for the r_1 coordinate) and 1.60 a_0 (r_1 value corresponding to the TS geometry).

4.2.2 Results and Comments

We obtained a proton transfer time of 30.5 fs for the 7-azaindole undeuterated dimer and 60.1 fs for the deuterated one. The results of our calculations are shown in Figure 4.1.

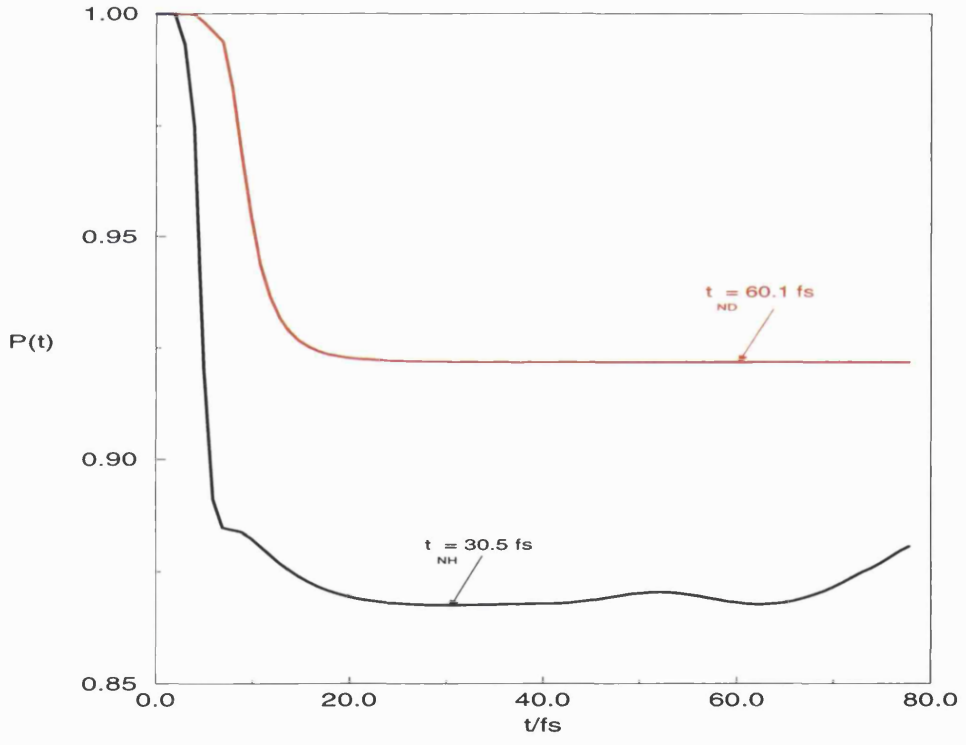

Figure 4.1: Representation of the probability of finding the H/D atom in the first well of the GS potential energy surface versus the propagation time. The black line represents the results for the undeuterated $(7\text{-AI})_2$ while the red one represents these results for the deuterated one.

It is not possible to compare these results with experimental ones as the proton transfer time of the $(7\text{-AI})_2$ ground state tautomerization reaction has not been determined experimentally. However, Fuke and Kaya [46] in their supersonic beams experiments estimated that the lifetime of the $(7\text{-AI})_2$ tautomeric form in the ground state was 10 μs. As the most stable form in the GS is the dimer its lifetime should be longer than that of the ground state tautomer and hence the transfer time should be more than 10 μs. This is clearly not the case as the transfer times determined in our calculations are in the femtosecond time scale.

4.3 First Excited State Calculations

4.3.1 Two Dimensional Calculations

These were the first calculations we carried out on the first excited state of the $(7\text{-AI})_2$ phototautomerization reaction. As in the previous case, in these calculations, $Q \equiv r_1$ (N-H distance) and $q \equiv r_2$ (N-N distance).

Numerical Details

The first calculations carried out on the excited state were performed using the potential energy surfaces generated in Subsection 3.1.2. In the calculations 150 $\phi_\alpha(r_1)$ functions and 20 $\psi_m(r_2)$ functions were used. The $\phi_\alpha(r_1)$ functions were obtained using 400 equally spaced DVR functions; from these initial 400 $\phi_\alpha(r_1)$ functions only 150 of them were considered as their corresponding energy $E_\alpha \leq 0.05$ E_h (maximum $V_{sys}(Q)$ value considered). The $\phi_\alpha(r_1)$ functions and the $V_{sys}(Q)$ potential were described in a grid of 402 equally spaced points (the same as in the previous case).

In order to reproduce the experimental conditions the r_1 component of the initial wavepacket was now chosen to be the first eigenstate of the ground state potential energy surface. This wavepacket was centred on the first well of the excited state potential energy surface. Having also in mind the experimental conditions different initial vibrational energies in the r_2 coordinate were considered. So, the r_2 component

of the initial wavepacket took different values along the calculations. The general form of the initial wavepacket was:

$$\Psi_0(r_1, r_2) = \phi_\alpha^{GS}(r_1)\psi_m(r_2) \tag{4.12}$$

where m=0,1,2,3,4 as these were the values used in the experiments carried out by Zewail and co-workers [49]. If m=0 there is no extra vibrational energy in the r_2 coordinate. By changing the value of m we should be able to determine the influence of the N-N vibration on the proton transfer time.

The reduced masses used in the calculations were the same as those used in the previous Section. r_2 was integrated over the whole r_2 space. In order to determine the first proton transfer time r_1 was integrated between -0.2330 a_0 (its minimum value) and 1.17 a_0 (r_1 value at the first TS geometry). To determine the second proton transfer time r_1 was integrated between -0.2330 a_0 and 1.59 a_0 (r_1 value corresponding to the second TS geometry).

Results and Comments

The results of our calculations are shown in the Tables 4.1 and 4.2 and plotted in Figures 4.2, 4.3 and 4.4.

m	$PES_{\varepsilon=-0.0007}$	$PES_{\varepsilon=-0.0005}$	$PES_{\varepsilon=-0.0003}$	$PES_{\varepsilon=-0.0001}$	$PES_{\varepsilon=0.00}$
0	14.8 (20.7)	14.7 (20.7)	14.6 (20.7)	14.6 (20.7)	14.6 (20.7)
1	13.4 (20.7)	14.7 (20.7)	14.6 (20.7)	14.6 (20.7)	14.6 (20.7)
2	13.4 (20.7)	14.7 (20.7)	14.6 (20.7)	14.6 (20.7)	14.6 (20.7)
3	13.4 (20.7)	14.7 (20.7)	14.6 (20.7)	14.6 (20.7)	14.6 (20.7)
4	13.4 (20.7)	14.7 (20.7)	14.6 (20.7)	14.6 (20.7)	14.6 (20.7)

Table 4.1: First proton transfer times obtained for the different first excited state potential energy surfaces and for the different initial N-N vibrational states. The values within brackets correspond to the deuterated $(7\text{-AI})_2$. All the values are given in fs.

m	$PES_{\varepsilon=-0.0007}$	$PES_{\varepsilon=-0.0005}$	$PES_{\varepsilon=-0.0003}$	$PES_{\varepsilon=-0.0001}$	$PES_{\varepsilon=0.00}$
0	32.5 (36.9)	33.7 (36.9)	33.7 (36.9)	33.7 (36.9)	33.7 (36.9)
1	32.2 (36.9)	33.7 (36.9)	33.7 (36.9)	33.7 (36.9)	33.7 (36.9)
2	32.2 (36.9)	33.7 (36.9)	33.7 (36.9)	33.7 (36.9)	33.7 (36.9)
3	32.2 (36.9)	33.7 (36.9)	33.7 (36.9)	33.7 (36.9)	33.7 (36.9)
4	32.2 (36.9)	33.7 (36.9)	33.7 (36.9)	33.7 (36.9)	33.7 (36.9)

Table 4.2: Second proton transfer times obtained using the different first excited state potential energy surfaces and the different initial N-N vibrational energies. The values within brackets correspond to the deuterated $(7\text{-AI})_2$. All the values are given in fs.

These results can be compared with those obtained by Zewail and co-workers [49] and by Castleman and co-workers [55]; these experimental results are showed in Table 4.3.

	τ_{1H}	τ_{2H}	τ_{1D}	τ_{2D}
m=0	650 fs	3300 fs		
m=3	360 fs	1700 fs	3000 fs	25000 fs
m=4	200 fs	1600 fs		
m=0^{C}	660 fs	5000 fs		

Table 4.3: Experimental transfer times obtained by Zewails's and Castleman's (^{C}) groups for the deuterated and undeuterated species.

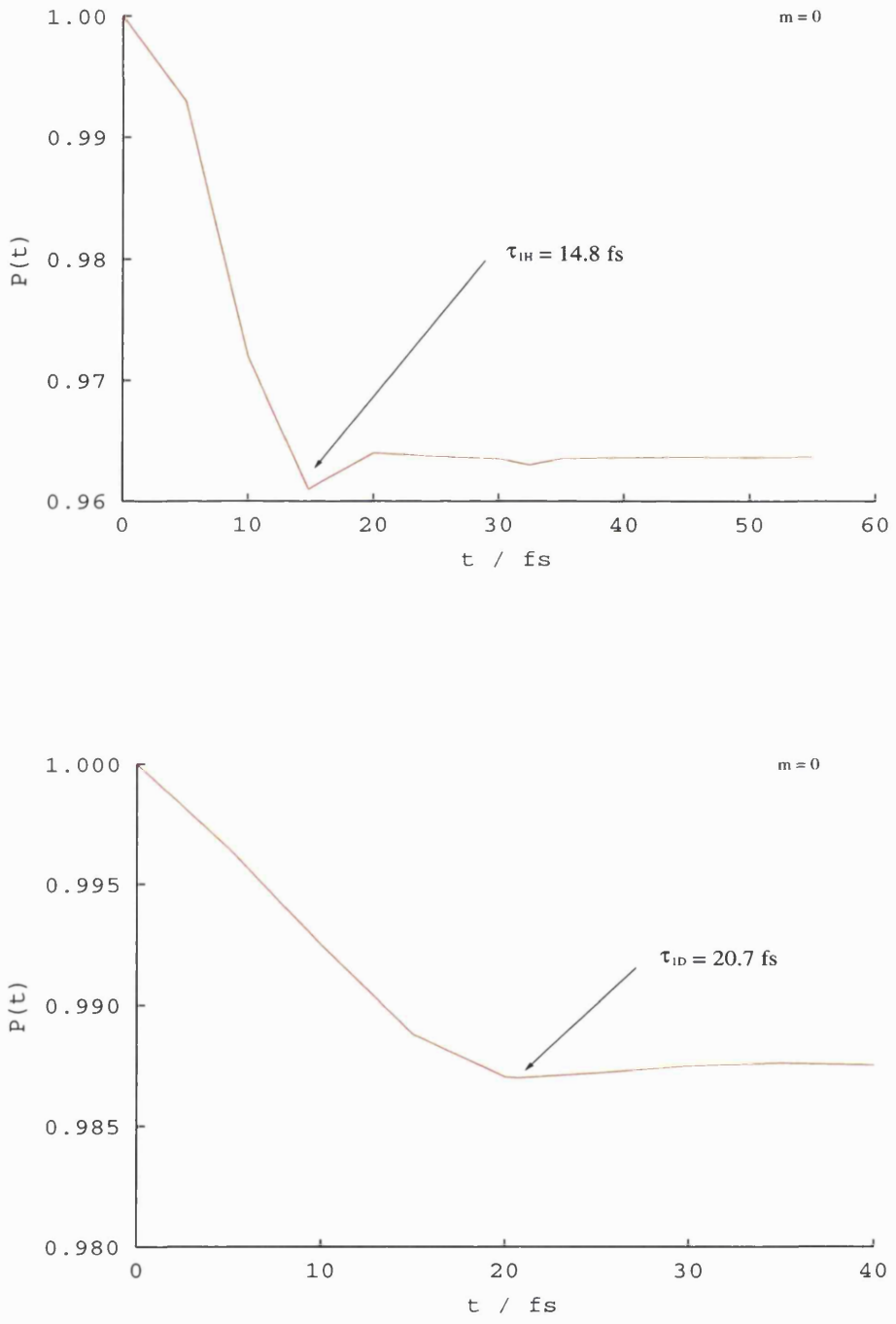

Figure 4.2: Probability of finding the H/D atom to the left of the first TS barrier *versus* the propagation time. The first figure presents the results for the undeuterated $(7\text{-AI})_2$ while the second one presents the results for the deuterated dimer. These results were obtained for m=0 (no extra-vibrational energy in the N-N coordinate) and ε=-0.0007 $E_h.a_0^{-2}$.

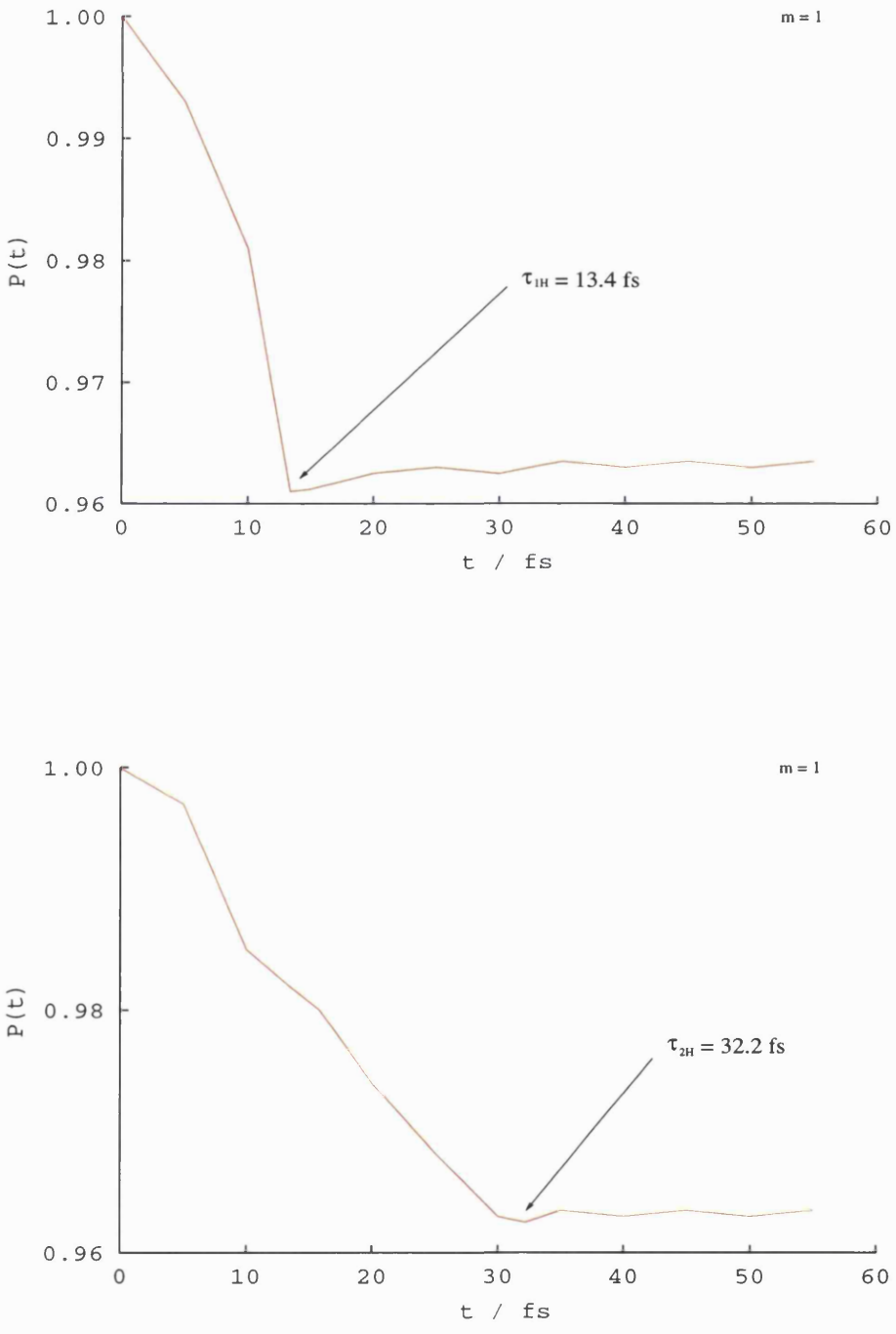

Figure 4.3: Probability of finding the H atom to the left of the first and second barrier *versus* the propagation time. The first figure presents the results of the first H jump while the results for the second H jump are presented in the second figure. These results were obtained for m=1 and ε=-0.0007 $E_h.a_0^{-2}$.

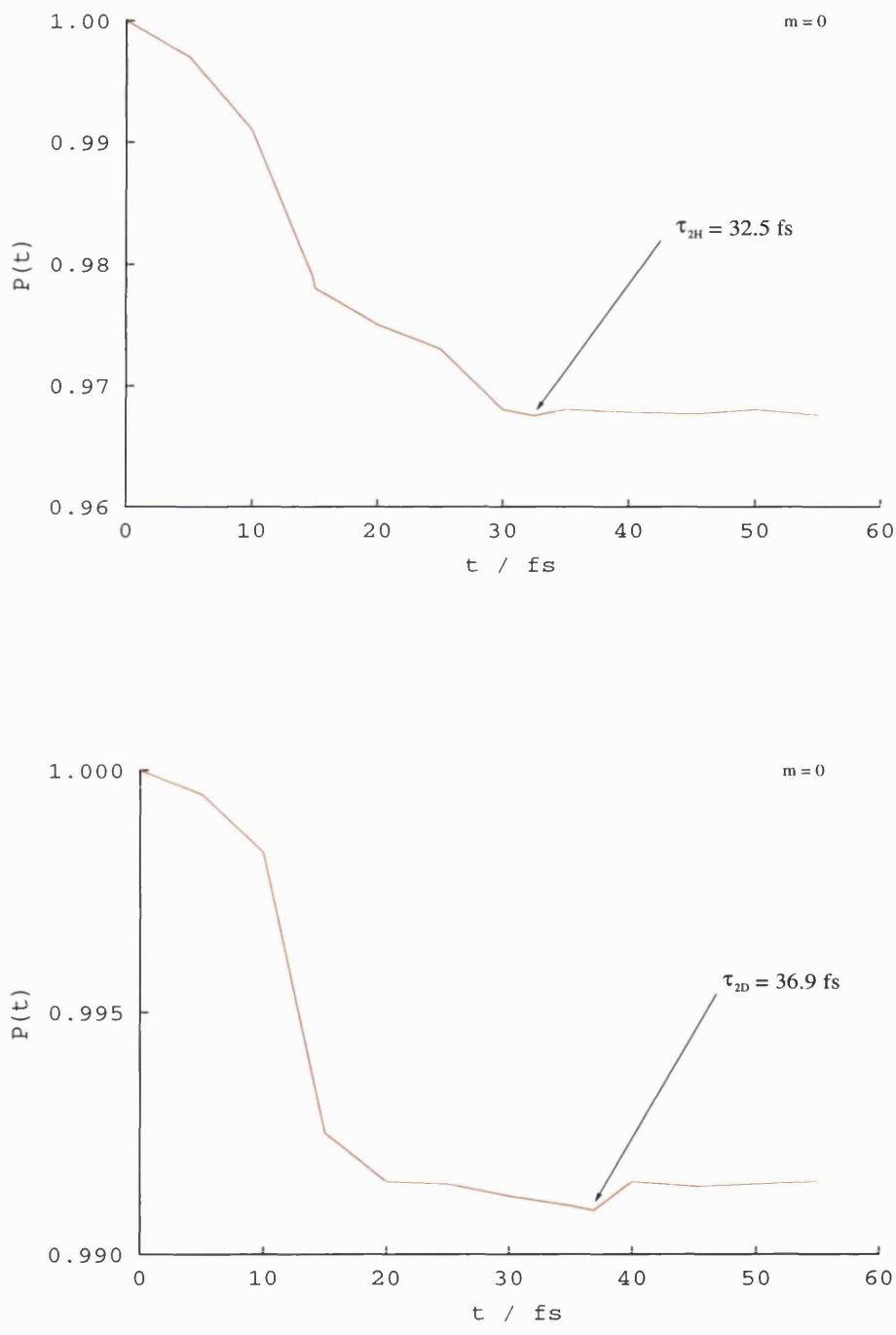

Figure 4.4: Probability of finding the H/D atom to the left of the second TS barrier *versus* the propagation time. The first figure presents the results for the undeuterated $(7\text{-AI})_2$ while the second one presents the results for the deuterated dimer. These results were obtained for m=0 (no extra-vibrational energy in the N-N coordinate) and ε=-0.0007 $E_h.a_0^{-2}$.

There are several differences between our theoretical H/D transfer times and the experimental ones reported by Zewail's and Castleman's groups. First of all, the results obtained by Zewail and co-workers change when the vibrational energy in the N-N bond is increased. Our theoretical results do not change much with this energy change. Only when ε=-0.0007 $E_h.a_0^{-2}$ the H transfer times go from τ_{1H}=14.8 fs and τ_{2H}=32.5 fs at m=0 to τ_{1H}=13.4 fs and τ_{2H}=32.2 fs if m>0. For the rest of the ε values the transfer times do not change as we vary the internal N-N vibrational energy. The D transfer times do not change at all with the N-N vibrational energy change.

It must also be noted that the change in the coupling term value from ε=-0.0007 $E_h.a_0^{-2}$ to ε=0.0000 $E_h.a_0^{-2}$ does not cause significant changes in the transfer times. τ_{1H}=14.8 fs if ε=-0.0007 $E_h.a_0^{-2}$ and τ_{1H}=14.6 fs if ε=0.0000 $E_h.a_0^{-2}$.

In general it can be said that all our transfer times are smaller than those reported by Zewail's and Castleman's groups. This difference is especially significant when we compare the results for the second proton transfer time (32.5 fs obtained theoretically *versus* 3300 fs obtained in the experiments); this difference increases for the deuterated form (36.9 fs versus 25000 fs). In the H case, the difference between the experimental and theoretical values is of a factor of 100 while in the D case the difference is of a factor of 650. This difference could be due, at least in part, to the fact that on the potential energy surfaces used in these calculations there is a very small barrier between the intermediate and the tautomeric forms. So, once the first H/D has jumped the second one jumps very quickly.

4.3.2 Two Dimensional Calculations Using The New Potential Energy Surface

In order to improve our previous results we carried out similar calculations on a new potential energy surface reported by Guallar *et al.* [56]. This new surface has a new and very stable covalent intermediate structure. So, by carrying out calculations on this surface we expected to obtain different H/D transfer times; as the surface has a deeper intermediate there is a higher barrier for the second H/D jump.

Numerical Details

These calculations were carried out on the first excited state potential energy surfaces generated in Subsection 3.2.1. As in the previous calculations $Q \equiv r_1$ and $q \equiv r_2$.

In these calculations 250 $\phi_\alpha(r_1)$ functions were used all of them having $E_\alpha \leq 0.05$ E_h, this being the maximum value given to $V_{sys}(Q)$. The $\phi_\alpha(r_1)$ functions were obtained from 800 equally spaced DVR functions. The $\phi_\alpha(r_1)$ functions and the $V_{sys}(Q)$ were described in a grid of 802 points. For the bath only 20 $\psi_m(r_2)$ were used. It was found that increasing the number of these functions did not make significant changes in the final results.

The initial wavepacket was chosen to be the same as in the previous case. The r_1 component of the initial wavepacket was the first eigenstate of the ground state potential energy surface considering it to be centred on the first well of the excited state potential energy surface. The r_2 component was given different values to try to reproduce the experimental results. So the form of the initial wavepacket was:

$$\Psi_0(r_1, r_2) = \phi_\alpha^{GS}(r_1)\psi_m(r_2) \tag{4.13}$$

where m=0,1,2,3,4. If m=0 there is no extra vibrational energy in the r_2 coordinate.

The reduced masses used in the calculations were the same as those used in the previous Sections. r_2 was integrated over the whole r_2 space. In order to determine the first proton transfer time r_1 was integrated between -0.04 a_0 (its minimum value) and 0.7068 a_0 (r_1 value at the first TS geometry). To determine the second proton

transfer time r_1 was integrated between -0.04 a_0 and 2.73 a_0 (r_1 value corresponding to the second TS geometry).

Results and Comments

The results of our calculations are shown in Tables 4.4 and 4.5 and plotted in Figures 4.5 and 4.6.

m	$PES_{\varepsilon=-0.0007}$	$PES_{\varepsilon=-0.0005}$	$PES_{\varepsilon=-0.0003}$	$PES_{\varepsilon=-0.0001}$	$PES_{\varepsilon=0.00}$
0	16.9 (60.2)	16.9 (60.2)	16.9 (60.2)	16.8 (60.2)	16.8 (60.2)
1	16.7 (60.2)	16.6 (60.2)	16.6 (60.2)	16.6 (60.2)	16.6 (60.2)
2	16.7 (60.2)	16.6 (60.2)	16.6 (60.2)	16.6 (60.2)	16.6 (60.2)
3	16.7 (60.2)	16.6 (60.2)	16.6 (60.2)	16.6 (60.2)	16.6 (60.2)
4	16.7 (60.2)	16.6 (60.2)	16.6 (60.2)	16.6 (60.2)	16.6 (60.2)

Table 4.4: First proton transfer times obtained for the different first excited state potential energy surfaces and for the different initial N-N vibrational states. The values within brackets correspond to the deuterated $(7\text{-AI})_2$. All the values are given in fs.

	$mPES_{\varepsilon=-0.0007}$	$PES_{\varepsilon=-0.0005}$	$PES_{\varepsilon=-0.0003}$	$PES_{\varepsilon=-0.0001}$	$PES_{\varepsilon=0.00}$
0	60.2 (124.8)	60.1 (124.8)	60.1 (124.8)	60.1 (124.8)	60.0 (124.8)
1	60.0 (124.8)	59.8 (124.8)	59.8 (124.8)	59.8 (124.8)	59.8 (124.8)
2	60.0 (124.8)	59.8 (124.8)	59.8 (124.8)	59.8 (124.8)	59.8 (124.8)
3	60.0 (124.8)	59.8 (124.8)	59.8 (124.8)	59.8 (124.8)	59.8 (124.8)
4	60.0 (124.8)	59.8 (124.8)	59.8 (124.8)	59.8 (124.8)	59.8 (124.8)

Table 4.5: Second proton transfer times obtained using the different first excited state potential energy surfaces and the different initial N-N vibrational energies. The values within brackets correspond to the deuterated $(7\text{-AI})_2$. All the values are given in fs.

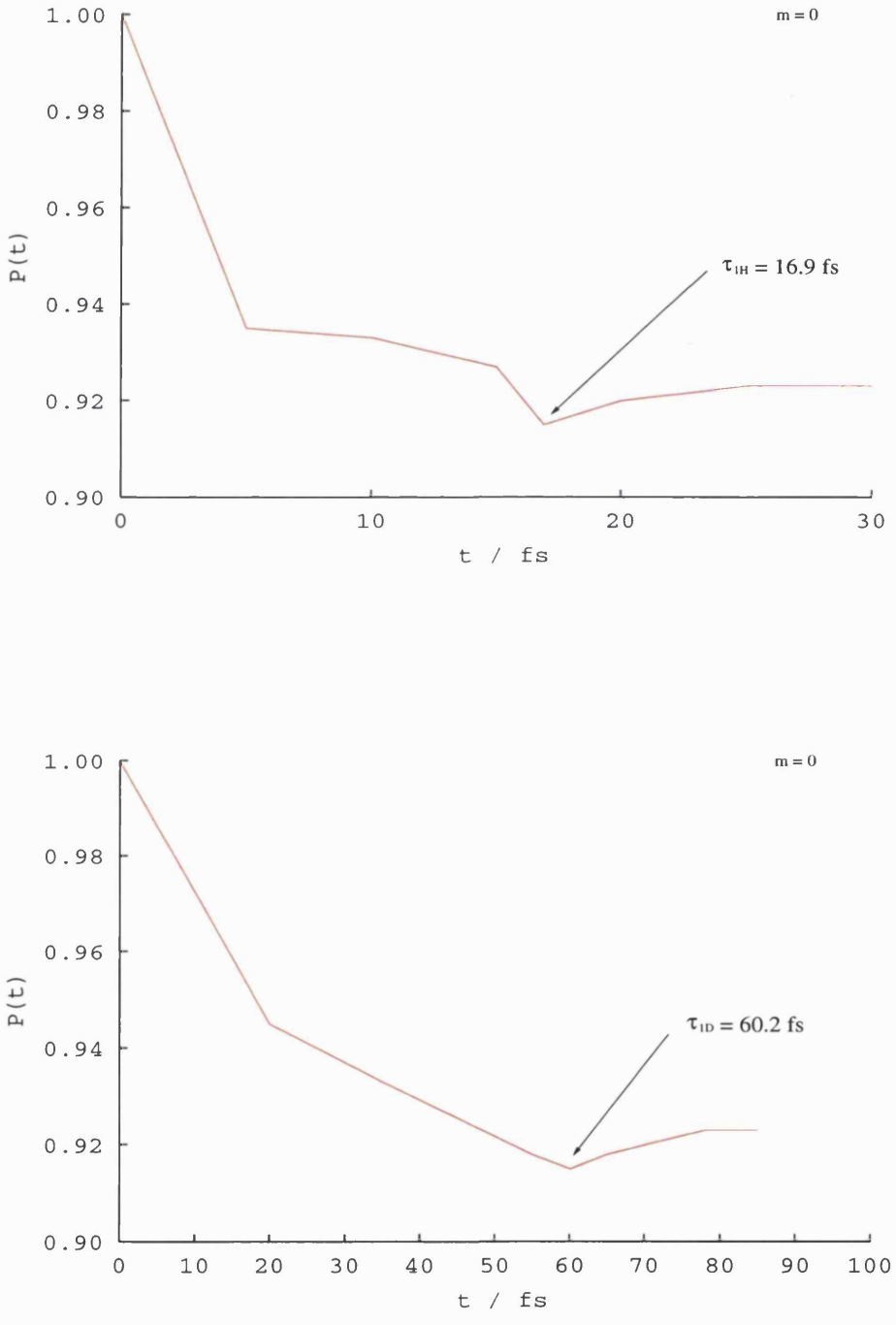

Figure 4.5: Probability of finding the H/D atom to the left of the first TS barrier *versus* the propagation time. The first figure presents the results for the undeuterated $(7\text{-AI})_2$ while the second one presents the results for the deuterated one. These transfer times were obtained for m=0 (no extra-vibrational energy in the N-N coordinate) and ε=-0.0007 $E_h.a_0^{-2}$.

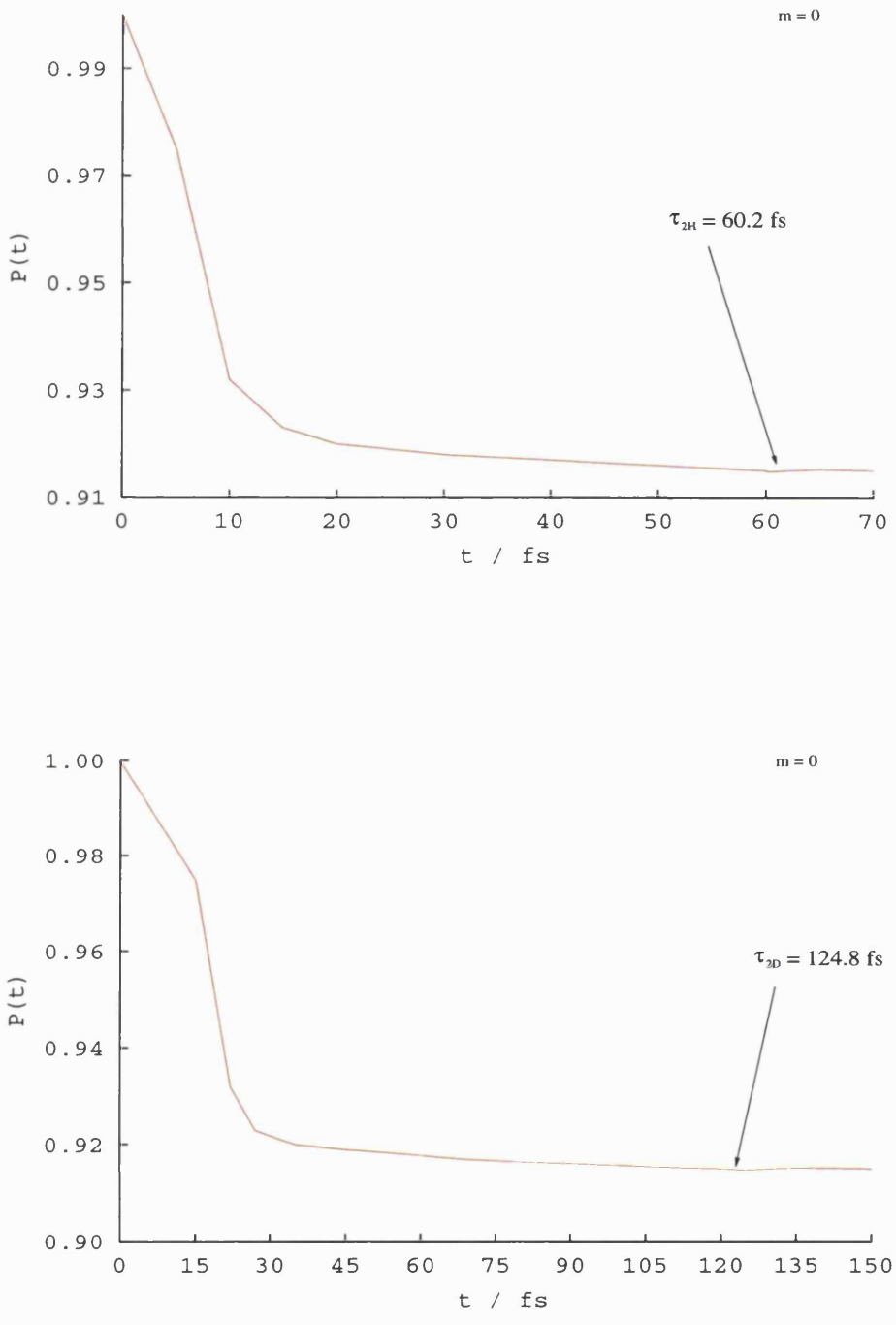

Figure 4.6: Probability of finding the H/D atom to the left of the second TS barrier *versus* the propagation time. The first figure presents the results for the undeuterated $(7\text{-AI})_2$ while the second one presents the results corresponding to the deuterated one. These results were obtained for m=0 (no extra-vibrational energy in the N-N coordinate) and ε=-0.0007 $E_h.a_0^{-2}$.

Several things can be pointed out if we compare these theoretical transfer times with the experimental ones reported by Zewail's and Castleman's groups and shown in Table 4.3.

First of all, it can be seen that there is still a big difference between the experimental and theoretical values. All theoretical transfer times are still on the femtosecond scale while some of the experimental ones are on the picosecond one. The theoretical results do not change much when the N-N vibrational energy is increased, the H transfer times only change two or three tenths of femtosecond when the vibrational quantum number goes from m=0 to m>0. The first D transfer times do not change at all with N-N vibrational energy change, the second D transfer times only change one or two tenths of a femtosecond with the change of the vibrational quantum number m.

If we compare these theoretical results with the previous ones we can see an improvement especially in the calculations carried out with the deuterated species. At ε=-0.0007 $E_h.a_0^{-2}$ the D transfer times go from τ_{1D}=20.7 fs to τ_{1D}=60.2 fs and from τ_{2D}=36.9 fs to τ_{2D}=124.8 fs. This improvement could be due to the fact that the potential energy barriers are much larger in these surfaces than on the ones used in the previous calculations (see details in Figures 3.6 and 3.10).

It must also be noted that the change in the coupling term from ε=-0.0007 $E_h.a_0^{-2}$ to ε=0.0000 $E_h.a_0^{-2}$ does not cause significant changes in the transfer times. τ_{1H}=16.9 fs if ε=-0.0007 $E_h.a_0^{-2}$ and τ_{1H}=16.8 fs if ε=0.0000 $E_h.a_0^{-2}$.

4.3.3 Three Dimensional Calculations

In order to improve the theoretical results we carried out a new set of calculations. In this case three dimensions were considered, r_1 (N-H distance) and r_2 (N-N distance) as the coordinates defining the system and R (global reorganization coordinate) describing the bath.

Numerical Details

The three dimensional calculations were performed using the potential energy surface reported by Guallar *et al.* [56] and depicted in Chapter 3. The calculations were carried out using 350 $\phi_\alpha(r_1,r_2)$ functions and 18 $\psi_m(R)$ functions. The $\phi_\alpha(r_1,r_2)$ functions were calculated using 40 DVR $\psi(r_1)$ functions and 42 DVR $\psi(r_2)$ functions. The potential energy surface $V_{sys}(r_1,r_2)$ and the $\phi_\alpha(r_1,r_2)$ functions were plotted in a grid of 1680 points (40 points in the r_1 coordinate and 42 points in the r_2 coordinate).

In this case the initial wavepacket was chosen to be a two dimensional gaussian wavepacket centred on the first well of the three dimensional potential energy surface. So, the final form of the initial wavepacket used in these calculations was:

$$\Psi_0(r_1, r_2, R) = \sqrt{\frac{\alpha_1}{\pi^{0.5}}}\exp^{-0.5(\alpha_1(r_1-r_1^0))^2}\sqrt{\frac{\alpha_2}{\pi^{0.5}}}\exp^{-0.5(\alpha_2(r_2-r_2^0))^2}\psi_0(R). \qquad (4.14)$$

where α_1=15 and α_2=10. Different values for these coefficients were used; their value determined the wavepacket's width but they did not change the final results. These calculations were the most demanding ones in computational resources that we performed. In order to obtain the $\Psi_E(Q,q)$ functions we had to solve Equation 2.9 and to diagonalise the matrix $\langle\Psi_{E'}|H|\Psi_E\rangle$ written in Equation 2.11. This is a 6300x6300 matrix. In order to diagonalise it we used a Nag routine making use of the fact that this matrix is banded [114].

Once the $\Psi_E(Q,q)$ functions were calculated we propagated the initial wavepacket $\Psi_0(r_1, r_2, R)$ in time using the Equation 2.15. Finally, we calculated the probability of finding the H or D atoms in a given region using Equation 2.24. In this case

the integral is a three dimensional integral, R was integrated between its maximum and minimum values (all of the R space), r_1 and r_2 were integrated between their minimum values and the values corresponding to the first barrier (for the first H/D transfer time) or to the values corresponding to the second barrier (for the second H/D transfer time). The values that define the barrier are given in Table 4.6.

r_2	r_1	r_2	r_1
-7.000000	1.450000	-7.000000	4.600000
-6.650000 - -4.900000	1.275000	-6.650000 - -6.300000	4.425000
-4.550000 - -2.450000	1.100000	-5.950000 - -5.600000	4.250000
-2.100000 - 0.350000	0.925000	-5.250000 - -4.900000	4.075000
0.700000 - 3.150000	0.750000	-4.550000 - -4.200000	3.900000
3.500000 - 5.250000	0.575000	-3.850000 - -3.150000	3.550000
5.600000 - 6.650000	0.400000	-2.800000 - -2.450000	3.375000
		-2.100000 - -1.750000	3.200000
		-1.400000 - -1.050000	3.025000
		-0.700000 - -0.350000	2.850000
		0.000000 - 0.350000	2.675000
		0.700000 - 1.050000	2.500000
		1.400000 - 1.750000	2.325000
		2.100000 - 2.450000	2.150000
		2.800000 - 3.150000	1.975000
		3.500000 - 3.850000	1.800000
		4.200000 - 4.550000	1.625000
		4.900000 - 5.250000	1.450000
		5.600000 - 5.950000	1.275000
		6.300000 - 6.650000	1.100000

Table 4.6: r_1 and r_2 values, in atomic units, that define the barriers. The data on the left define the first TS barrier and those on the right define the second TS barrier.

Results and Comments

The results of these calculations are plotted in Figures 4.7, 4.8, 4.9 and 4.10. Table 4.7 shows the comparison between the experimental and theoretical results.

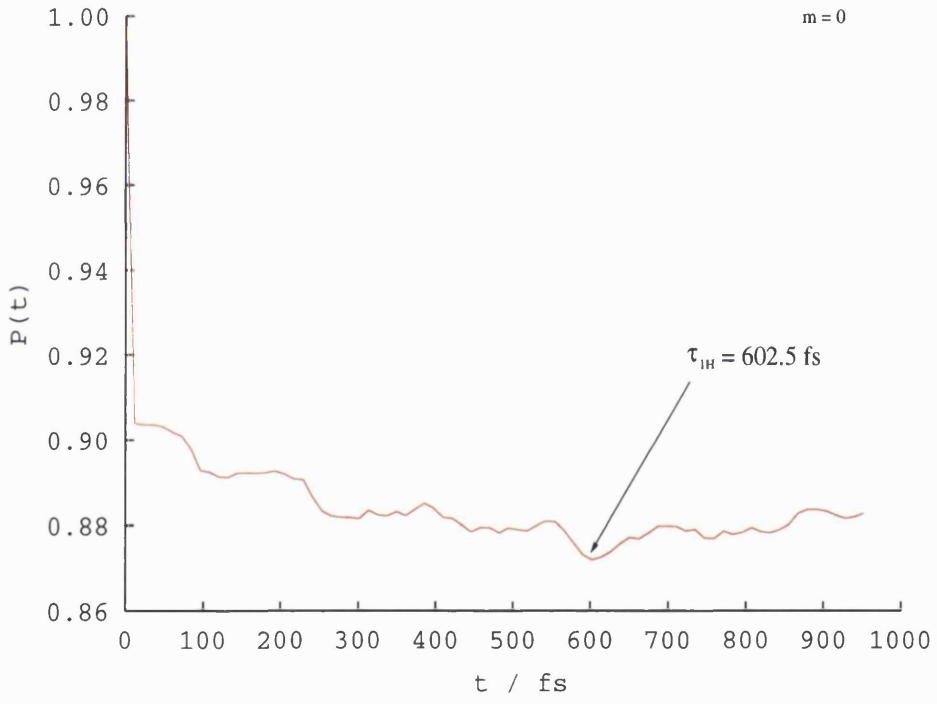

Figure 4.7: Probability of finding the H atom in the first well of the 3D potential energy surface *versus* the propagation time.

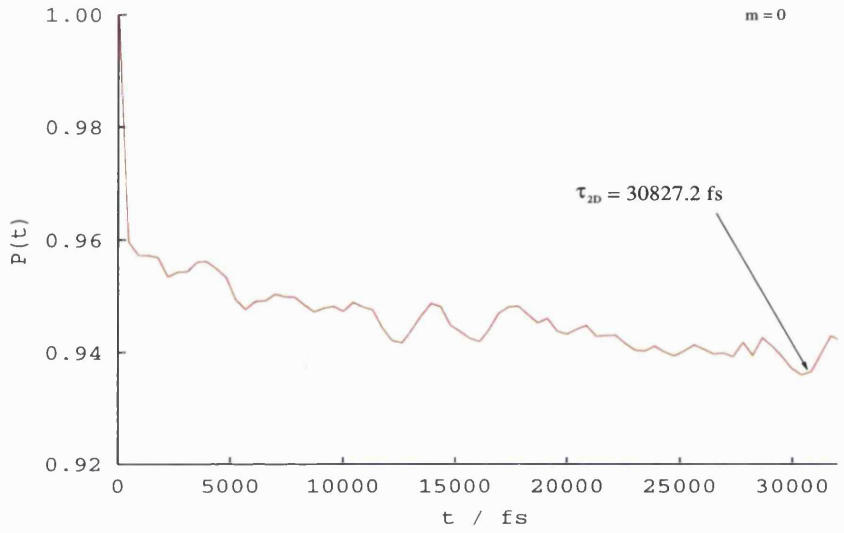

Figure 4.8: Probability of finding the H atom to the left of the second barrier of the 3D potential energy surface *versus* the propagation time.

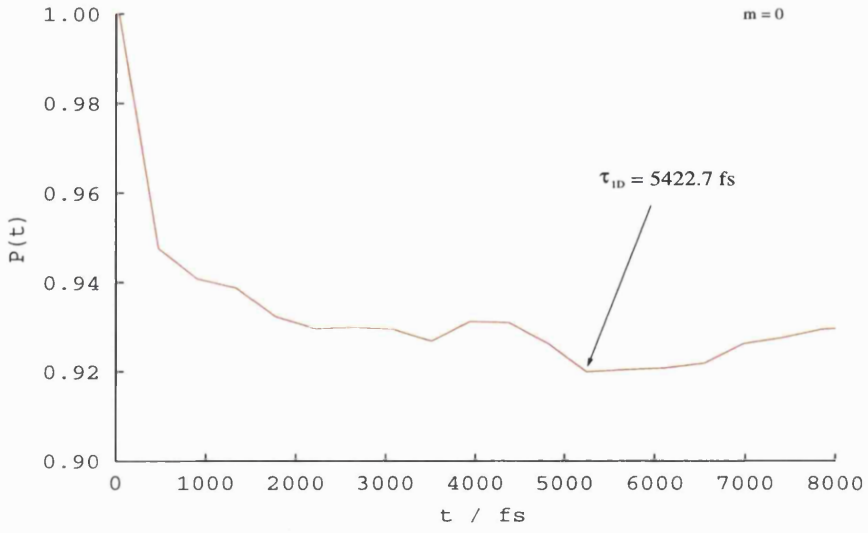

Figure 4.9: Probability of finding the D atom in the first well of the 3D potential energy surface *versus* the propagation time.

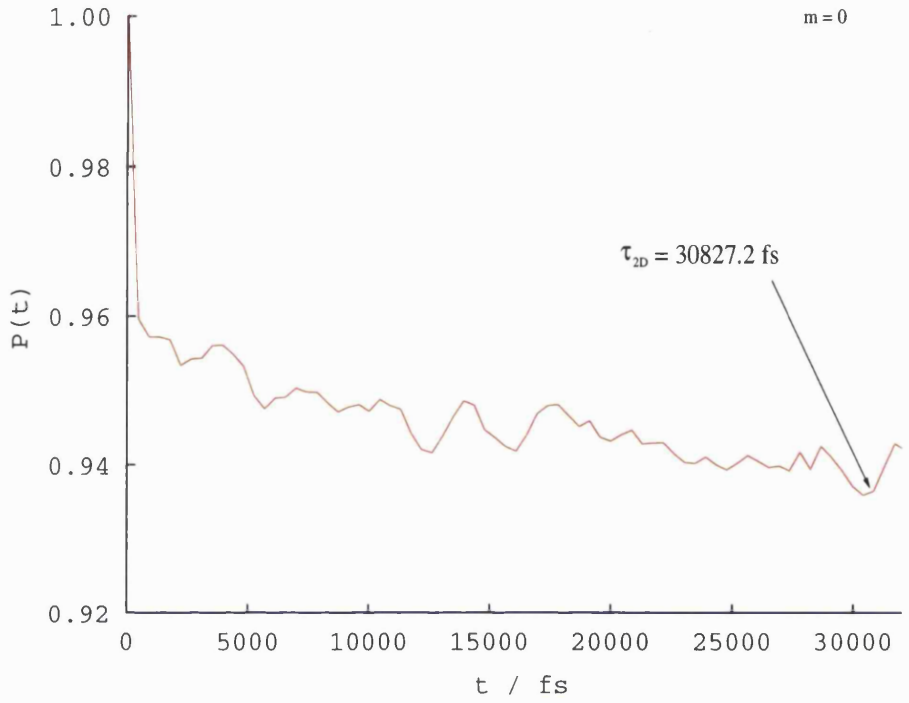

Figure 4.10: Probability of finding the D atom to the left of the second barrier of the 3D potential energy surface *versus* the propagation time.

	τ_{1H}	τ_{2H}	τ_{1D}	τ_{2D}
Zewail m=0	650	3300		
Zewail m=3	360	1700	3000	25000
Castleman m=0	660	5000		
theoretical m=0	602.5	4940.7	5422.7	30827.2

Table 4.7: Comparison of the experimental and theoretical H/D transfer times (in fs).

The first thing to notice is a large improvement in these results compared with the previous theoretical ones shown in Tables 4.1, 4.2, 4.4 and 4.5. These new results are more similar to the experimental ones. The first proton transfer time obtained in the calculations is 602.5 fs while the experimental one reported by Zewail's group is 650 fs and Castleman's group reported 660 fs. The second proton transfer time is 4940.7 fs while the experimental one was reported to be 3300 fs by Zewail's group and 5000 fs by Castleman's group. For the deuterated species the theoretical transfer times are 5422.7 fs and 30837.2 fs obtained with m=0, while the experimental ones are 3000 fs and 25000 fs obtained at m=3. In the two dimensional approach calculations were carried out with $m \geq 0$. In these calculations the r_2 coordinate constituted the bath and it was simulated by a harmonic potential, it was easy then to introduce extra vibrational energy in the N-N bond to observe the influence of the internal N-N vibrational energy on the proton transfer times. However, in the three dimensional calculations the r_2 coordinate is treated as part of the system which makes it more difficult to introduce extra vibrational energy into the N-N bond so the calculations were carried out only at m=0. The theoretical results show the importance of the role played by the N-N bond in this reaction. When this bond is treated explicitly as part of the system the results obtained improved dramatically when compared with experiments. The potential energy surfaces used here are very approximate, but qualitative insight is gained. The results show clearly that at least three dimmensions are required to model this type of problem to get realistic comparison with experiment.

Chapter 5

Conclusions

This thesis describes how the proton transfer reactions in large systems can be treated using the quantum tunnelling in a dissipative environment method. In particular it has been shown that this method allows us to reduce the dimensionality of the calculations while still obtaining results in general agreement with experiments.

The quantum tunnelling in a dissipative environment method treats separately the harmonic and anharmonic molecular degrees of freedom. The harmonic ones, those that change very little during the reaction, constitute the bath and are simulated using a harmonic potential. The anharmonic degrees of freedom, those that change most during the reaction, constitute the system and are treated explicitly.

This method was applied to the double proton transfer reaction in the 7-azaindole dimer. The aim of this work was to obtain the proton and deuterium transfer times, at the same time throwing some light on the reaction mechanism which has been a subject of discussion over the last few years. We wanted to observe the influence of the atom-donor atom-acceptor (in our case the N-N bond) initial vibrational energy and of the isotopic changes on the final transfer times.

By carrying out two and three dimensional calculations we were able to show the importance of the role played by the N-N bond. Treating it explicitly (as part of the system) allowed us to reach quite good agreement with the experimental transfer times. We have also demonstrated that this reaction occurs mainly through quantum tunnelling; this fact is confirmed by the variation of the transfer times with the

isotopic change.

The two dimensional calculations allow us to see the importance of the reaction barrier. The agreement with experiment improved with the presence of a deeper intermediate well which implies a higher barrier for the second proton or deuterium transfer times.

The transfer times obtained in the three dimensional calculations reached a good agreement with the experimental values. The fact that the first H transfer time, when there is no extra vibrational energy in the atom-donor atom-acceptor bond, is in the femtosecond scale confirms Zewail's suggestion that the reaction is direct and does not involve the entire molecule. It can then be said that the proton transfer time is localised in the N-H$\cdots$N coordinate.

In conclusion, it can be said that the quantum tunnelling in a dissipative environment method is suitable for studying proton transfer reactions in large systems providing that at least two degrees of freedom are treated explicitly. Double proton transfer is a common process, particularly in biological environments. The method and findings described here could be useful in future studies of this important process.

Appendix A

Ground State $(7\text{-AI})_2$ DFT Points

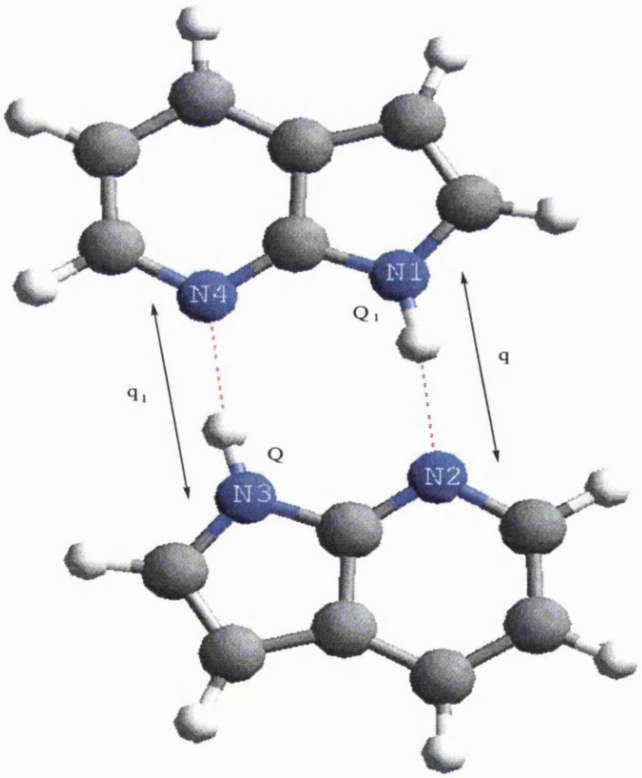

Figure A.1: Coordinates used in the DFT calculations.

Table A.1: DFT points of the (7-AI)$_2$ ground state potential energy surface.

q/Å	q_1/Å	Q/Å	Q_1/Å	Energy/Hartree
2.985606	2.985159	1.013300	1.013300	-759.740822972
			1.110297	-759.737499907
			1.207311	-759.727357234
			1.304342	-759.715205255
			1.401382	-759.704203030
			1.498433	-759.696015969
			1.595491	-759.691306806
			1.692556	-759.689983652
			1.789626	-759.690918754
			1.886701	-759.690918754
			1.983778	-759.687422439
		1.110250	1.013300	-759.737505300
			1.110297	-759.734291307
			1.207311	-759.724375085
			1.304342	-759.712531034
			1.401382	-759.701869558
			1.498433	-759.694062179
			1.595491	-759.689804518
			1.692556	-759.688955037
			1.789626	-759.690376010
			1.886701	-759.691501752
			1.983778	-759.687588926
		1.207219	1.013300	-759.727372537
			1.110297	-759.724385119
			1.207311	-759.714699410
			1.304342	-759.703242442
			1.401382	-759.693024934
			1.498433	-759.685715989
			1.595491	-759.682000756
			1.692556	-759.681787950
			1.789626	-759.683769374
			1.886701	-759.685358078
			1.983778	-759.681867458
		1.304203	1.013300	-759.715230228
			1.110297	-759.712550715
			1.207311	-759.703252127
			1.304342	-759.692276535
			1.401382	-759.682600395
			1.498433	-759.675927395
			1.595491	-759.672883912
			1.692556	-759.673290157
			1.789626	-759.675913228
			1.886701	-759.678093348
			1.983778	-759.675113085
		1.401198	1.013300	-759.704235447
			1.110297	-759.701896512
			1.207311	-759.693041794

Table A.1: DFT points of the (7-AI)$_2$ ground state potential energy surface.

q/Å	q_1/Å	Q/Å	Q_1/Å	Energy/Hartree
2.985606	2.985159	1.401198	1.304342	-759.682607467
			1.401382	-759.673585614
			1.498433	-759.667635204
			1.595491	-759.665348855
			1.692556	-759.666520364
			1.789626	-759.669878744
			1.886701	-759.672718448
			1.983778	-759.670236444
		1.498203	1.013300	-759.696052123
			1.110297	-759.694092711
			1.207311	-759.685736193
			1.304342	-759.675937686
			1.401382	-759.667638505
			1.498433	-759.662521459
			1.595491	-759.661095277
			1.692556	-759.663124043
			1.789626	-759.667230260
			1.886701	-759.670717836
			1.983778	-759.668763185
		1.595215	1.013300	-759.691342090
			1.110297	-759.689834106
			1.207311	-759.682019995
			1.304342	-759.672893349
			1.401382	-759.665351278
			1.498433	-759.661094321
			1.595491	-759.660533984
			1.692556	-759.663369899
			1.789626	-759.668245744
			1.886701	-759.672358644
			1.983778	-759.670907294
		1.692233	1.013300	-759.690014593
			1.110297	-759.688980134
			1.207311	-759.681802180
			1.304342	-759.673294661
			1.401382	-759.666526766
			1.498433	-759.663118529
			1.595491	-759.663365009
			1.692556	-759.666921007
			1.789626	-759.672507835
			1.886701	-759.677232138
			1.983778	-759.676264759
		1.789257	1.013300	-759.690941973
			1.110297	-759.690393165
			1.207311	-759.683775647
			1.304342	-759.675909462
			1.401382	-759.669867741
			1.498433	-759.667215948

Table A.1: DFT points of the (7-AI)$_2$ ground state potential energy surface.

q/Å	q_1/Å	Q/Å	Q_1/Å	Energy/Hartree
2.985606	2.985159	1.789257	1.595491	-759.668232556
			1.692556	-759.672499630
			1.789626	-759.678718830
			1.886701	-759.683961538
			1.983778	-759.683409728
		1.886285	1.013300	-759.691657067
			1.110297	-759.691506014
			1.207311	-759.685353919
			1.304342	-759.678080092
			1.401382	-759.672697925
			1.498433	-759.670694158
			1.595491	-759.672336053
			1.692556	-759.677214649
			1.789626	-759.683952272
			1.886701	-759.689642510
			1.983778	-759.689416150
		1.983317	1.013300	-759.687430181
			1.110297	-759.687590579
			1.207311	-759.681858293
			1.304342	-759.675094076
			1.401382	-759.670210235
			1.498433	-759.668733884
			1.595491	-759.670878749
			1.692556	-759.676241917
			1.789626	-759.683395243
			1.886701	-759.689411179
			1.983778	-759.689492580
2.900000	2.900000	1.013300	1.013300	-759.740394439
			1.101763	-759.738096430
			1.190240	-759.729869961
			1.278728	-759.719726930
			1.367226	-759.710312262
			1.455731	-759.703063572
			1.544242	-759.698607184
			1.632759	-759.696810751
			1.721280	-759.696672108
			1.809805	-759.696083365
			1.898333	-759.691191025
		1.101760	1.013300	-759.738096327
			1.101763	-759.735889252
			1.190240	-759.727892460
			1.278728	-759.718043347
			1.367226	-759.708952660
			1.455731	-759.702060026
			1.544242	-759.698014855
			1.632759	-759.696659939
			1.721280	-759.696959975

Table A.1: DFT points of the (7-AI)$_2$ ground state potential energy surface.

q/Å	q_1/Å	Q/Å	Q_1/Å	Energy/Hartree
2.900000	2.900000	1.101760	1.809805	-759.696711425
			1.898333	-759.692144818
		1.190236	1.013300	-759.729869173
			1.101763	-759.727891963
			1.190240	-759.720156423
			1.278728	-759.710655646
			1.367226	-759.701974710
			1.455731	-759.695549246
			1.544242	-759.692034931
			1.632759	-759.691152886
			1.721280	-759.691937710
			1.809805	-759.692123082
			1.898333	-759.687958461
		1.278726	1.013300	-759.719725437
			1.101763	-759.718042105
			1.190240	-759.710654882
			1.278728	-759.701604152
			1.367226	-759.693412594
			1.455731	-759.687561806
			1.544242	-759.684565980
			1.632759	-759.684272752
			1.721280	-759.685608871
			1.809805	-759.686326079
			1.898333	-759.682576612
		1.367225	1.013300	-759.710309969
			1.101763	-759.708950555
			1.190240	-759.701973137
			1.278728	-759.693411872
			1.367226	-759.685810685
			1.455731	-759.680557416
			1.544242	-759.678250328
			1.632759	-759.678634658
			1.721280	-759.680596872
			1.809805	-759.681869053
			1.898333	-759.678577348
		1.455731	1.013300	-759.703060741
			1.101763	-759.702057559
			1.190240	-759.695547343
			1.278728	-759.687560929
			1.367226	-759.680557078
			1.455731	-759.676048966
			1.544242	-759.674472672
			1.632759	-759.675581390
			1.721280	-759.678205886
			1.809805	-759.680047164
			1.898333	-759.677218561

Table A.1: DFT points of the (7-AI)$_2$ ground state potential energy surface.

q/Å	q_1/Å	Q/Å	Q_1/Å	Energy/Hartree
2.900000	2.900000	1.544245	1.013300	-759.698604633
			1.101763	-759.698012756
			1.190240	-759.692033314
			1.278728	-759.684565208
			1.367226	-759.678250228
			1.455731	-759.674473031
			1.544242	-759.673632428
			1.632759	-759.675449772
			1.721280	-759.678727552
			1.809805	-759.681127713
			1.898333	-759.678763848
		1.632764	1.013300	-759.696898721
			1.101763	-759.696658133
			1.190240	-759.691152212
			1.278728	-759.684272861
			1.367226	-759.678635570
			1.455731	-759.675582719
			1.544242	-759.675450772
			1.632759	-759.677864308
			1.721280	-759.681756258
			1.809805	-759.684700943
			1.898333	-759.682785765
		1.721288	1.013300	-759.696671448
			1.101763	-759.696960084
			1.190240	-759.691938737
			1.278728	-759.685610728
			1.367226	-759.680599562
			1.455731	-759.678209035
			1.544242	-759.678730242
			1.632759	-759.681758071
			1.721280	-759.686215246
			1.809805	-759.689625040
			1.898333	-759.688092831
		1.809816	1.013300	-759.696084556
			1.101763	-759.696713128
			1.190240	-759.692126084
			1.278728	-759.686329864
			1.367226	-759.681873801
			1.455731	-759.680052340
			1.544242	-759.681132513
			1.632759	-759.684704850
			1.721280	-759.689627123
			1.809805	-759.693473948
			1.898333	-759.692259846
		1.898347	1.013300	-759.691193064
			1.101763	-759.692147610
			1.190240	-759.687962157

Table A.1: DFT points of the (7-AI)$_2$ ground state potential energy surface.

q/Å	q_1/Å	Q/Å	Q_1/Å	Energy/Hartree
2.900000	2.900000	1.898347	1.278728	-759.682581285
			1.367226	-759.678583141
			1.455731	-759.677224796
			1.544242	-759.678769767
			1.632759	-759.682790817
			1.721280	-759.688095967
			1.801757	-759.692251907
			1.898333	-759.691313067
2.782545	2.782586	1.013300	1.013300	-759.740822972
			1.013302	-759.737694738
			1.088641	-759.736571800
			1.164210	-759.730874232
			1.239965	-759.723484508
			1.315878	-759.716304802
			1.391920	-759.710392618
			1.468072	-759.706255014
			1.544317	-759.703860099
			1.620644	-759.702470880
			1.697040	-759.700367060
			1.773495	-759.694810541
		1.088636	1.013302	-759.736572266
			1.088641	-759.735585611
			1.164210	-759.730099907
			1.239965	-759.722955560
			1.315878	-759.716059556
			1.391920	-759.710469223
			1.468072	-759.706670754
			1.544317	-759.704611862
			1.620644	-759.703551747
			1.697040	-759.701782476
			1.773495	-759.696516341
		1.164202	1.013302	-759.730875334
			1.088641	-759.730100546
			1.164210	-759.724920929
			1.239965	-759.718070499
			1.315878	-759.711512011
			1.391920	-759.706312942
			1.468072	-759.702929194
			1.544317	-759.701275589
			1.620644	-759.700608341
			1.697040	-759.699211359
			1.773495	-759.694272418
2.782545	2.782586	1.239955	1.013300	-759.723486272
			1.088641	-759.722956860
			1.164210	-759.718071138
			1.239965	-759.711616692
			1.315878	-759.705454664

Table A.1: DFT points of the (7-AI)$_2$ ground state potential energy surface.

q/Å	q_1/Å	Q/Å	Q_1/Å	Energy/Hartree
2.782545	2.782586	1.239955	1.391920	-759.700703887
			1.468072	-759.697811404
			1.544317	-759.696637178
			1.620644	-759.696414106
			1.697040	-759.695428580
			1.773495	-759.690861437
		1.315864	1.013300	-759.716307075
			1.088641	-759.716061371
			1.164210	-759.711513166
			1.239965	-759.705455179
			1.315878	-759.699733561
			1.391920	-759.695490384
			1.468072	-759.693135275
			1.544317	-759.692506673
			1.620644	-759.692773262
			1.697040	-759.692233245
			1.773495	-759.687996582
		1.391902	1.013302	-759.710395155
			1.088641	-759.710471297
			1.164210	-759.706314345
			1.239965	-759.700704660
			1.315878	-759.695490642
			1.391920	-759.691759832
			1.468072	-759.689967053
			1.544317	-759.689910357
			1.620644	-759.690709884
			1.697040	-759.690648895
			1.773495	-759.686846011
		1.468051	1.013302	-759.706257608
			1.088641	-759.706672870
			1.164210	-759.702930617
			1.239965	-759.697812175
			1.315878	-759.693135540
			1.391920	-759.689967052
			1.468072	-759.688767765
			1.544317	-759.689270273
			1.620644	-759.690635437
			1.697040	-759.691037415
			1.773495	-759.687647259
		1.544294	1.013302	-759.703862455
			1.088641	-759.704613765
			1.164210	-759.701276791
			1.239965	-759.696637726
			1.315878	-759.692506706
			1.391920	-759.689910125
			1.468072	-759.689270057
			1.544317	-759.690348304

Table A.1: DFT points of the (7-AI)$_2$ ground state potential energy surface.

q/Å	q_1/Å	Q/Å	Q_1/Å	Energy/Hartree
2.782545	2.782586	1.239955	1.620644	-759.692202779
			1.697040	-759.693063674
			1.773495	-759.690061893
		1.620616	1.013300	-759.702472893
			1.088641	-759.703553292
			1.164210	-759.700609165
			1.239965	-759.696414270
			1.315878	-759.692772916
			1.391920	-759.690634858
			1.468072	-759.692202382
			1.544317	-759.694508150
			1.620644	-759.695778101
			1.697040	-759.695778101
			1.773495	-759.693129088
		1.697009	1.013300	-759.700368800
			1.088641	-759.701783787
			1.164210	-759.699211828
			1.239965	-759.695428398
			1.315878	-759.692232562
			1.391920	-759.690647958
			1.468072	-759.691036490
			1.544317	-759.693062931
			1.620644	-759.695777764
			1.697040	-759.697410343
			1.773495	-759.695072492
		1.773461	1.013302	-759.694812249
			1.088641	-759.696517420
			1.164210	-759.694272799
			1.239965	-759.690861169
			1.315878	-759.687995822
			1.391920	-759.686845018
			1.468072	-759.687646294
			1.544317	-759.690061111
			1.620644	-759.693128721
			1.697040	-759.695072479
			1.773495	-759.693011789
2.839999	2.840000	1.013300	1.013300	-759.739551905
2.939996	2.940000	1.013300	1.013300	-759.740786921
2.839999	2.840000	1.304203	1.013300	-759.717546239
2.939996	2.940000	1.304203	1.013300	-759.716180822
2.839999	2.840000	1.692233	1.013300	-759.699795402
2.939996	2.940000	1.692233	1.013300	-759.690014593

Bibliography

[1] A.H. Zewail, *J. Phys. Chem.*, **100**, 12701 (1996).

[2] A.H. Zewail, *J. Phys. Chem. A*, **104**, 5660 (2000).

[3] A.H. Zewail, *FEMTOCHEMISTRY: Ultrafast Dynamics of the Chemical Bond, Vols. I and II*, (World Scientific, 20^{th} Century Chemistry Series, New Jersey, Singapore, 1994).

[4] Lectures' notes, *Femtochemistry and Femtobiology*, El Escorial Summer School (2000).

[5] *Femtosecond Chemistry, Vols. 1 and 2*, J. Manz and L. Wöste (Eds.), (VCH Publishers, Weinheim, Germany, 1995).

[6] Royal Swedish Academy of Science. Nobel Prize Chemistry 1903. Presentation speech.

[7] F.A. Lindemann, *Trans. Faraday Soc.*, **17**, 598 (1922).

[8] *The Kinetics of Chemical Change in Gaseous Systems*, C.N. Hinshelwood, (Calendron, Oxford, 1926).

[9] H. Eyring, *J. Chem. Phys.*, **3**, 107 (1935).

[10] H. Eyring, *J. Chem. Phys.*, **17**, 65 (1935).

[11] M.G. Evans, M. Polanyi, *Trans. Faraday Soc.*, **31**, 875 (1935).

[12] O.K. Rice, H.C. Ramsperger, *J. Am. Chem. Soc*, **32**, 225 (1928.

[13] R.A. Marcus, O.K. Rice, *J. Phys. Colloid. Chem.*, **55**, 894 (1951).

[14] R.A. Marcus, *J. Chem. Phys.*, **20**, 359 (1952).

[15] W. Heitler, F. London, *Z. Phys.*, **44**, 455 (1927).

[16] F. London, *Probleme der Modernen Physik*; Sommerfeld Fetschrift; 104 (1928).

[17] H. Eyring, M. Polanyi, *Z. Phys. Chem. B*, **12**, 279 (1931).

[18] H.A. Kramers, *Physicaa*, **7**, 284 (1940).

[19] J.O. Hirschfelder, H. Eyring, B. Topley, *J. Chem. Phys.*, **4**, 170 (1936).

[20] A.H. Zewail, R.B. Bernstein, *Chem. and Eng. News*, Nov. 7, 24 (1988).

[21] Royal Swedish Academy of Science. Nobel Prize Chemistry 1967. Presentation speech.

[22] Royal Swedish Academy of Science. Nobel Prize Chemistry 1986. Presentation speech.

[23] R.L. Fork, C.H. Brito Cruz, P.C. Becker, C.V. Shank, *Opt. Lett.*, **12**, 483 (1987).

[24] D.E. Spence, P.N. Kean, W. Sibbett, *Opt. Lett.*, **16**, 42 (1991).

[25] M. Dantus, M.J. Rosker and A.H. Zewail, *J. Chem. Phys.*, **87**, 1451 (1987).

[26] M. Dantus, M.J. Rosker and A.H. Zewail, *J. Chem. Phys.*, **89**, 6128 (1988).

[27] T.S. Rose, M.J. Rosker and A.H. Zewail, *J. Chem. Phys.*, **88**, 6672 (1988).

[28] V. Engel, H. Metiu, R. Almeida, R.A. Marcus and A.H. Zewail, *Chem. Phys. Lett.*, **152**, 1 (1988).

[29] T.S. Rose, M.J. Rosker and A.H. Zewail, *J. Chem. Phys.*, **91**, 7415 (1989).

[30] N.F. Scherer, C. Sipes, R.B. Bernstein and A.H. Zewail, *J. Chem. Phys.*, **92**, 5239 (1990).

[31] M.J. Rosker, M. Dantus and A.H. Zewail, *J. Chem. Phys.*, **89**, 6113 (1988).

[32] Royal Swedish Academy of Science. Nobel Prize Chemistry 1999. Presentation speech and press release.

[33] A.V. Smirnov, D.S. English, R.L. Rich, J. Lane, L. Teyton, A.W. Schwabacher, S. Luo, R.W. Thornburg and J.W. Petrich, *J. Phys. Chem. B*, **101**, 2758 (1997).

[34] J.D. Watson and F.H.C. Crick, *Nature*, **171**, 737, 964 (1953).

[35] J.A. Syage, *J. Phys. Chem.*, **99**, 5772 (1995).

[36] T. Koyama and A. Wakisaka, *J. Chem. Soc., Faraday Trans.*, **93**, 3813 (1997).

[37] D.E. Folmer, E.S. Wisniewski, S.M. Hurley and A.W. Castleman Jr., *Proc. Natl. Acad. Sci.*, **96**, 12980 (1999).

[38] C.A. Taylor, M.A. El-Bayoumi and M. Kasha, *Proc. Natl. Acad. Sci. USA*, **63**, 253 (1969).

[39] K.C. Ingham, M. Abu-Elgheit and M.A. El-Bayoumi, *J. Am. Chem. Soc.*, **93**, 5023 (1971).

[40] K.C. Ingham and M.A. El-Bayoumi, *J. Am. Chem. Soc.*, **96**, 1674 (1974).

[41] H. Bulska and A. Chodkowska, *J. Am. Chem. Soc.*, **102**, 3259 (1980).

[42] M.A. El-Bayoumi, P. Avouris and W.R. Ware, *J. Chem. Phys.*, **62**, 2499 (1975).

[43] W.M. Hetherington, R.H. Micheels and K.B. Eisenthal, *Chem. Phys. Lett.*, **66**, 230 (1979).

[44] J. Catalán and P. Pérez, *J. Theor. Biol.*, **81**, 213 (1979).

[45] K. Fuke, H. Yoshiuchi and K. Kaya, *J. Phys. Chem.*, **88**, 5840 (1984).

[46] K. Fuke and K. Kaya, *J. Phys. Chem.*, **93**, 614 (1989).

[47] K. Tokumura, Y. Watanabe and M. Itoh, *J. Phys. Chem.*, **90**, 2362 (1986).

[48] P.-T. Chou, C.-Y. Wei, C.-P. Chang and K. Meng-Shin, *J. Phys. Chem.*, **99**, 11994 (1995).

[49] A. Douhal, S.K. Kim and A.H. Zewail, *Nature*, **378**, 260 (1995).

[50] A. Douhal, V. Guallar, M. Moreno and J.M. Lluch, *Chem. Phys. Lett.*, **256**, 370 (1996).

[51] R. Lopez-Martens, P. Long, D. Solgadi, B. Soep, J. Syage and Ph. Millie, *Chem. Phys. Lett.*, **273**, 219 (1997).

[52] A. Nakajima, M. Hirano, R. Hasumi, K. Kaya, H. Watanabe, C.C. Carter, J.M. Williamson and T.A. Miller, *J. Phys. Chem. A*, **101**, 392 (1997).

[53] J. Catalán, J.C. del Valle and M. Kasha, *Chem. Phys. Lett.*, **318**, 629 (2000).

[54] V. Guallar, M. Moreno and J.M. Lluch, *Chem. Phys.*, **228**, 1 (1998).

[55] D.E. Folmer, L. Poth, E.S. Wisniewski and A.W. Castleman Jr., *Chem. Phys. Lett.*, **287**, 1 (1998).

[56] V. Guallar, V.S. Batista and W.H. Miller, *J. Chem. Phys.*, **110**, 9922 (1999).

[57] M. Moreno, A. Douhal, J.M. Lluch, O. Castaño and L.M. Frutos, *J. Phys. Chem. A*, **105**, 3887 (2001).

[58] J. Catálan, J.C. del Valle and M. Kasha, *Proc. Natl. Acad. Sci. USA*, **96**, 8338 (1999).

[59] J.C. del Valle, M. Kasha and J. Catalán, *Int. J. Quantum Chem.*, **77**, 118 (2000).

[60] D.E. Folmer, E.S. Wisniewski and A.W. Castleman, Jr., *Chem. Phys. Lett.*, **318**, 637 (2000).

[61] A. Douhal, M. Moreno and J.M. Lluch, *Chem. Phys. Lett.*, **324**, 75 (2000).

[62] A. Douhal, M. Moreno and J.M. Lluch, *Chem. Phys. Lett.*, **324**, 81 (2000).

[63] S. Takeuchi and T. Tahara, *Chem. Phys. Lett.*, **277**, 340 (1997).

[64] S. Takeuchi and T. Tahara, *J. Phys. Chem. A*, **102**, 7740 (1998).

[65] M. Chachisvilis, T. Fiebig, A. Douhal and A.H. Zewail, *J. Phys. Chem. A*, **102**, 669 (1998).

[66] T. Fiebig, M. Chachisvilis, M. Manger, A.H. Zewail, A. Douhal, I. García-Ochoa and A. de La Hoz Ayuso, *J. Phys. Chem. A*, **103**, 7419 (1999).

[67] J. Catalán and M. Kasha, *J. Phys. Chem. A*, **104**, 10812 (2000).

[68] P.O. Löwdin, *Rev. Mod. Phys.*, **35**, 724 (1963).

[69] P.O. Löwdin, *Adv. Quantum Chem.*, **2**, 213 (1965).

[70] R.P. Bell, *The Tunnel Effect in Chemistry*, Chapman and Hall, London, UK (1980).

[71] M.M. Nieto, V.P. Gutschick, C.M. Bender, F. Cooper and D. Strottman, *Phys. Lett. B*, **163**, 336 (1985).

[72] M. Razavy, *Can. J. Phys.*, **73**, 131 (1995).

[73] A. Douhal, *Science*, **276**, 221 (1997).

[74] H.-H. Limbach and J. Manz, *Ber. Bunsenges. Phys. Chem.*, **102**, 289 (1998).

[75] M.F. Hineman, G.A. Brucker, D.F. Kelley and E.R. Bernstein, *J. Chem. Phys.*, **97**, 3341 (1992).

[76] A. Douhal, F. Lahmani and A.H. Zewail, *Chem. Phys.*, **207**, 477 (1996).

[77] A.Z. Weller, *Elektrochem.*, **60**, 1144 (1956).

[78] J. Catalán, J. Palomar and J.L.G. de Paz, *J. Phys. Chem. A*, **101**, 7914 (1997).

[79] Y. Kim, S. Lim and Y. Kim, *J. Phys. Chem. A*, **103**, 6632 (1999).

[80] A. Kyrychenko, J. Herbich, M. Izydorzak, M. Gil, J. Dobkowski, F. Wu, R.P. Thummel and J. Waluk, *Israel J. Chem.*, **39**, 309 (1999).

[81] E. Bardez, *Israel J. Chem.*, **39**, 319 (1999).

[82] V. Guallar, A. Douhal, M. Moreno and J.M. Lluch, *J. Phys. Chem. A*, **103**, 6251 (1999).

[83] J. Brickmann and H. Zimmermann , *J. Chem. Phys.*, **50** , 1608 (1969).

[84] J. Brickmann, in *The hydrogen bond*, eds. P. Schuster, G. Zundel and C. Sandorfy, North-Holland Publishing Company (1976). Chapter 4.

[85] V.K. Babamov and R.A. Marcus, *J. Chem. Phys.*, **74**, 1790 (1981).

[86] W.H. Miller, N.C. Handy and J.E. Adams, *J. Chem. Phys.*, **72**, 99 (1980).

[87] T. Carrington Jr. and W.H. Miller, *J. Chem. Phys.*, **81**, 3942 (1984).

[88] T. Carrington Jr. and W.H. Miller, *J. Chem. Phys.*, **84**, 4364 (1986).

[89] N. Sato and S. Iwata, *J. Chem. Phys.*, **89**, 2932 (1988).

[90] W.H. Miller and S. Schwartz, *J. Chem. Phys.*, **77**, 2378 (1982).

[91] A.O. Caldeira and A.J. Leggett, *Ann. Phys.*, **149**, 374 (1983).

[92] M. Hron and M. Razavy, *Can. J. Phys.*, **70**, 719 (1992).

[93] A.J. Horsewill, D.F. Brougham, R.I. Jenkinson, C.J. McGloin, H.P. Trommsdorff and M.R. Johnson, *Ber. Bunsenges. Phys. Chem.*, **102**, 317 (1998).

[94] N. Došlić, O. Kühn and J. Manz, *Ber. Bunsenges. Phys. Chem.*, **102**, 292 (1998).

[95] S.M. Anderson, J.I. Zink and D. Neuhauser, *Chem. Phys. Lett.*, **291**, 387 (1998).

[96] G.D. Billing, *Chem. Phys. Lett.*, **30**, 391 (1975).

[97] R.B. Gerber, V. Buch and M.A. Ratner, *J. Chem. Phys.*, **77**, 3022 (1982).

[98] J.C. Tully and R.K. Preston, *J. Chem. Phys.*, **55**, 562 (1971).

[99] J.C. Tully, *J. Chem. Phys.*, **93**, 1061 (1990).

[100] R.P. Feynman and A.R. Hibbs, *Quantum Mechanics and Path Integrals*, McGraw-Hill, New York, (1965).

[101] X. Sun and W.H. Miller, *J. Chem. Phys.*, **106**, 916 (1996).

[102] W.H. Miller, *Adv. Chem. Phys.*, **25**, 69 (1974).

[103] J.V. Lill, G.A. Parker and J.C. Light, *Chem. Phys. Lett.*, **89**, 483 (1982).

[104] J.C. Light, I.P. Hamilton and J.V. Lill, *J. Chem. Phys.*, **82**, 1400 (1985).

[105] J.T. Muckerman, *Chem. Phys. Lett.*, **173**, 200 (1990).

[106] J. Echave and D.C. Clary, *Chem. Phys. Lett.*, **190**, 225 (1992).

[107] L.S. Costa, *Cálculo de Estados Metaestáveis de Sistemas Moleculares*, Dissertação de Mestrado, Departamento de Física, Universidade de Brasilia, Brazil (1996).

[108] J.C. Light and T. Carrington Jr., *Adv. Chem. Phys.*, **114**, 263 (2000).

[109] M.J. Frisch, G.W. Trucks, H.B. Schlegel, G.E. Scuseria, M.A. Robb, J.R. Cheeseman, V.G. Zakrzewski, J.A. Montgomery, Jr., R.E. Stratmann, J.C. Burant, S. Dapprich, J.M. Millam, A.D. Daniels, K.N. Kudin, M.C. Strain, O. Farkas, J. Tomasi, V. Barone, M. Cossi, R. Cammi, B. Mennucci, C. Pomelli, C. Adamo, S. Clifford, J. Ochterski, G.A. Petersson, P.Y. Ayala, Q. Cui, K. Morokuma, D.K. Malick, A.D. Rabuck, K. Raghavachari, J.B. Foresman, J. Cioslowski, J.V. Ortiz, B.B. Stefanov, G. Liu, A. Liashenko, P. Piskorz, I. Komaromi, R. Gomperts, R.L. Martin, D.J. Fox, T. Keith, M.A. Al-Laham, C.Y. Peng, A. Nanayakkara, C. Gonzalez, M. Challacombe, P.M.W. Gill, B. Johnson, W. Chen, M.W. Wong, J.L. Andres, C. Gonzalez, M. Head-Gordon, E.S. Replogle, and J.A. Pople, *Gaussian 98, Revision A.3* Gaussian, Inc., Pittsburgh PA, (1998).

[110] Y.T. Chang and W.H. Miller, *J. Phys. Chem*, **94**, 5884 (1990).

[111] A. Warshel, *J. Phys. Chem.*, **86**, 2218 (1982).

[112] W.H. Press, S.A. Teukolsky, W.T. Vetterling and B.P. Flannery, *Numerical Recipes in Fortran*, (Cambridge University Press, Cambridge, 1992).

[113] *NAG Fortran Library* , The Numerical Algorithms Group Ltd., Oxford, UK (1999).

[114] F08JEF routine, *NAG Fortran Library* , The Numerical Algorithms Group Ltd., Oxford, UK (1999).